Fine-scale temporal and spatial variability in the coastal waters of Clayoquot Sound

by

Stephanie King
B.Sc., The University of Victoria, 2006

A Thesis Submitted in Partial Fulfillment
of the Requirements for the Degree of

MASTER OF SCIENCE

in the Department of Geography

Supervisory Committee

Fine-scale temporal and spatial variability in the coastal waters of Clayoquot Sound

by

Stephanie King
B.Sc., The University of Victoria, 2006

Supervisory Committee

Olaf Niemann (Department of Geography)
Supervisor

Jim Gower (Department of Geography)
Departmental Member

David A. Duffus (Department of Geography)
Departmental Member

Abstract

Supervisory Committee

Olaf Niemann (Department of Geography)
Supervisor

Jim Gower
Departmental Member

David A. Duffus
Departmental Member

An oceanographic buoy with 10 atmospheric and oceanographic instruments was deployed in Clayoquot Sound on the west coast of Canada in 2007. The high-resolution time series was used to monitor the fine-scale variability in the coastal ocean. Over 700 CTD profiles measuring temperature, salinity and chlorophyll fluorescence made in the region of the buoy were used to relate the buoy data to spatial patterns. Analysis showed that large-scale upwelling in combination with the localized winds and tidal currents affect water properties at time scales of hours to days. At low tide the buoy represented inland water and at high tide the buoy represented offshore water. Both the buoy data and CTD profiles measured a strong offshore/onshore gradient. For temperature the gradient depended on the direction of the wind, salinity was always higher offshore compared to onshore, and the chlorophyll fluorescence was higher onshore in the early spring and higher offshore for the rest of the time series. The fine scale temporal resolution of the buoy was able to capture the variability measured by the CTD profiles in a 40km^2 area. This work shows the importance of making high-resolution temporal measurements in the coastal ocean. However, these types of moorings also require frequent maintenance. In Clayoquot Sound, the optical sensors needed to be cleaned every 4-6 days.

Table of Contents

List of Tables

Chapter 2 tables

Chapter 3 tables

Chapter 4 tables

List of Figures

Chapter 1 figures

Chapter 2 figures

Chapter 3 figures

Chapter 4 figures

Acknowledgments

First, thanks to my supervisor Olaf Niemann for support and encouragement. On my occasional appearance, Olaf and my lab mates made coming to school a pleasure. Humour and warmth from GQ, RL, FV and DP was particularly appreciated from the beginning. In the field HM, LJF, KM, KD, CP and several enthusiastic interns made a summer of fantastic science, friendship, campfires, music and card games, and one I'll never forget. To Duff who encouraged us to be scientists, captains, explorers, mechanics, lumberjacks, chefs and rock-stars. Thanks for an opportunity of a lifetime and many thought provoking conversations. To Hughie Clark for his consistency, humour and countless favours. To Keith Clark and RP for being helpful and calm when we went to rescue the buoy. To the Ahousaht First Nation for being supportive and interested in our research. To Chris Ledger from Mainstream Aquaculture for supplying an anchor, and Nick Gubby from Axys for answering many questions.

My friends and family, SM, IC, MM, TB, SK, KF, and SB have been a tremendous support through this process, and buoy, what a process! To TL for continual inspiration. To Jim Gower for objectivity and comments on the thesis, for a being a wonderful boss, but most of all for friendship. Lastly and mostly, to Mum and Dad, who have encouraged me, supported me, put up with me and loved me, every step of the way. I am very fortunate.

Chapter 1. General Introduction

1.1. The Project

In spring 2006 and 2007 an oceanographic buoy was deployed in Clayoquot Sound to investigate the challenges and value of making fine-scale measurements in coastal waters. The project was funded through the Center for Applied Remote Sensing, Modeling and Simulation (CARMS) and the Canadian Buoyed Monitoring Network, both based at the University of Victoria. Axys Technologies in Sidney, BC, Canada, developed the system and managed the instrument integration. A similar buoy was deployed in Kyuquot Sound, but those data are not discussed here. Research shows that strategically placed instrumented buoys provide invaluable tools for long-term monitoring of the ocean environment (Dickey, 1991; Cullen, 1997) and are appropriate for the temporal scales operating in the coastal environment (Jannasch, 2008). While a buoy is making measurements at a fixed point the data can represent a larger area because the water moving around the buoy represents space. We ask how much can be learnt from the buoy about processes and patterns in the area surrounding buoy?

The combination of dynamic ecosystem and societal pressure in Clayoquot Sound makes the region a suitable location for coastal monitoring. In addition, the University of Victoria (UVic) Whale Research Lab (WRL) has a field camp on Flores Island, which provided logistic support and was a convenient base for field work. The WRL has been based in the Sound since the late 1980s and has identified the importance of high temporal resolution monitoring of the atmospheric and oceanographic properties in the area. The buoy data supported the WRL's activities. The buoy data was also monitored by local fish farmers.

Following the 2006 trial deployment, the buoy was retrieved from the water for the duration of the winter storm season. The data from 2006 is not discussed in this thesis due to problems with the instruments and maintenance. However, this initial deployment was valuable in designing a research program and maintenance schedule for the following year. In spring 2007 the buoy was redeployed and operational on March 24 to October 14. The buoy was rigorously maintained and calibrated through the 2007 field season. From March to September 2007 it was serviced 25 times. Water profiles of

temperature, salinity and chlorophyll fluorescence at 41 stations were also collected in the vicinity of the buoy on 18 days from June to September of 2007.

The 2007 buoy data and water profiles combine to form a dataset that is used in this thesis. The objective of which is threefold: 1) to describe the fine-scale temporal and spatial oceanographic patterns and processes in a dynamic coastal ecosystem, 2) to look at the links between the biological and physical components, and 3) to evaluate the functionality and logistics of autonomous data collection in coastal waters.

This thesis is organized into five chapters. This chapter introduces the study area and discusses the issue of scale in the coastal ocean. Chapter 2 uses the buoy data to describe the fine-scale temporal variability over 6 months in Clayoquot Sound. From these data, and with additional sources such as tidal models, upwelling indices, an offshore buoy and satellite imagery, we extend the fixed-point measurement to have spatial meaning. Chapter 3 describes the water profiles for temperature, salinity and chlorophyll fluorescence and relates the patterns observed to processes in space and time using empirical orthogonal function analysis. In chapter 4 we describe fouling on the buoy and discuss fouling rates compared to other studies. Lastly, in chapter 5 we conclude by combining the discussions from chapters 2 and 3.

1.2. Background

1.2.1. Clayoquot Sound

Clayoquot Sound on the west coast of Vancouver Island, Canada covers an area of 3500km^2 including both coastal ocean (coastline to the continental shelf) and the mountainous surrounding terrain (Figure 1-1). Water depths on the western seaward side range from 0 to 30m. In contrast, inlets to the east have glacial sills and depths greater than 100m. The continental shelf is broad, extending about 40km westward into the Pacific Ocean. The region is a temperate rainforest with the annual precipitation for the town of Tofino (Figure 1-1) at 325.7cm/year (Environment Canada, 2009). Rainfall is highest between October and April with fresh water entering the sound through many streams and small rivers. Mulkins *et al.* (2002) described the region as an estuary with significant freshwater input in the winter and spring. However, in the summer input flow

from many of the rivers and streams are significantly reduced and these types of estuaries can be considered an extension of the coastal ocean (Hickey and Banas, 2003).

The region has significant cultural value and supports several communities whose livelihoods depend on the productivity of the waters. Industries such as tourism and aquaculture have seen major expansion in recent years and therefore coastal monitoring is becoming increasingly important. Active aquaculture sites in the Sound generate questions about water quality. For example, how the water affects fish health (Whyte *et al.*, 2001) and how the farms impact the environment (Winsby, 1996).

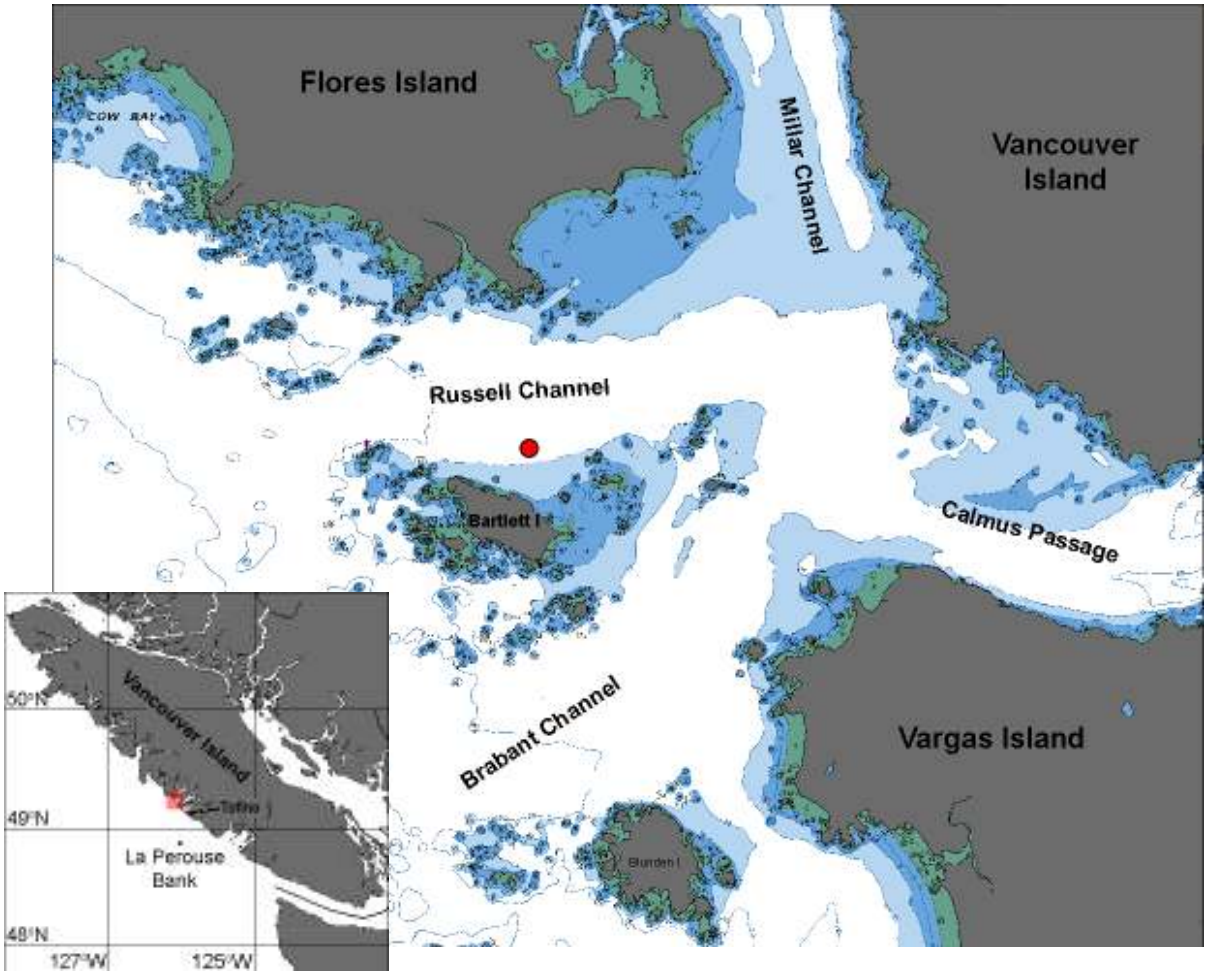

Figure 1-1. Map of the study area in Clayoquot Sound. The red circle is the location of the buoy in Russell Channel.

Research in the Sound has covered such topics as marine mammals, predator-prey relationships, and biological spatio-temporal analyses, e.g. Nelson *et al.* 2008; Kerr &

Duffus, 2005; Mulkins *et al.*, 2002. These research activities have focused on biological interactions and, while taking into account the physical parameters, have missed the fine-scale link between the physical parameters and lower trophic levels. These studies have also identified the fine-scale variability at higher trophic levels in terms of patchiness in lower trophic levels and physical parameters.

1.2.2. Local oceanography

There has been much work done on the oceanography off western Canada including such topics as physical oceanography (Thompson, 1981; Crawford & Thompson, 1991), plankton variability (Mackas & Yelland, 1999; Denman & Dower, 2001), marine mammals (Dunham & Duffus, 2001; Kerr & Duffus, 2005), ocean colour remote sensing (Gower *et al.*, 2007), harmful algal blooms (Taylor & Haigh, 1996; Whyte *et al.*, 2001) and aquaculture (Winsby, 1996; Whyte *et al.*, 2001). Most of this work is concentrated on the continental shelf and further offshore, and at coarse time scales (several times a year) and over large areas.

Large-scale oceanographic features are principally driven by dominant winds that vary with the season. In the winter the prevailing coastal winds are southeast to southwest. In the summer winds are west to northwest with a lower average wind speed. Summer winds create regions of upwelling on the west coast of Vancouver Island (Whitney *et al.*, 2005), which brings cold saline water to the surface (Thompson, 1981). This upwelled water is rich in nutrients providing a foundation for high biological productivity. In winter the change in dominant wind direction creates downwelling. In the summer upwelling along the shelf brings cold saline water to the surface with highest salinities seen in July to September. Whitney *et al.* (2005) describe river discharge, tidal mixing, and estuarine circulation in addition to upwelling as major sources for nutrients that drive productivity (Crawford & Thompson, 1991).

Dominant currents vary with season and proximity to the shore. In winter the flow is northward along the continental shelf and intensified closer to land. In summer the flow on the edge of the continental shelf is southward; however, closer to shore the flow continues to be northward (Freeland, 1997). This coastal northward flow is called the Vancouver Island Coastal Current and is probably driven by buoyancy from freshwater sources. Large-scale tidal currents flood to the north and ebb to the south.

Ocean currents that overlay the tidal currents are more dominant and dictate the direction of flow. These currents include the California Current, the California Undercurrent, the Davidson Current and the Vancouver Island Coastal Current (Thompson, 1981). The tides near the shore are largely semi-diurnal. In Clayoquot Sound tidal heights range from 1 to 4 m (measured by Tideview) and currents range from 0 to 1.2 m/s (measured by the buoy).

1.2.3. Coastal measurements and the issue of scale

The question of scale is a fundamental issue in addressing the spatial and temporal variability of the water properties in the vicinity of moored buoys. Scale is the temporal and spatial dimension of how a problem is approached and can be explained in terms of extent and grain (Wiens, 1989; Lewis, 1996; Folt, 1998). Temporal extent is the duration of the study. Spatial extent is the area of the study. Temporal grain-size or resolution is the frequency of the measurement. Spatial grain-size or resolution is the size of the individual measurements. This is of application to the buoy when combining datasets and interpreting processes from point measurements.

Clayoquot Sound is a complex and dynamic coastal ecosystem. Research in this type of environment requires high resolution (temporal and spatial) measurements as processes operate at short-time scales (hours to years) and over small areas (meters to a few kilometres) (Mackas *et al.*, 1985). Physical processes affect the productivity in coastal waters. Therefore, resolving the physical patterns is a key factor in understanding the biological response. The literature describes a knowledge gap in understanding the scales of variability and processes driving the patterns found in the coastal ocean (Narvaez *et al.*, 2007; Otero & Siegel, 2004; Wieters, 2003; Freeland, 1997). Coastal waters respond to open-ocean forcing, terrestrial inputs and atmospheric exchanges. Studying the coastal zone is further complicated because it is difficult to generalize conditions between coastal locations. Site-specific drivers dominate patterns and processes; what is true at one site may not be applicable at another (Cloern, 1996; Cloern & Jassby, 2008).

The relationship between physical processes and plankton has been studied at very fine scales where turbulence can effect predator-prey interactions and other aspects

of plankton ecology (Dower & Denman, 2001). This type of research is frequently conducted in a laboratory setting. Therefore, it is difficult to extrapolate these relationships to population scales and to the natural environment. There is a known interaction between patchiness in plankton and higher trophic levels (Dunham & Duffus, 2001); however, the physical patterns related to plankton patchiness at fine scales are less well understood. For example, not only does temperature affect the rate of chemical reactions, but salinity and temperature determine the density of water which influences plankton. In addition, nutrients, sunlight, grazing, winds and currents may contribute to plankton heterogeneity. Very little is understood about the scales of variability of phytoplankton biomass in coastal waters, and even less about the processes driving this variation (Wieters *et al.* 2003).

Descriptive studies with high spatial and temporal resolution are necessary for determining the scales operating in the coastal zone. Autonomous moorings are often used for data collection in these waters because measurements must be made at a relatively high temporal frequency to resolve the dynamic range of conditions (Dickey, 1991).

1.3. Questions and hypothesis

I entered this research project with several questions to guide the evaluation of the temporal and spatial variability in Clayoquot Sound using buoy data and water profiles. The objective of this thesis is to answer the questions:

- What are the fine-scale temporal and spatial patterns in the Sound?
- What are the processes that drive these patterns?
- What are the challenges associated with an autonomous mooring?
- What is the representative area of the buoy?

I developed hypotheses and specific objectives based on the literature. I expected there to be a strong tidal signal in the buoy data that shows higher salinity values at high tide and lower salinity values at low tide. Density processes are dominated by salinity in the northwest Pacific (Thompson, 1981). This is true in Clayoquot Sound, which has a significant input of fresh water. When the tide is ebbing there should be more fresh water

in Russell Channel. Water temperature should be closely related to season and solar heating. I expected to see warmer water temperatures coming from offshore in the spring and warmer temperatures coming from inland later in the summer. From past field work in the area the water colour was observed to be highly patchy in space and time. I expected to see this reflected in the buoy chlorophyll fluorescence time series. Patterns in spatial measurements should be related to driving processes such as wind and tides. I anticipated there to be challenges with keeping the instruments on the buoy free from biofouling.

1.4. Literature Cited

Cloern, JE. 1996. Phytoplankton bloom dynamics in coastal ecosystems: A review with some general lessons from sustained investigation of San Francisco Bay, California. Reviews of Geophysics 34, no. 2 (May): 127-168.

Cloern, JE and AD Jassby. 2008. Complex seasonal patterns of primary producers at the land-sea interface. Ecology Letters 11, no. 12 (December): 1294-1303. doi:10.1111/j.1461-0248.2008.01244.x.

Crawford, WR and RE Thomson. 1991. Physical oceanography of the western Canadian continental shelf. Continental Shelf Research 11, no. 8-10 (October): 669-683. doi:10.1016/0278-4343(91)90073-F.

Denman, KL and JF Dower, 2001. Patch dynamics, pp. 2107-2114, In: JH Steele, SA Thorpe and KK Turekian (eds.), Encyclopedia of Ocean Sciences, Academic Press, London.

Dickey, TD. 1991. The Emergence of Concurrent High-Resolution Physical and Bio-Optical Measurements in the Upper Ocean and their Applications. Reviews of Geophysics 29, no. 3 (August): 383-413.

Dunham, JS and DA Duffus. 2002. Diet of gray whales Eschrichtius Robustusin, Clayoquot Sound, British Columbia, Canada. Marine Mammal Science 18, no. 2: 419-437. doi:10.1111/j.1748-7692.2002.tb01046.x.

Environment Canada, 2009. National Climate Data and Information Archive. http://www.climate.weatheroffice.ec.gc.ca. Accessed March 2009.

Freeland, HJ 1992. The physical oceanography of the west coast of Vancouver Island. Pages 10-14 of proceedings of a symposium on "The Ecology, Status and Conservation of Sea and Shoreline Birds on the West Coast of Vancouver Island", eds. K. Vermeer, R.W. Butler and K. H. Morgan. Canadian Wildlife Service Occasional Paper #75, Ottawa, Ont. 1992.

Gower, J, and S King. 2007. Validation of chlorophyll fluorescence derived from MERIS on the west coast of Canada. International Journal of Remote Sensing 28, no. 3: 625–636.

Hickey, B and N Banas. 2003. Oceanography of the U.S. Pacific Northwest Coastal Ocean and estuaries with application to coastal ecology. Estuaries and Coasts 26, no. 4: 1010-1031.

Kerr, KA and DA Duffus. 2005. Timing of larval release in the porcelain crab, Petrolisthes cinctipes (Decapoda, Anomura), in Clayoquot Sound, British Columbia. Crustaceana 78 (October): 1041-1051.

Mackas, DL, KL Denman, and MR Abbott. 1985. Plankton patchiness – biology in the physical vernacular. Bulletin of Marine Science 37, no. 2 (September): 652-674.

Mackas, DL and DR Yelland. 1999. Topical Studies in Oceanography : Horizontal flux of nutrients and plankton across and along the British Columbia continental margin. Deep Sea Research Part II 46, no. 11-12 (November): 2941-2967. doi:10.1016/S0967-0645(99)00089-2.

Mulkins, LM, DE Jelinski, JD Karagatzides, and A Carr. 2002. Carbon isotope composition of mysids at a terrestrial-marine ecotone, Clayoquot Sound, British Columbia, Canada. Estuarine Coastal and Shelf Science 54, no. 4 (April): 669-675. doi:10.1006/ecss.2001.0851.

Narváez, DA, E Poulin, G Leiva, E Hernández, JC Castilla, and SA Navarrete. 2004. Seasonal and spatial variation of nearshore hydrographic conditions in central Chile. Continental Shelf Research 24, no. 2: 279–292.

Nelson, TA., DA Duffus, C Robertson, and LJ Feyrer. 2008. Spatial-temporal patterns in intra-annual gray whale foraging: Characterizing interactions between predators and prey in Clayquot Sound, British Columbia, Canada. Marine Mammal Science 24, no. 2: 356-370. doi:10.1111/j.1748-7692.2008.00190.x.

Otero, MP, and DA Siegel. 2004. Spatial and temporal characteristics of sediment plumes and phytoplankton blooms in the Santa Barbara Channel. Deep-sea Research Part II – Topical Studies in Oceanography 51, no. 10-11: 1129-1149. doi:10.1016/j.dsr2.2004.04.004.

Taylor, FJR and R Haigh. 1996. Spatial and temporal distributions of microplankton during the summers of 1992–1993 in Barkley Sound, British Columbia, with emphasis on harmful species. Canadian Journal of Fisheries and Aquatic Sciences 53, no. 10: 2310–2322.

Thomson, RE. 1981. Oceanography of the British Columbia coast. Gordon Soules Book Pub.

Whitney, FA, WR Crawford, and P Harrison. 2005. Physical processes that enhance nutrient transport and primary productivity in the coastal and open ocean of the subarctic NE Pacific. Deep-sea Research Part II – Topical Studies in Oceanography 52, no. 5-6: 681-706. doi:10.1016/j.dsr2.2004.12.023.

Whyte, JNC, N Haigh, NG Ginther, and LL Keddy. 2001. First record of blooms of Cochlodinium sp.(Gymnodiniales, Dinophyceae) causing mortality to aquacultured salmon on the west coast of Canada. Phycologia 40, no. 3: 298–304.

Wieters, EA, DM Kaplan, SA Navarrete, A Sotomayor, J Largier, KJ Nielsen, and F Veliz. 2003. Alongshore and temporal variability in chlorophyll a concentration in Chilean nearshore waters. Marine Ecology – Progress Series 249: 93-105.

Winsby, M. 1996. Environmental Effects of Salmon Netcage Culture in British Columbia. BC, Ministry of Environment, Lands & Parks, Environmental Protection Dept.

Chapter 2. Temporal and spatial oceanographic conditions measured from a buoy in Clayoquot Sound

2.1. Introduction

The coastal waters of Vancouver Island are a dynamic system and are considered to be of significant ecological and economic value (Whyte *et al.*, 2001). However, little is known about oceanographic variability in near-shore west coast waters (Taylor & Haigh, 1996) or about the processes driving this variation (Wieters *et al.* 2003). Previous work in the Sound identifies the need for high temporal resolution measurements to understand the patterns in oceanographic variability (Kerr, 2005). The deployment of the Clayoquot Sound oceanographic buoy provides the opportunity for a high temporal resolution perspective into this complex system. In this chapter I describe the temporal patterns of the variables measured at the buoy and relate these measurements to measurements near the buoy. These patterns are analysed at different temporal scales and then compared to multi-scale processes. For example, wind driven upwelling is a large-scale driver in terms of oceanographic patterns measured at the buoy and, while local winds measured at the buoy may reflect a component of these large-scale winds, they have a far more localized impact in terms of space and time.

The literature describes a knowledge gap on the topic of links between processes and patterns, particularly in the context of temporal and spatial scale (Dickey, 1991). Denman and Dower (1991) describe a lag time between environmental variables and use the example of plankton variability. A snapshot of the plankton variability at one point in time may have some correlation with another property or process from an earlier time at a different scale. In Dickey *et al.*'s (2006) review on remote sensing in optical oceanography, a relationship is shown between the temporal and spatial scale of oceanographic processes and the instruments used to measure them. Remote sensing is relevant on spatial scales of meters to thousands of kilometres and on temporal scales of minutes to decades. The Dickey *et al.* review suggests moorings are relevant on similar time scales, but only on spatial scales of centimetres to tens of centimetres. In this chapter we show that a buoy can represent a larger spatial area than centimetres or metres, particularly when used with other data sources. The buoy time series is described

in terms of temperature, salinity and chlorophyll fluorescence. Patterns in these parameters are related to and explained by other measurements: on the buoy, tidal models, upwelling indices, and satellite images.

2.2. Methods

2.2.1. Buoy instrumentation

The Clayoquot Sound buoy was developed by Axys Technologies in Sidney, BC, with a payload of oceanographic and atmospheric instruments (Figure 2-1). In the air, at 2m above the water line, the variables measured were wind speed, wind gust, wind direction, air temperature, relative humidity, dew point temperature, pressure, photosynthetically active radiation, and irradiance and radiance in 7 bands, at 412, 443, 560, 620, 665, 682, 705 nm. In the water, an ADCP measured current through a moon pool in the hull of the buoy. The current was measured at about 2m below the surface with a blanking area in the water closest to the instrument to minimize values affected by turbulence. Two chains suspended over the side of the buoy supported conductivity (for salinity), temperature and oxygen sensors, and a biowiping fluorometer at 4m depth. At 3.5m depth a Satlantic hyperspectral sensor measured downwelling irradiance in the same bands as the above water radiometers. The hyperspectral sensor was mounted at an angle looking upward and outward at an angle of 12^{o}. This was to avoid looking at the bottom of the yellow buoy. The underwater package was weighted to maintain a near vertical orientation. Data was collected and managed using the Watchman 500 acquisition system, and relayed in real-time using Iridium telemetry. During the 2007 deployment the instruments made a measurement every 30-minutes from an average of a 2-minute sample period. The average and maximum wind speed was taken from a 10-minute sample period.

2.2.2. Data collection, calibration and analysis

The Clayquot buoy was deployed on March 25, 2007 and broke free from its mooring on October 14 during a severe, early winter storm. A software problem on the buoy resulted in measurements being made hourly (instead of half-hourly) from July 22 to 26.

Every 5 to 10 days from May to September, the instruments on the buoy were cleaned with a cloth or a mild bleach solution (table 4-1). Fouling was a major problem as discussed in chapter 4. However, no correction for fouling was needed for the data used in this chapter.

	Instrument	Property measured
1	RM Young 05103 Anemometer	Wind speed/gust/direction
2	Ro-tronic HygroClip S	Temperature/dewpoint/ humidity/pressure
2	Freescale MPX4115AP barometer	Atmospheric Pressure
3	Licor pyranometer LI – 200SA	Solar radiation
4/5	Satlantic OCR-507 RO3A/ICSA	Irradiance and Radiance in 7 wavelengths with a field of view of 3°
6	Satlantic HyperOCR1	Irradiance in 7 wavelengths with a cosine response
7	YSI 5775 DO sensor (AMS)	Dissolved oxygen
8	Applied Micro Systems T/S	Water temperature, conductivity
9	Wetlabs fluorometer FLNTU	Chlorophyll Fluorescence
10	Nortek Aquadopp ADCP current meter	Current speed and direction, tilt, roll

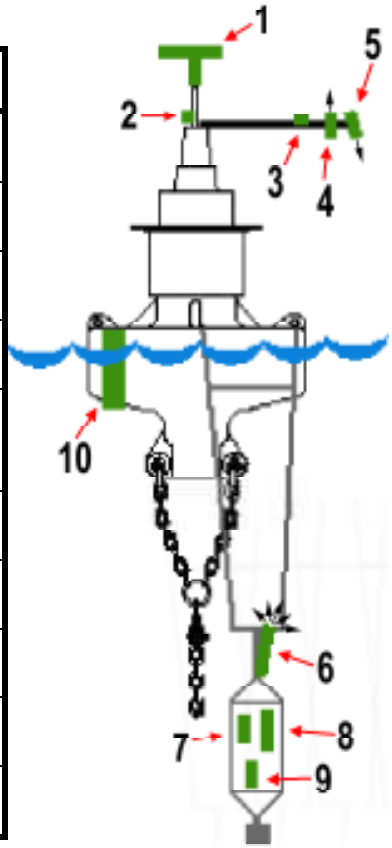

Figure 2 - 1. Instruments and variables measured on the buoy. Numbers in the table correspond to the numbered arrows on the diagram.

The modeled tidal cycle was calculated by tidal prediction software WXTide32 (available at http://www.wxtide32.com) and Tideview (available at http://dive.bc.ca/tideviewdownload.html). The daily upwelling index for 48°N, 125°W was taken from the Pacific Fisheries Environmental Laboratory (PFEL) website (available at http://www.pfeg.noaa.gov/). There is a gap in the current meter dataset (speed, direction, tilt and roll) from May 26 to July 4. The instrument became severely encrusted with barnacles, covering the transducers and preventing the instrument from

working. This is also discussed in chapter 4 with respect to fouling. During this period the Tideview and Wxtide models were used. There is no current data available for Clayoquot Sound other than what was measured on the buoy. Tide height was used as a proxy for current direction and speed.

Water profiles using a Seabird 19plus CTD and additional Wetlabs fluorometer were collected to show the vertical structure of temperature, salinity and chlorophyll fluorescence in the water column. These casts are described in detail in chapter 3. The CTD casts were used to calibrate the temperature, salinity and chlorophyll fluorescence as described below. Table 2-2 describes the relationships of the calibrations.

Buoy time series are presented in this section as plots with lines drawn between measurements. This is for visualization purposes only. There are no data between points. The dates labeling vertical lines on plots are the start of the day or month with which it's labeled. All times are in UTC unless otherwise stated.

2.2.2.1. Temperature and salinity calibration on the buoy

The buoy temperature and salinity were calibrated with a recently calibrated CTD. Calibration measurements were made 22 times throughout the field season. The CTD made a calibration measurement at 4.5m depth (beside the buoy's instruments), or the buoy's instruments were lifted and held at the surface beside the CTD (table 2-2). The temperature and salinity measured by the CTD have a strong linear relationship with the temperature and salinity measured by the buoy (Figure 2-2) with an r^2 value of 0.99 and 0.96 for temperature and salinity respectively. The error for this relationship is $\pm 0.17^{o}C$ for temperature and ±0.18 PSU for salinity.

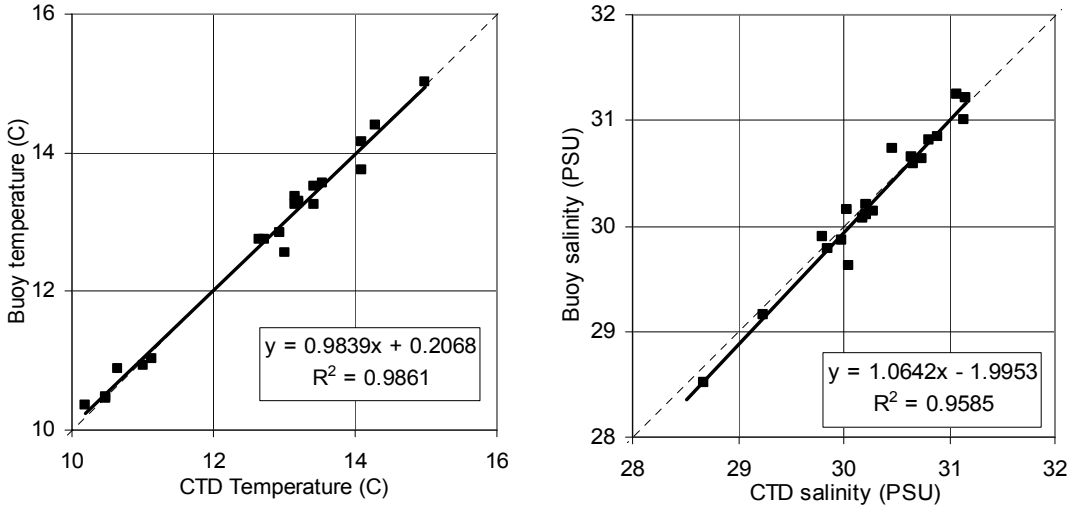

Figure 2 - 2. Comparison of buoy and CTD temperature (right) and salinity (left). The dashed line shows the 1 to 1 line and the solid line shows the linear best fit.

2.2.2.2. Fluorometer calibration on the buoy

Extracted chlorophyll samples were collected to calibrate both the buoy fluorometer and the CTD fluorometer (table 2-2). Factory calibration coefficients can be improved upon in the field because measurements can be dependant on many in-situ variables such as physiology, species, morphology, and light history (Nittis *et al.*, 2001; www.wetlabs.com).

The in-situ chlorophyll samples were filtered with 47mm GF/F filters, frozen and extracted in acetone 1 to 3 weeks later. Chlorophyll measurements were made according to the protocols for the Joint Global Ocean Flux Study (JGOFS) Core Measurements described by Knap *et al.* (1996). Many of the duplicate samples had high variability. Duplicate samples with variability greater than 10% were rejected, however, duplicates were only made on a small number of samples. The filtered chlorophylls were stored in a standard freezer for 1 to 4 weeks and transported on dry ice back to the Institute of Ocean Sciences (IOS) in Sidney, BC, for analysis. High variability in the duplicate samples may be attributed to the length of time before analysis and difficulty in refrigeration during transport. These issues likely resulted in degradation of the chlorophyll before extraction and analysis. Chlorophylls were analyzed in 4 sessions: on

August 4, August 14, September 6 and September 19. The samples from August 14 were not used in these comparisons because they were left out of refrigeration for too long during the transport back to IOS.

The regression equations for all fluorometer calibration fits shown below are forced with a zero y-intercept to avoid negative values in the fluorometer data. This is justified by the buoy and CTD fluorometers having values close to zero (and never negative) in air (zero chlorophyll). Only samples measured at the surface were used in the fluorescence calibration to have more control over the sampling area.

Ideally, the buoy chlorophyll fluorescence would have been calibrated with extracted chlorophyll, but there were only 7 surface samples taken at the buoy and the relationship was poor (Figure 2 - 3). The r^2 value for this relationship is 0.0121. There is no known reason for this poor agreement. However, potential issues may have been related to the inherent patchiness of chlorophyll. Photoinhibition may also have been a factor. Samples were collected in daylight and when the fluorometers were making measurements at the surface the cells' fluorescence may have been inhibited by bright sunlight.

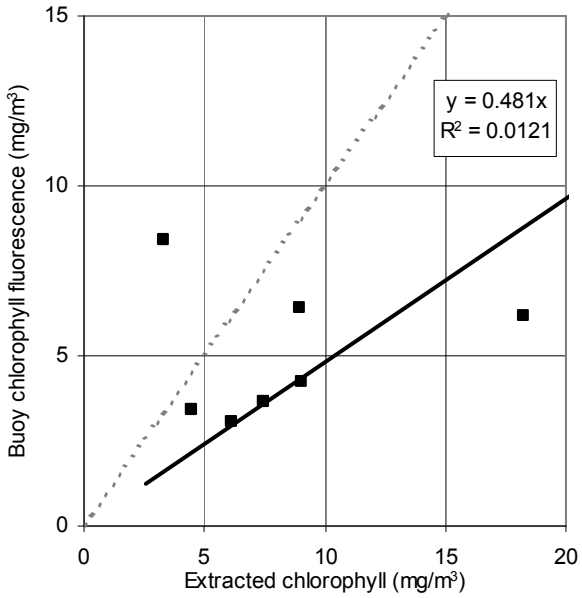

Figure 2 - 3. The relationship of the extracted chlorophyll with the buoy chlorophyll fluorescence measurements made at the surface.

Instead of calibrating the buoy chlorophyll fluorescence directly with the extracted chlorophylls we calibrated the CTD fluorometer with the extracted chlorophyll and calibrated the buoy fluorometer with the CTD fluorometer. There were 27 extracted chlorophyll samples to compare with the CTD fluorometer and a more robust relationship between measurements with an r^2 value of 0.55 (Figure 2 – 4).

The corrected CTD chlorophyll fluorescence was used to correct the buoy fluorometer. The r^2 value for this linear relationship is low (0.33) but can be partly explained by a data point from July 16 where the buoy measured 8.44 mg/m^3 and the CTD measured 3.26 mg/m^3. It is reasonable that the natural patchiness or a small piece of drifting vegetation could cause this difference. When this data point is removed the r^2 value becomes 0.73. The buoy fluorometer was corrected with corrected CTD fluorometer and the equation used with the July 16 point removed. The CTD fluorometer underestimates chlorophyll compared to the extracted chlorophyll and the buoy fluorometer underestimates chlorophyll compared to the CTD fluorometer. The error for this relationship is ±1.4mg/m^3.

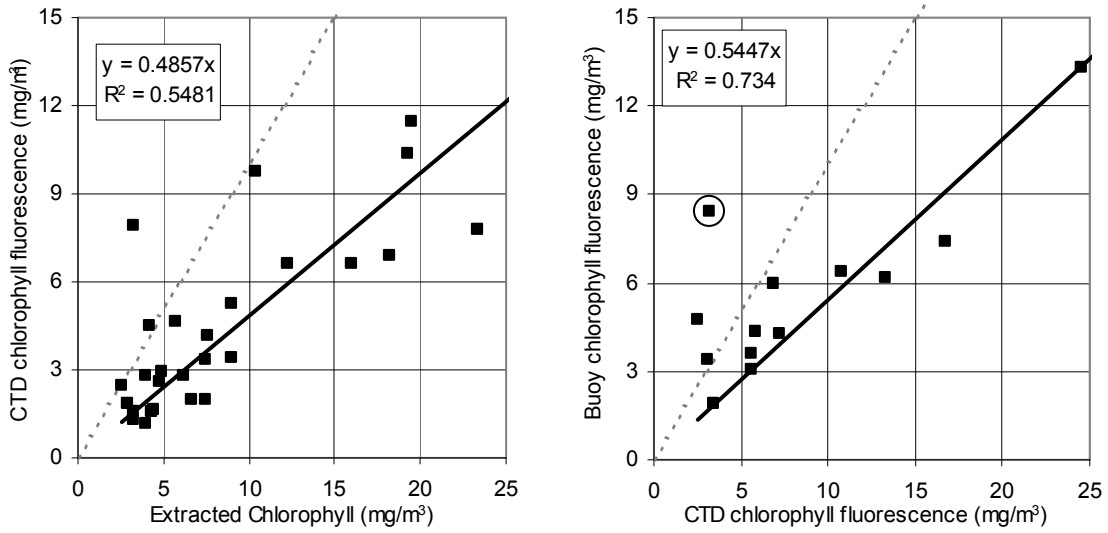

Figure 2 - 4. The relationship of CTD chlorophyll fluorescence and extracted chlorophyll (left) is used to correct the CTD chlorophyll fluorescence. The corrected CTD chlorophyll fluorescence is used to correct the buoy chlorophyll fluorescence (right). The circled point on the right plot was from July 16 and was not used for the best-fit line.

#	Calibration	Linear relationship	R^2
1	Buoy temperature corrected with CTD temperature	y = 0.9839x +0.2068	0.99
2	Buoy salinity corrected with CTD salinity	y = 1.064x – 1.9953	0.96
3	Buoy fluorescence corrected with extracted chlorophyll	y = 0.481x	0.01
4	CTD fluorescence corrected with extracted chlorophyll	y = 0.486x	0.55
5	Buoy fluorometer corrected with corrected CTD fluorometer	y = 0.56x	0.33
6	Buoy fluorometer corrected with corrected CTD fluorometer with suspect point removed	y = 0.54x	0.73

Table 2 - 1. The best fit line equations for correcting the buoy data to the CTD (temperature and salinity) and in situ sample (chlorophyll).

Date	**Time (PDT)**	**Depth of CTD calibration with the buoy**	**Number of extracted chlorophyll samples**	
			With B/CTD	**With CTD**
May 26	11:50:40	4.5		
Jun 3	9:24:47	4.5		
Jun 5	14:00:00	S		
Jun 3	10:04:22	4.5		
Jun 21	10:01:09	S		
Jun 22	7:06:00	4.5		
Jul 4	16:10:59	4.5		
Jul 7	11:57:44	S	1	
Jul 14	16:04:39	4.5		
Jul 16	8:59:42	S	1	
Jul 25	6:58:03	S		3
Jul 29	13:28:13	S	1	2
Aug 07	16:30:00	S	1	
Aug 09	9:29:53	4.5	1	4
Aug 12	10:00:25	S		
Aug 12	15:59:47	S	1	3
Aug 21	9:30:59	S	1	3
Aug 25	8:59:52	S	1	2
Aug 30	8:00:19	S		3
Sep 03	15:30:37	S	1	3
Sep 12	15:00:33	S	1	3
Sep 13	15:31:05	4.5	1	3

Table 2 - 2. Calibration of temperature, salinity, chlorophyll fluorescence on the buoy with CTD. S is for surface. Extracted chlorophyll samples were taken starting in July. 'With B/CTD' means that the sample was taken at the buoy at the same time as the calibration case. "With CTD' means that the extracted chlorophyll was taken at the same time as a CTD cast at another station. Grey fill means that were problems with the extraction methods and data are not used for calibration.

2.2.2.3. Satellite imagery

Satellite imagery from the European Space Agency's sensor MERIS was used to look at spatial patterns of chlorophyll fluorescence in Clayoquot Sound. The sensor is an imaging spectrometer aboard the satellite ENVISAT and has a spatial resolution of 300m at full resolution and 1200m at reduced resolution. This high spatial resolution is required for narrow waters such as Russell Channel and is not available on any other ocean colour sensor. The satellite gives global coverage every 3 days and, given the 1100km swath width, the temporal coverage is 2 of 3 days. The spectral resolution is 15 bands ranging from 412 to 900nm. Three bands at 664, 685 and 709nm are optimally positioned to measure the chlorophyll fluorescence peak at 685nm using the algorithm, the Fluorescence Line Height (FLH) (Gower *et al.*, 2007). This equation measures the height of the fluorescence peak above a linear baseline between 664nm and 709nn. It is particularly useful in coastal waters as it uses level 1 radiance data rather than the level 2 atmospherically corrected reflectance data. The FLH imagery shown is in radiance units, $W*sr^{-1}*m^{-2}*u^{-1}$, and images are enhanced on the same scale. For Figure 2-15 a wide baseline using bands at 664, 681 and 753nm was used for the calculation to avoid negative FLH values due to red-tide conditions. For the purpose of this paper imagery is used qualitatively; however, FLH is related to chlorophyll using the colour legend shown in Figure 2-14. The land and cloud are masked to black, and all images are projected with the same parameters.

2.3. Results

2.3.1. Variability at different timescales

Oceanographic conditions in mid-March to mid-October 2007 in Russell Channel are summarized in this chapter using buoy time series for temperature, salinity and chlorophyll fluorescence. Scale plays a key role in understanding the relationship between processes and patterns in the water property time series. Wind and current measured at the buoy are described to place the oceanographic conditions in context of driving processes. The oceanographic conditions were analysed at two temporal scales: seasonal and daily.

2.3.1.1. Seasonal currents and wind

The Clayoquot buoy was in a location exposed to periods of strong current and high wind. These play a strong role in the variability of the water properties measured by the buoy. The strongest tidal currents are in an eastward direction (80^o) on the flood and in a west-southwest direction (230^o) on the ebb (Figure 2-5a). The current meter shows current speeds up to 1.3m/s with all values above 1m/s measured on an ebb tide. The current speed predicted by Tideview for Russell Channel is generally lower with maximum currents up to 0.7m/s. The timing and direction of the current measured by the current meter is well matched by the model. The discrepancy between the current speed may be related to additional wind stress and also a scaling problem where the spatial resolution of the Tideview model is not sufficient to resolve tides in the narrow channel. When current data on the buoy wasn't available the tide height from WXtide was used. The change in tide height indicates a change in direction of current. In addition larger tidal height ranges tend to correspond with larger currents.

Strongest winds come primarily from the east-southeast (100^o) and west (265^o) (Figure 2-5b). These speeds and directions are consistent with Environment Canada weather buoy, ODAS 46206, on La Perouse Bank (48.834^o N, 126.000^o W), which have more range in direction, but similar wind speeds. The difference in direction is likely due to the local topography of land surrounding the buoy. The wind is frequently calm in early morning and increases in the afternoon.

In shallow, coastal areas Ekman transport doesn't apply (Stewart, 2008) and the current due to wind is parallel to the direction of the wind. Wind can create drift from 1% to 3.5% of the wind speed (Stewart, 2008; Wu, 1983). The highest current velocities occur mostly at moderate wind speeds of 2 to 5m/s. However, for all current values above 1m/s the tide is ebbing and the wind is mostly from the north to east (Figure 2-5c). This may suggest a correlation between the alignment of the wind and current at high current speeds. An example of the effect of wind on current is shown in the August example below. Note that wind is measured in the direction it is coming from and current is measured in the direction it is going.

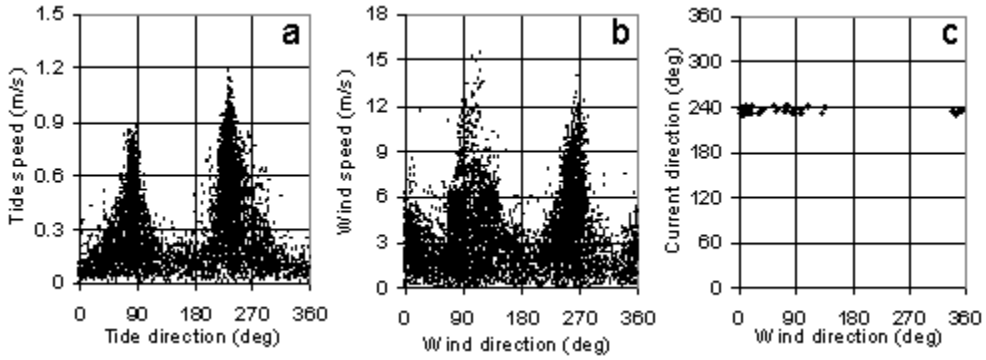

Figure 2 - 5. Wind and tide data from the Clayoquot Buoy for mid-March to mid-October 2007 show (a) the highest tidal currents go to 235^{o} (the ebb) and 80^{o} (the flood), (b) the highest wind speeds come from the west to southwest (230-280^{o}), east to southeast (80-140^{o}) and to lesser extent the north (350-30^{o}). Plot (c) shows the current direction for all currents above 1m/s. These are all on an ebb tide and when the wind is from the north to east. Note that wind is measured in the direction it's coming from and current is measured in the direction it's going.

2.3.1.2. Seasonal temperature and salinity

The temperature time series (Figure 2-6a) shows a gradual increase in water temperature into August followed by cooling in late August into October. The daily temperature range is highest during late May and lowest in March and April. This range can be 2^{o}C in a 24hour period. On average the daily temperature range is 1^{o}C. The salinity time series (Figure 2-6a) shows an increase in salinity from April to June, no trend from June to mid-September and decreasing salinity after mid-September. This is likely related to seasonal trends in precipitation and snowmelt. Salinity has more daily variation in the spring and early summer compared with late summer, which can be explained by decreased fresh water input through the time period. For salinity, the daily range is highest in the spring and fall with changes of over 4.5 PSU/day. On average the daily salinity range is 1.8 PSU.

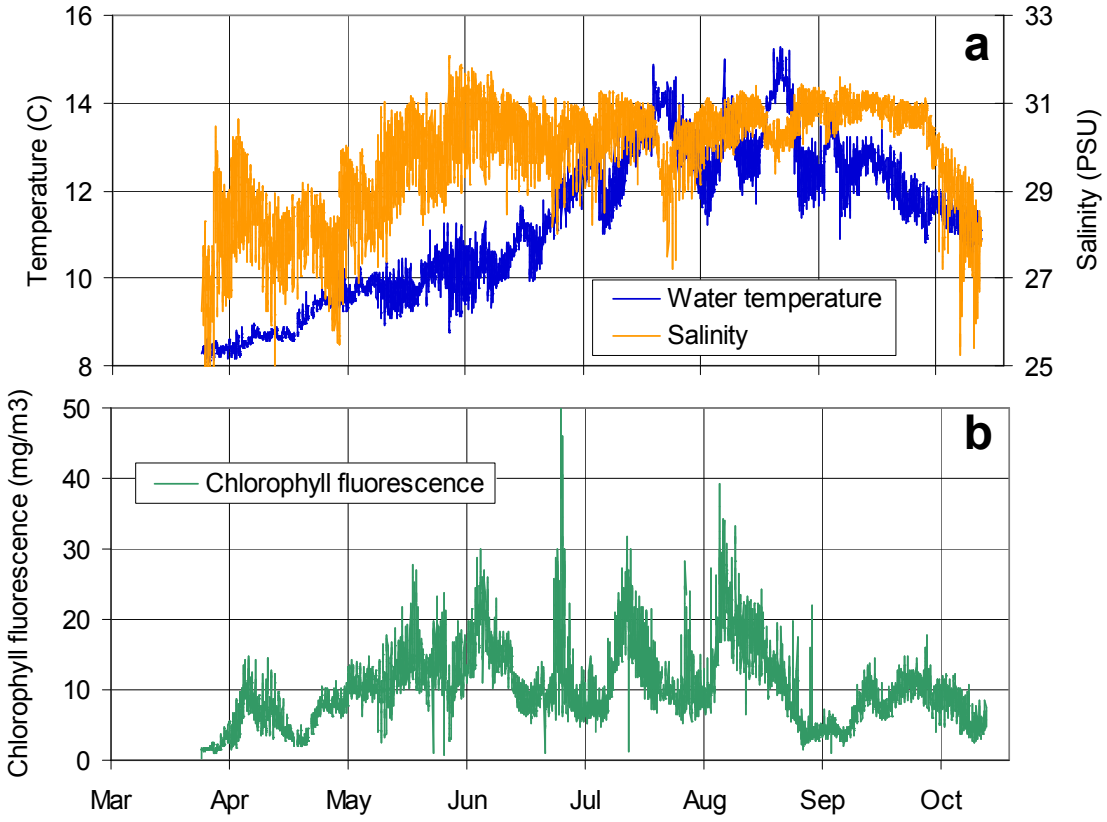

Figure 2 - 6. Half hourly measurements of temperature and salinity (a) and chlorophyll fluorescence (b) measured on the buoy in 2007. The month label indicates the start of each month.

On a seasonal timescale the temperature and salinity are positively correlated where temperature and salinity increase during the spring and summer and decrease in the fall. Over shorter timescales (hours to days) the temperature and salinity are frequently inversely correlated and related to a semi-diurnal tidal signal.

2.3.1.3. Seasonal chlorophyll fluorescence

The buoy chlorophyll fluorescence time series (Figure 2-6b) shows episodic blooms throughout the summer with concentrations seldom decreasing below 5mg/m^3. Low concentrations after deployment and near the end of the time series (late August) suggest that sensor drift was not a problem. This is discussed further in chapter 4. In late June there is a short-lived event where chlorophyll levels increase above 50mg/m^3.

Other events (mid-July and early August) are longer in duration, but have more moderate chlorophyll concentrations with a maximum around 25mg/m^3.

2.3.1.4. Tides and large area winds related to oceanographic variability

The daily range for temperature, salinity and chlorophyll fluorescence is correlated with the tidal cycle (Figure 2-7), but most strongly in salinity. At low tide the salinity is always lower than at high tide at the buoy, which suggests that the salinity is always lower inland compared to offshore. The temperature difference at high and low tide is more variable (Figure 2-7a). For late March and April there is little change in temperature with tide height. During May to early June and mid-September to mid-October the warmer water is associated with a low tide, indicating an inland source. In the summer months, June to August, the relationship changes with a frequency of about 1 to 2 weeks. While both the high and low tide temperature time series follow the same pattern (Figure 2-7a), the high tide temperatures have more extreme values.

The chlorophyll difference also shows a difference between high tide and low tide (Figure 2-7c), although not with any notable relationship to either temperature or salinity. Early in the time series is the only period when high chlorophyll is associated with low tides for a significant period of time. For the rest of the series the blooms either have an offshore origin, indicated by high chlorophyll at high tide, or show little difference between the high and low tides (mid to late April, mid-June, September and October).

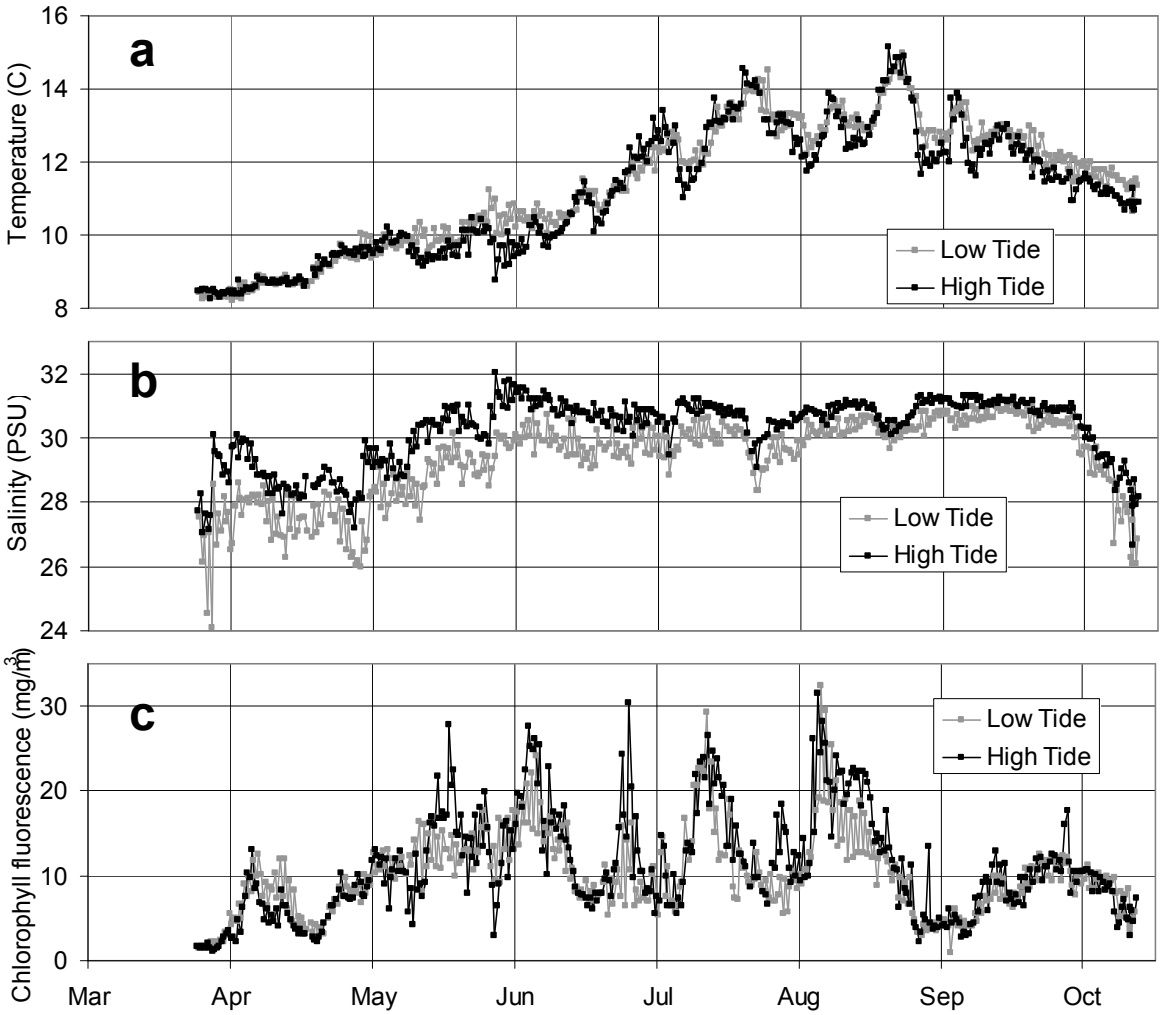

Figure 2 - 7. Temperature (a), salinity (b) and chlorophyll fluorescence (c) at high and low tide measured at the buoy in 2007. The month label indicates the start of each month.

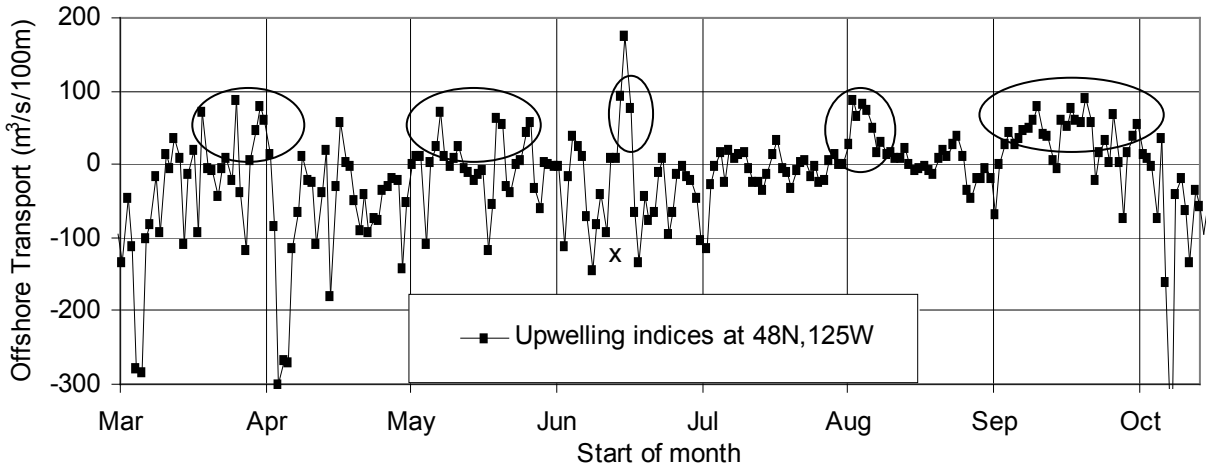

Figure 2 - 8. The PFEL upwelling index for 48°N, 125°W. Ovals mark periods of upwelling.

When compared to the upwelling index (Figure 2-8) the temperature time series appears to have temperature decreases related to periods of upwelling. For example, the upwelling in early May corresponds to a temperature decrease, especially at high tide, around May 9. Other similar examples are in mid-June and early August. A relationship between salinity and upwelling is difficult to see. Peaks in chlorophyll fluorescence at the buoy appear to follow periods of upwelling (circled peaks on figure 2-8). However, there is no obvious relationship between the difference between high and low tide and upwelling for chlorophyll.

In late August, a period of high temperatures, low salinities and decreasing chlorophyll concentrations, as well as a small range between high and low tide for all three variables, corresponds with a period of no transport in the upwelling indices. The tidal range for this period is also low. A similar combination occurs in late July with low tidal range and no transport.

2.3.1.5. Variability at short time scales

2.3.1.5.1. August 1 to 7, 2007: Water masses and the combined effect of tide and wind

Figure 2-9a shows an example of an inverse relationship between temperature and salinity in early August that is typical at time scales on the order of hours to days. The relationship varies with the current speed and direction (Figure 2-9b). The current speed and direction agrees with the tidal model where high and low tidal heights correspond low current and a change in direction (Figure 2-9e). When the current is moving in a westward direction (an ebb tide) the water becomes warmer and less saline. When the current is moving in an eastward direction (flood tide) the water mass becomes cooler and more saline. A wind from the west increases each day from local noon to mid-afternoon, and decreases during the night. This pattern in wind speed and direction is a result of solar heating over land creating an onshore wind during the local afternoon.

The Tideview output validated by showing the wind effect on three different tidal conditions on August 1 and 2 (Figure 2-10). During a flood tide on August 1 at 20:00 UTC (Figure 2-10a) with no wind the current direction is in an eastward direction. By adding in the wind speed and direction (Figure 2-10b), which was 6m/s wind from the

SSW, the model predicts that the wind will increase the current from 0.4m/s to 0.6m/s. At high tide, three hours later (Figures 2-10c and d), the current is slack and the wind is 9m/s from the WSW. This increases the current speed from the near slack to 0.2m/s in the direction the wind is going. On the ebb tide on August 2 at 2:00 UTC a 8m/s wind from the west decreases the current from 0.3m/s to 0.2m/s. The direction changes from WSW to SSW. On August 2 at 20:00 UTC there is a large flood tide with a current measured at 0.8m/s. This corresponds with an 8m/s wind from the west (Figure 2-9). Another large flood on August 3 at 21:00 UTC with currents of 0.6m/s corresponds with a 3-4m/s wind from the SW. This drop in current speed between the two flood tides is likely due to the decrease in wind speed.

The strong westerly wind in the afternoon appears to orient the flood in an eastward direction with little variation. This strong afternoon wind is coordinated with a strong flood, however, the strength of both the flood and the ebb are increased. As the wind speed decreases and the direction becomes more variable, both the flood and the ebb's direction has a greater range and currents decrease. After August 4, when wind speeds decrease, the temperature and salinity ranges also decrease.

From August 1 to 4 the chlorophyll varies between 8 and 12mg/m^3, but does not show a strong tidal signature as with temperature and salinity. Starting on August 5 there is an increase in chlorophyll near the end of the large ebb. The bloom peaks on August 6 at concentrations close to 40mg/m^3. It persists at concentrations higher than 10mg/m^3 until the end of August. Starting on August 5 the bloom also shows a strong tidal signature. The highest chlorophyll concentrations occur at the same time as the highest high tides. This indicates the bloom comes from an offshore source. Isolated peaks in the time series, such as on August 3 at 15:40 UTC, are likely plant matter drifting in front of the fluorometer.

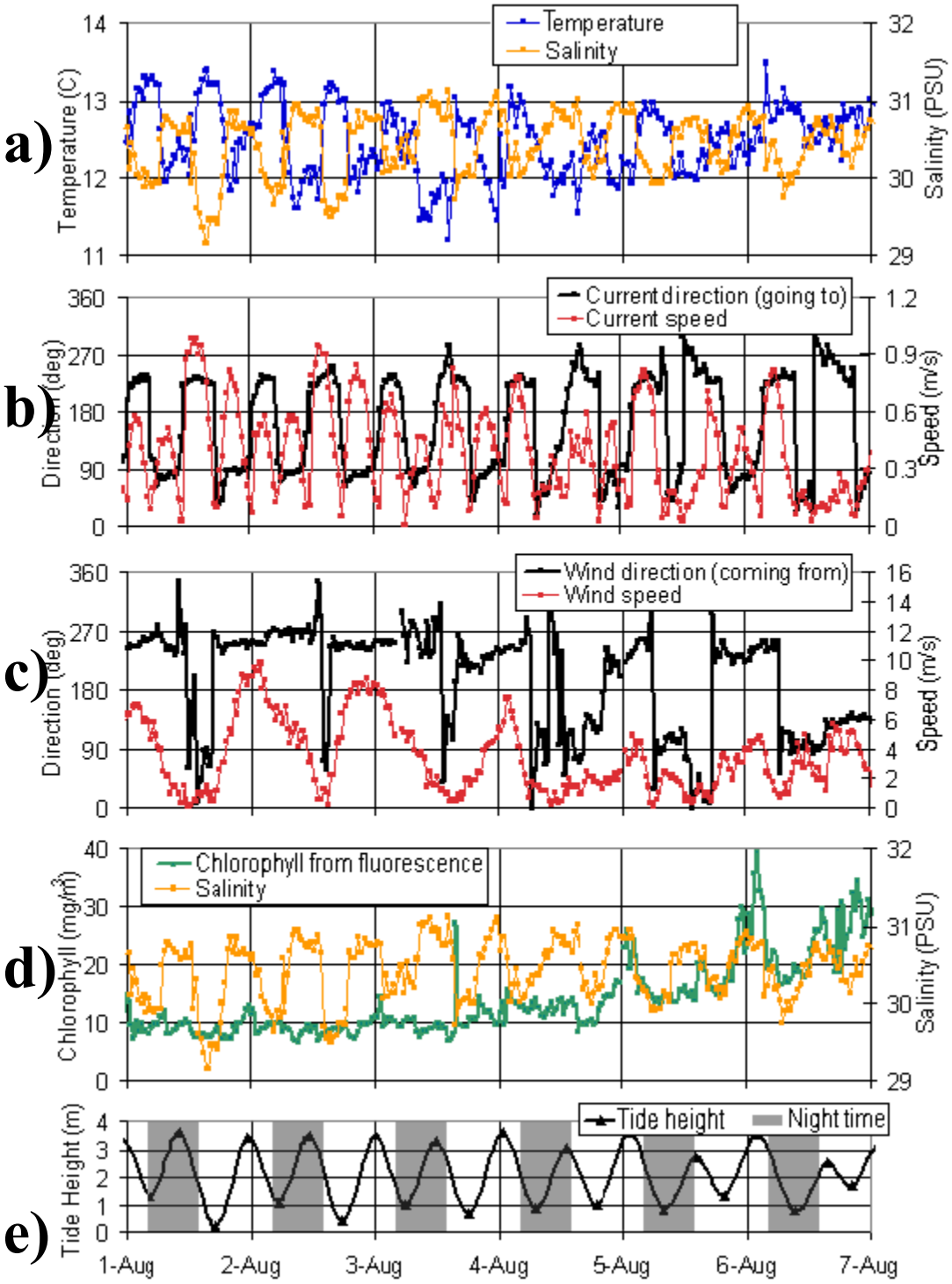

Figure 2 - 9. Fine temporal scale plots for a) water temperature and salinity, b) current direction and speed, c) wind direction and speed, e) chlorophyll fluorescence, and e) the modeled tide height for on August 1 to 7 2007 (UTC). The date label indicates the start of day.

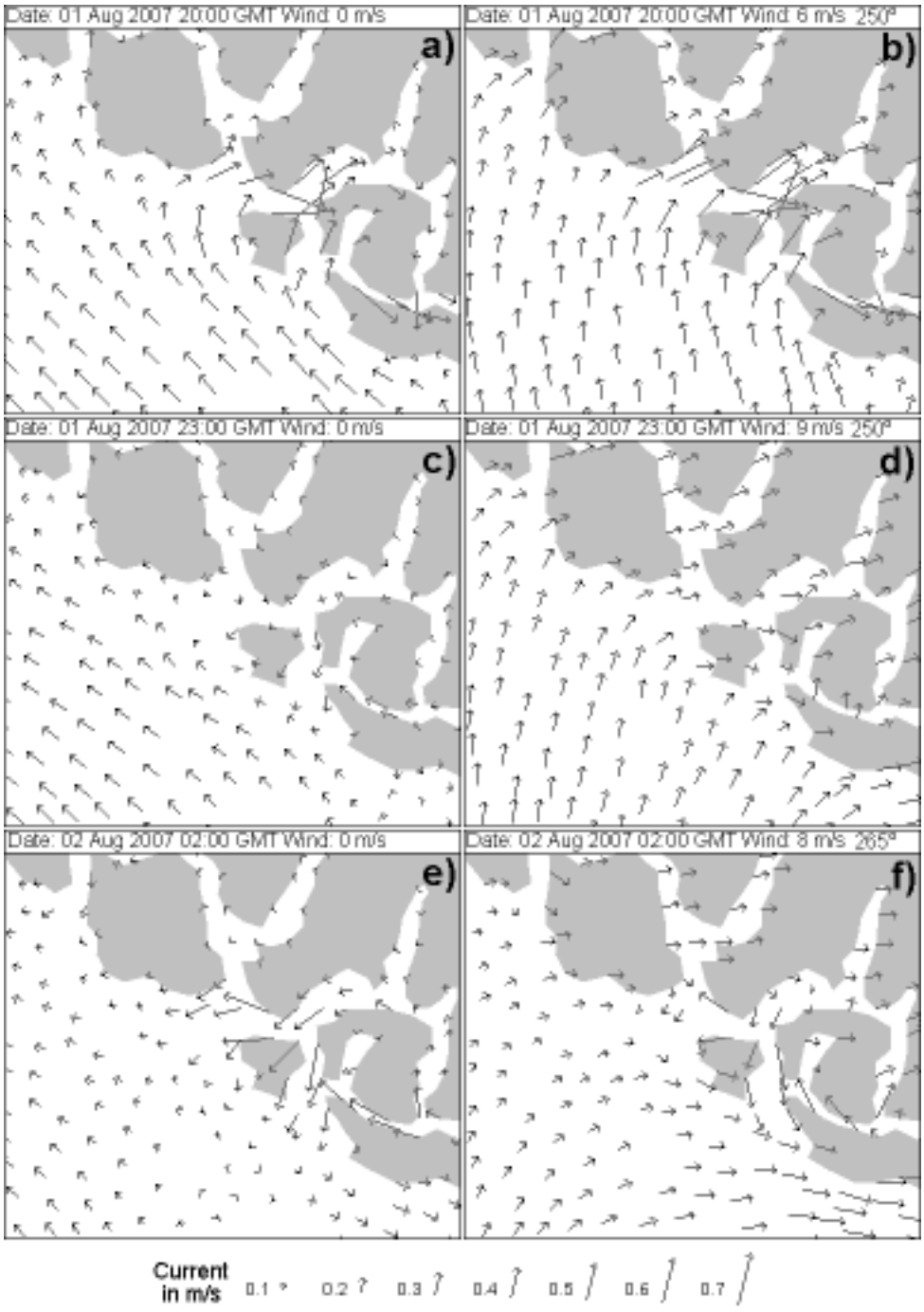

Figure 2 - 10. The Tideview current prediction for different tide and wind conditions on August 1 and 2, 2007. The left column are the predicted currents under no-wind conditions for a a) flood tide, c) slack high tide, and e) ebb tide. The right column are for the same time and same tidal conditions under b) 6m/s wind from the WSW, d) 9m/s from the WSW, and f) 8m/s from the W.

2.3.1.5.2. May 7 to 13, 2007 – Change in wind pattern reflected in water properties

Prior to May 9 low salinity water is correlated with low temperatures at low tide and high salinity and high temperatures at high tide (figure 2-11). This indicates that warm saline water is from an offshore source and cold fresh water is from an inland source. There is little temperature range (less than 0.5^{o}C) and the salinity range is about 1PSU. Chlorophyll concentrations are between 10 and 15mg/m^{3} with slightly lower concentrations on the high tide and the following large ebb.

Starting on May 9 there is a shift in the relationship between the water variables that can be related to wind. High salinities, low temperatures and low chlorophyll are correlated with high tides. Low salinities, high temperatures and high chlorophyll are correlated with low tides. The daily salinity range is over 3 PSU and the temperature range is 1.5^{o}C. The chlorophyll peak at low tide increases in concentration from May 9 to May 14 with a range of 15mg/m^{3}. A shift in water properties coincides with a strong change in wind speed and direction on May 8 (Figure 2-11c). Wind speeds change from low velocity winds from the south and southeast to strong (>10m/s) afternoon (local time) winds from the west.

The tides at the start of this period are mixed, with a large difference between the two lows in each tidal day. The tides become more semi-diurnal by May 13. When the tidal model in figure 2-11e is compared to the current data in figure 2-11b there is a change in the pattern on May 8 that can also be related to wind. Before midday on May 8 both the large flood and small flood can be associated with the current flowing approximately eastward, but ranging from northeast to southeast. Starting late on May 8 this direction becomes directly eastward on the large flood. This is likely due to the large flood corresponding with high winds from the west, which increases the current from 0.4m/s to 0.7m/s after the wind increases from the west. This is consistent with an increase in current that is 2.5% of the wind, which is within the range suggested by some authors (Stewart, 2008; Wu, 1983). On the small flood the current velocity is low (<0.2m/s), and is oriented in an eastward direction prior to May 9, during low wind speeds. After May 9 the small flood is slightly slower and in a northwest direction. The change in the small flood corresponding with increased winds seems to have a strong effect on the water properties.

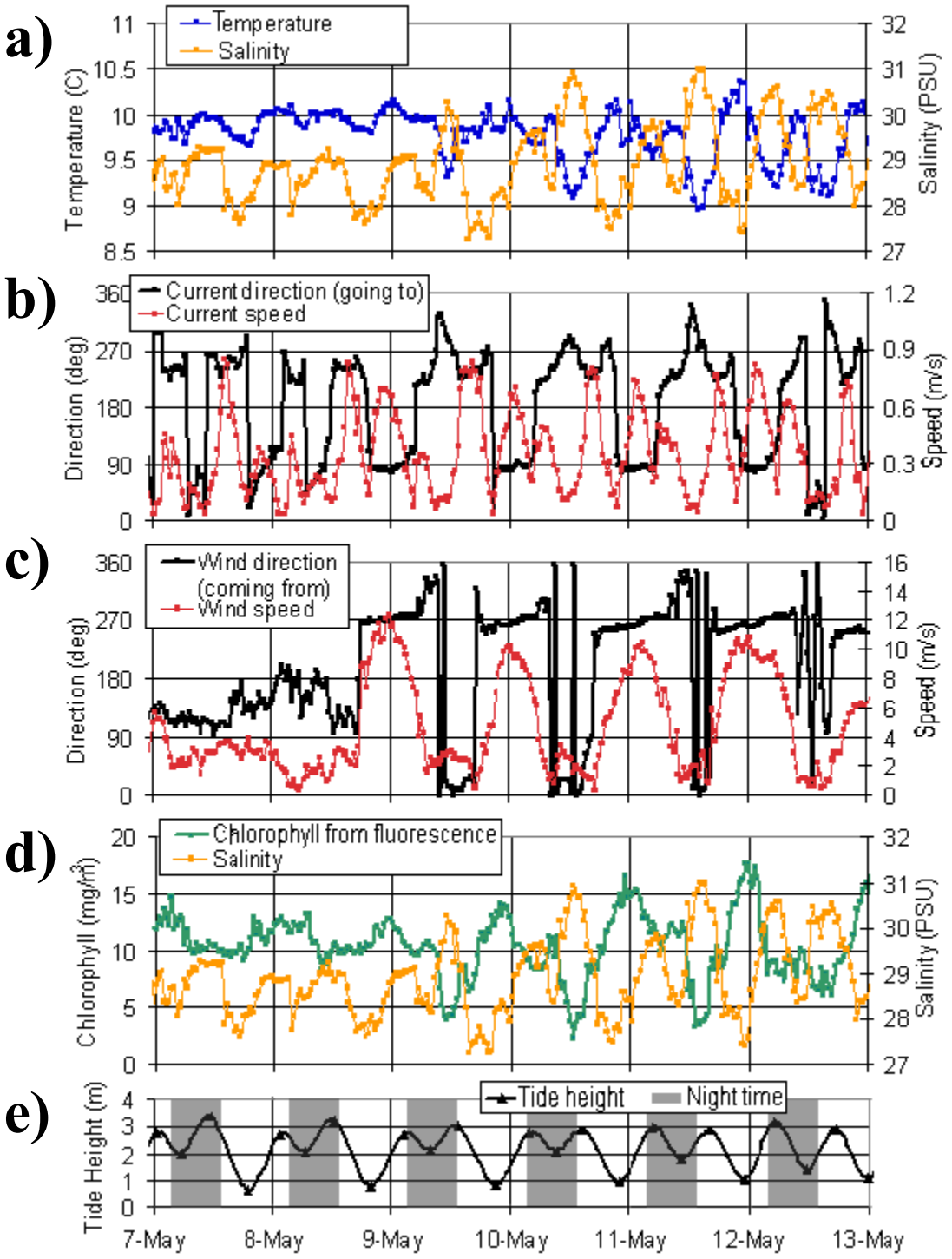

Figure 2 - 11. Fine temporal scale plots for a) water temperature and salinity, b) current direction and speed, c) wind direction and speed, d) chlorophyll fluorescence and salinity, and d) the modeled tide height for May 7 to 13 2007 (UTC). The date label indicates the start of day.

The highest salinity, lowest temperatures, and lowest chlorophylls occur after the small flood. The direction of the small flood suggests that the water comes from the small islets to southeast, which may have contributed to mixing and localized upwelling of deeper offshore water entering Brabant Channel. CTD casts conducted through the summer in the region confirm that the deep water in Brabant channel is usually more dense (colder and saltier) than in Russell Channel.

The major change in water properties is at high tide where the values of temperature and salinity don't change significantly at low tide over the 6 day time series. This suggests a change in the offshore water or the direction from which the water generally comes. This shift in wind at the buoy also coincides with winds measured at the La Perouse Bank buoy (Figure 2-12), which are from the south before midday on May 8 and from the northwest after midday on May 8. The change in direction is a switch from downwelling favourable winds to upwelling favourable winds.

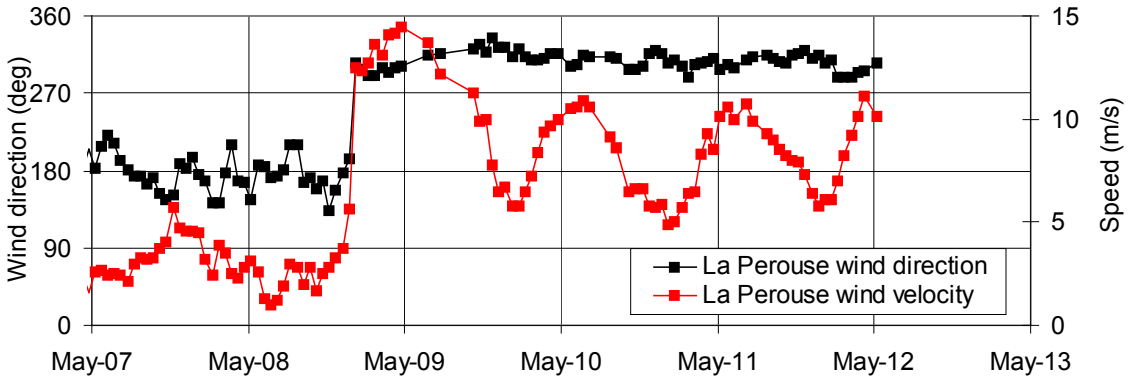

Figure 2 - 12. La Perouse buoy, (ODAS 46206) wind speed and direction for May 7 to 12. The buoy stopped transmitting on May 12 2007. The label indicates the start of each day.

2.3.1.5.3. June 23 to 30, 2007 – Very strong chlorophyll bloom

A bloom in late June shows a strong tidal signal and also reaches the highest concentrations of chlorophyll seen in the 2007 time series. The relationship between temperature and salinity (Figure 2-13a) is not inversely correlated as seen in the previous examples. There is no current data from the current meter for this period, although the tidal prediction software shows mixed tides increasing in height toward the end of the period. The wind was below 8m/s and mostly from the north or east during the night

(Figure 2-13b). During the day it was variable. The chlorophyll begins to show a tidal signal on June 24 when concentrations increase above 20mg/m^3 on the high tide and return to below 10mg/m^3 on the low tide. This peak gets higher on the high tide through to June 26. Without the actual current data it is difficult to know more specifically where the high chlorophyll water originates.

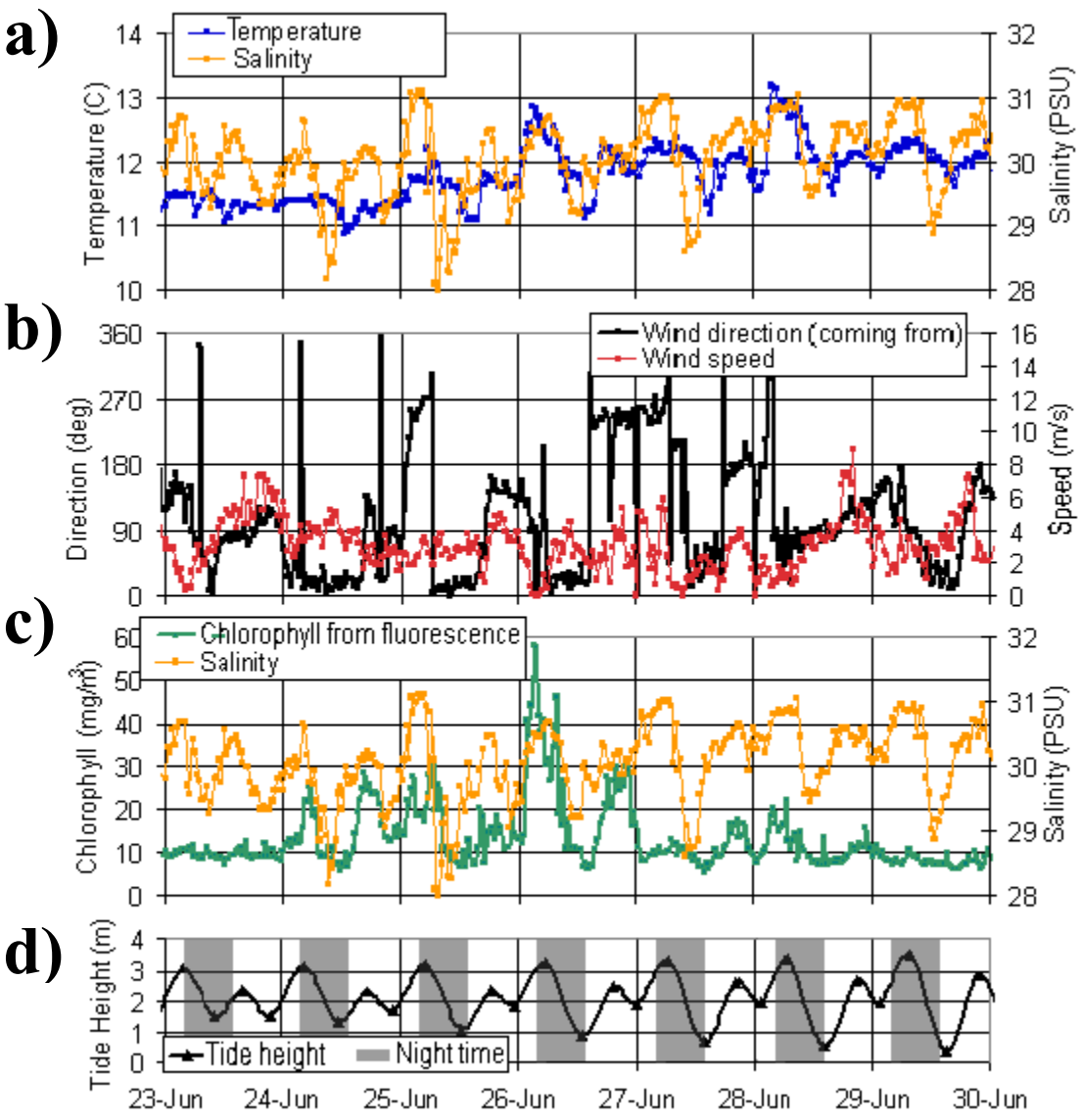

Figure 2 - 13. Fine temporal scale plots for a) water temperature and salinity, b) wind direction and speed, c) chlorophyll fluorescence and salinity, and d) the modeled tide height for June 23 to 30 2007 (UTC). No current data was available from the buoy at this time. The label indicates the start of each day.

2.3.2. Satellite imagery

The spatial conditions can also be evaluated in terms of satellite imagery. The MERIS sensor has 300m spatial resolution which is appropriate for assessing the spatial component of the buoy's time series. For example, an average current velocity of 0.5m/s represents about 900m of space between two measurements on the buoy. This is the same as about three MERIS pixels at the spatial resolution of 300m. MERIS has an orbital pattern which gives repeat coverage every 2 of 3 days. There are 113 possible images that cover Clayoquot Sound for the period March 25 to October 15. However, this number is limited by cloud and high-resolution data availability, and is narrowed down to 22. The most common spatial feature of the 22 images is higher chlorophyll offshore than onshore.

Figure 2-14 shows four examples of the spatial patterns of chlorophyll fluorescence using MERIS FLH. These images are compared to tide height and the temporal patterns of buoy chlorophyll fluorescence. There are cloud free MERIS images for the three time periods described in the previous section. However, for the bloom in late June only reduced resolution (1000m) imagery was available (Figure 2-15). The 1000m resolution data, which is the common resolution of ocean colour satellite sensors, is not sufficient to give data in Clayoquot Sound.

The MERIS pass for April 2 at 19:14 UTC shows a bloom in Millar Channel (Figure 2-14a). The chlorophyll time series for this period also shows higher chlorophyll around low tide. Using current direction and velocity to show the possible extent of 'space' measured by the buoy, the surface bloom in Millar Channel is too far away to be the same high chlorophyll measured by the buoy. At the time of the pass, the higher signal water is about 5000m away from the buoy. The water moves 2500m on the flood and 3000m on the ebb based on current velocities of 0.25 and 0.35m/s on the flood and ebb, respectively, measured at the buoy . The path of the water from the buoy is assumed to be toward Millar Channel on the flood and reversed on the ebb. However, there are many unknown variables such as the direction and velocity of the current away from the buoy. Another source of error may be related to depth of the bloom and stratification, where MERIS only measures the surface layer and the buoy is measuring at 4m.

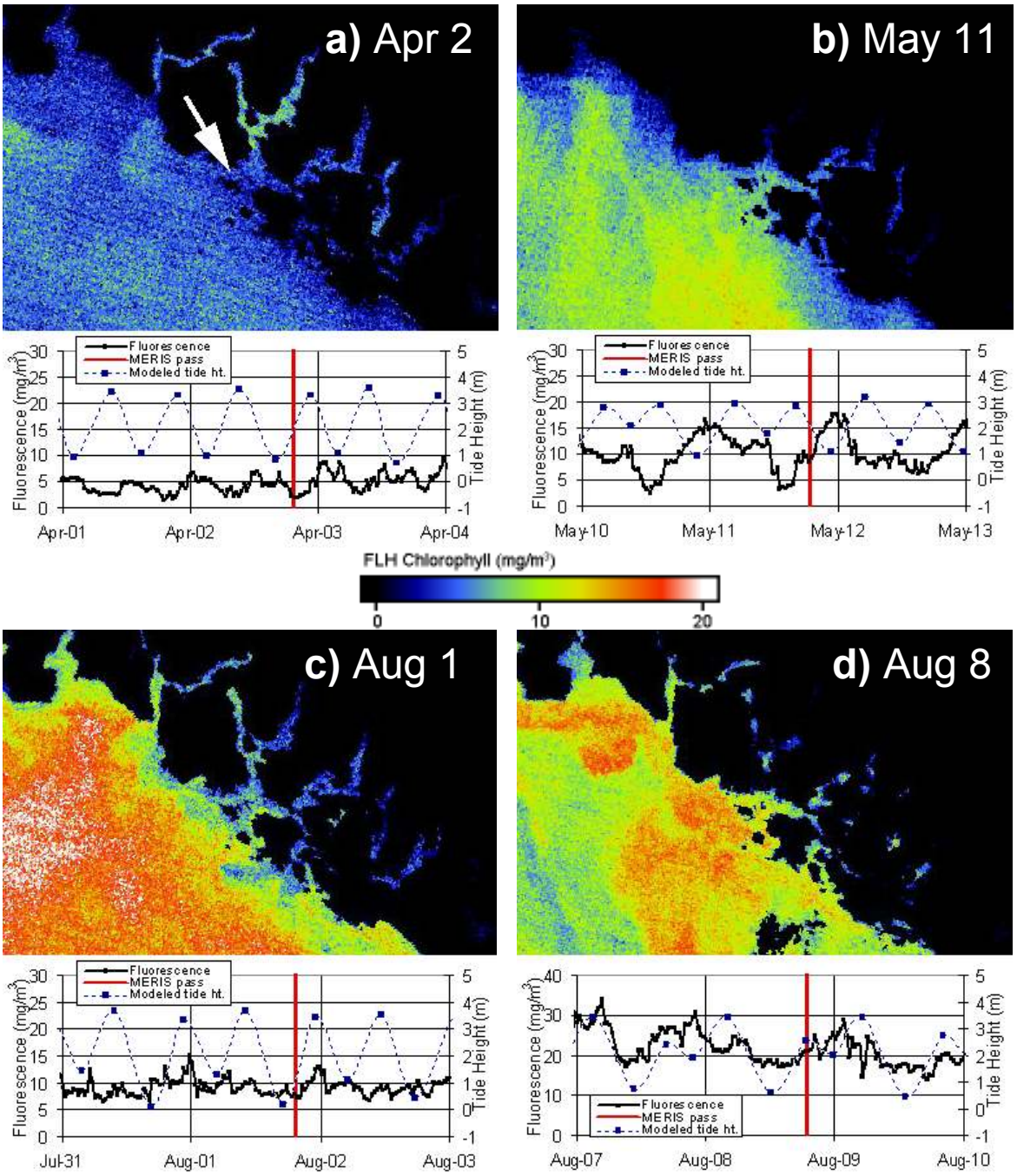

Figure 2 - 14. The MERIS 300m spatial resolution FLH images for a) April 2, b) May 12, c) Aug 1, and d) Aug 8. The colour legend relates FLH to chlorophyll concentrations. The buoy chlorophyll fluorescence and modeled tide height are shown for the period before and after each satellite pass. The white arrow in a) points to the location of the buoy. The red line on each plot is the time of the satellite pass. The labels on the plots indicate the start of the day (UTC).

The MERIS image for May 11 at 18:58 UTC, during an ebb tide shows higher chlorophyll in Brabant Channel and offshore than in Russell Channel (Figure 2-14b). The pass corresponds with the period after the wind shift on May 8, which was related to a strong change in temperature, salinity and chlorophyll with the tide. After low tide and during the flood, chlorophyll fluorescence peaks at the buoy after the current has been moving in a west-southwest direction to a east direction. It is difficult to use the satellite imagery to explain this pattern in the buoy data.

Figures 2-14c and 2-14d show the chlorophyll fluorescence from MERIS on August 1 at 19:11 and August 8 at 18:51, respectively. The MERIS pass close to low tide on August 1 shows lower concentrations onshore than offshore. The buoy data show a small tidal signal in the chlorophyll fluorescence. Slightly higher chlorophyll concentrations are seen after the large flood on August 1 and August 2. The MERIS image for August 8 shows the higher chlorophyll concentrations persisting offshore as well as moved closer to shore. The image is taken at a high tide and the buoy data show a small tidal signal where higher chlorophyll water is associated with a high tide. During this period the satellite images confirm that an offshore bloom moves onshore. The orientation of the wind and tide as discussed in the previous section are likely the driving process for the onshore movement of the high chlorophyll waters. The August 8 MERIS image was at high tide and the August 1 image at low tide which may also contribute to the difference in spatial patterns between the two images.

The 1000m resolution MERIS image from June 25 at 18:32 (Figure 2-15) demonstrates the value of the higher resolution (300m) data. The inland waters cannot be resolved at the lower spatial resolution. There is no high-resolution image available on this date. The scene is at the edge of the pass, which cuts off the image in the west and stretches pixels near the edge. However, the image demonstrates the extremely high chlorophyll seen offshore that coincides with the strong bloom seen at high tide on June 25 and 26 buoy chlorophyll fluorescence data.

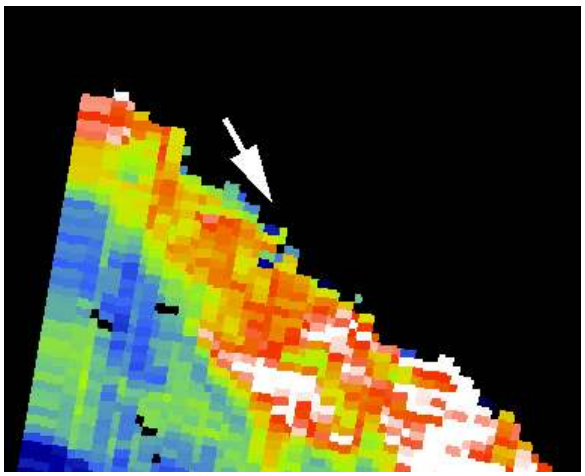

Figure 2 - 15. The 1000m spatial resolution MERIS FLH image for June 25. The area is the same as images in figure 2-14. The white arrow points to the location of the buoy.

2.4. Discussion and conclusions

The temperature time series has the highest range at high tides compared to low tides indicating offshore processes have the most impact on temperature variations (figure 2-7). The temperature range does not seem to be related to spring or neap tides. Hickey and Banas (2003) describe a mechanism for coastal variability related to the transition between coastal upwelling and downwelling; coastal upwelling brings cold water to the surface which then moves onshore during downwelling. Winds operating at different scales seem to have a strong influence on the variability measured at the buoy. At a large scale, prevailing winds produce Ekman transport in the form of upwelling and downwelling (Thompson, 1981). At a smaller scale, local winds create wind drift currents (Wu, 1983), which the buoy data show are parallel to the direction of the wind. Hickey and Banas (2003) describe fluctuations in water properties on the west coast to be dominated by wind forcing over scales of 3-10days. This is at a similar scale to the temperature variations between high and low tide described above.

In both the May and August examples (figures 2-9 and 2-11) the local westerly wind occurs with a northwesterly, upwelling wind offshore at La Perouse Bank. When the winds are strong and from the west at the buoy there is a strong inverse relationship

between temperature and salinity and also a greater range in both values. Also in both examples the tide and wind are oriented to the east, which increases onshore transport. This transport brings high nutrient water and potential for bloom conditions onshore.

The May 7 to 13 time series demonstrates the complexity of the system. The afternoon winds occur during the large flood tide, but there is little change in water properties. The major change in water properties occurs after the small flood, on the highest tide. The high tide is associated with high salinity, low temperature and low chlorophyll after the water has been moving in a northwest direction. Typically, during a flood tide the water moves in an eastward direction. However, after May 8 the small ebb is a low velocity northward current. This is the result of the complex interaction between wind and tide forcing. Water is pushed onshore by strong wind. When the wind relaxes and water flows back offshore the tide is weakly flooding and the resulting current direction is northward. Upwelled saline, cold, and low chlorophyll fluorescence water entering Brabant Channel moves into Russell Channel on the small flood.

In August the bloom develops after the upwelling winds subside. Cloern (1996) describes cases where plankton blooms develop during calm periods and neap tides when plankton accumulate near the surface. However, calm winds may not be a factor in this case. It is more likely that the August bloom was a result of a nutrient influx due to upwelling.

The upwelling index shows two periods in late August and late July when the transport is close to zero. These periods also coincide with a periods of small tidal range which has potential for stratification. However, neither time corresponds to a bloom. The spatial area measured by the buoy is small during this period as indicated by the small range of values between high and low tide. Likewise during periods of high wind and/or high tidal range and range in values measured by the buoy is large.

Photoinhibition is a problem for buoy chlorophyll fluorescence described in other studies (Blain *et al.* 2004). Photoinhibition occurs when strong sunlight stresses the phytoplankton and results in a decrease in chlorophyll fluorescence. There is no evidence for photoinhibition in the Clayoquot Sound buoy data. The fluorometer is down at 4m and is likely deep enough to avoid sufficient light penetration. Field observations in other coastal waters around Vancouver Island have shown photoinhibition only in the top

3m (Jim Gower, 2010, pers. comm.). The chlorophyll fluorescence is low in most CTD profiles for the top 1-2m, which probably suggests photoinhibition. This has serious implications for the calibration of the fluorometers. Calibration measurements with the buoy and CTD where all done in daylight hours when photoinhibition would have effected the fluorescence but not the extracted chlorophyll.

The current or tide height was used to determine the direction of flow and therefore the origin of water masses measured at the buoy. The buoy was anchored behind Bartlett Island to give it protection from wind and waves. This location also means the measurements were sheltered which effects the interpretations in this chapter. The Tideview current model was used, but the spatial resolution was coarse for such a small area. The buoy data demonstrate that wind was a factor in determining the speed and direction of the current. The relationship may have been different if the buoy was anchored in a different location; stronger winds, waves and current in a more exposed location, and lighter winds, waves and current in a less exposed location. The length of time the wind was blowing was not considered in this study. Wind will continue to effect the movement of the water after the wind calms.

The remotely sensed imagery offers another spatial perspective that is comparable to the spatial area measured at the buoy. However, the distance of the bloom on April 1 and the direction of the source of high chlorophyll on May 11 don't make sense in terms of the buoy space-time series. This may be a problem related to both patchiness of chlorophyll in the water and the difference in depth of measurement between the two sensors.

2.5. Literature cited

Blain, S, J Guillou, P Tréguer, P Woerther, L Delauney, E Follenfant, O Gontier, M Hamon, B Leilde, A Masson, C Tartu, R Vuillemin. 2004. High frequency monitoring of the coastal marine environment using the MAREL buoy. Journal of Environmental Monitoring: JEM 6, no. 6 (June): 569-575. doi:10.1039/b314073c.

Cloern, JE. 1996. Phytoplankton bloom dynamics in coastal ecosystems: A review with some general lessons from sustained investigation of San Francisco Bay, California. Reviews of Geophysics 34, no. 2 (May): 127-168.

Denman, KL, and JF Dower, 2001. Patch dynamics, pp. 2107-2114, In: J.H. Stee.

Dickey, T, M Lewis, and G Chang. 2006. Optical oceanography: Recent advances and future directions using global remote sensing and in situ observations (March 31). Review of Geophysics 44, RG1001, doi:10.1029/2003RG000148.

Dickey, TD. The Emergence of Concurrent High-Resolution Physical and Bio-Optical Measurements in the Upper Ocean and their Applications. Review of Geophysics 29, no. 3, 383–413.

Gower, J and S King. 2007. Validation of chlorophyll fluorescence derived from MERIS on the west coast of Canada. International Journal of Remote Sensing 28, no. 3: 625–636.

Gower, J., S King, and P Goncalves. 2008. Global monitoring of plankton blooms using MERIS MCI. International Journal of Remote Sensing 29, no. 21: 6209-6216.

Hickey, B, and N Banas. 2003. Oceanography of the U.S. Pacific Northwest Coastal Ocean and estuaries with application to coastal ecology. Estuaries and Coasts 26, no. 4: 1010-1031. doi:10.1007/BF02803360.

Kerr, K. 2005. Nearshore Oceanography and Planktonic Prey (Family Porcellanidae) of Gray Whales, *Eschrichtius robustus*, in Clayoquot Sound, British Columbia. Masters Thesis, University of Victoria, Victoria, Canada.

Knap, A, A Michaels, A Close, H Ducklow, and A Dickson. 1996. Protocols for the Joint Global Ocean Flux Study (JGOFS) Core Measurements. JGOFS Report Nr. 19, 170pp. Reprint of the IOC Manuals and Guides No. 29, UNESCO 1994.

Nittis K, V Zervakis, L Perivoliotis, A Papadopoulos, and G Chronis. 2001. Operational Monitoring and Forecasting in the Aegean Sea: System Limitations and Forecasting Skill Evaluation. Marine Pollution Bulletin 43 (July): 154-163. doi:10.1016/S0025-326X(01)00055-8.

Stewart, R. 2008. Introduction to Physical Oceanography, Department of Oceaongraphy, Texas A&M University, available at http://oceanworld.tamu.edu/ocean410/

Taylor, FJR, and R Haigh. 1996. Spatial and temporal distributions of microplankton during the summers of 1992–1993 in Barkley Sound, British Columbia, with emphasis on harmful species. Canadian Journal of Fisheries and Aquatic Sciences 53, no. 10: 2310–2322.

Thomson, RE. 1981. Oceanography of the British Columbia Coast. Can. Special Pub. Fish. Aquat. Sci. 56. Ottawa, 291p.

Whyte, JNC, N Haigh, NG Ginther, and LL Keddy. 2001. First record of blooms of Cochlodinium sp.(Gymnodiniales, Dinophyceae) causing mortality to aquacultured salmon on the west coast of Canada. Phycologia 40, no. 3: 298–304.

Wieters, EA, DM Kaplan, SA Navarrete, A Sotomayor, J Largier, KJ Nielsen, and F Veliz. 2003. Alongshore and temporal variability in chlorophyll a concentration in Chilean nearshore waters. MARINE ECOLOGY-PROGRESS SERIES 249: 93-105.

Wu, Jin. 1983. Sea-Surface Drift Currents Induced by Wind and Waves. Journal of Physical Oceanography 13, no. 8 (August 1): 1441-1451 .

Chapter 3. the spatio-temporal relationship between physical and biological fine-scale oceanographic CTD observations

3.1. Introduction

In this chapter I describe the fine-scale spatio-temporal oceanographic conditions of temperature, salinity and chlorophyll fluorescence in Clayoquot Sound from late May to mid-September 2007. In the pervious chapter I presented time series data from the buoy to describe spatial patterns. Here, a different approach is taken to describe the spatio-temporal patterns using vertical profiles collected in the vicinity of the buoy. I emphasise the linkage between fine-scale physical and biological measurements using the depth profiles measured multiple times over a 41-station grid. The grid was sampled 18 times from June to mid-September over a range of oceanographic conditions. The buoy data are related to the CTD profiles, which help determine the representative area the buoy represents. The results are presented in two parts. The first is a descriptive analysis of the water profiles. In the second part, I explore the spatial variability using empirical orthogonal function analysis. The focus of this chapter is the mechanisms driving spatial patterns over time and the link between the physical parameters and chlorophyll fluorescence.

3.2. Methods

3.2.1. Oceanographic CTD measurements

Profiles of temperature, salinity and chlorophyll fluorescence to a depth of 10 to 15m were collected in a 40km^2 region centred around the buoy. The measurements were made at 41 stations in the Bartlett Island region, south of Flores Island (Figure 3-1). The red circle in figure 3-1 is station 1 and the location of the Clayoquot Sound Buoy, with a latitude and longitude of 49^{o}13.8', 126^{o}4.9'. The sampling was repeated every 3 to 10 days depending on weather and boat access. These constraints allowed 18 sample dates over a range of oceanographic and atmospheric conditions between June and September 2007. The 41 profiles for each sample day were completed in 2 to 4 hours giving a near-

snapshot representation of the conditions. Station locations were picked to include backwaters, tidal channels and open water. Stations were sampled in order from Station 1 (at the buoy) to 41.

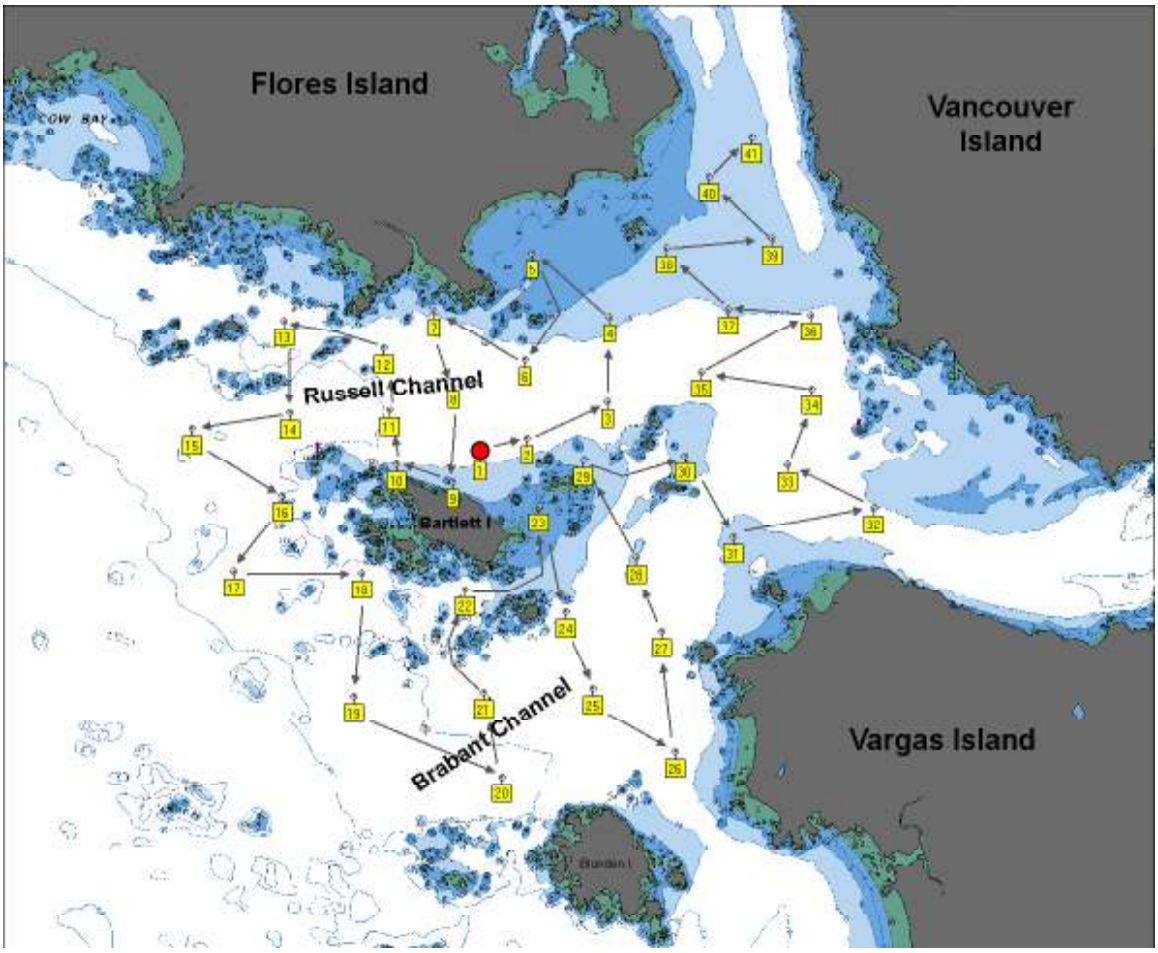

Figure 3 - 1. Positions of CTD sampling stations. The large red circle shows the location of the buoy, which is also station 1. It has a latitude and longitude of 49°13.8', 126°4.9'.

On July 7, low batteries in the CTD meant that 3 stations were missed and 5 stations were cut short (table 3-1). Station 12, Station 11, and Station 35 were missed on July 4, July 29, and August 9, respectively due to errors in instrument operation. Stations are grouped together by proximity and water mass. Stations 1-12 are called the Russell Channel stations, stations 13-22 and 25-26 are called the outside stations, stations 23-24 and 27-33 are called the Brabant stations, and stations 34-41 are called the inside stations.

Sample date	Start time (PDT)	# of stns sampled	Comments
Jun 3	09:24	41	
Jun 13	10:04	41	
Jun 22	07:06	41	Heavy rain
Jun 25	10:19	41	
Jul 4	13:20	40	Station 12 missed due to operating error
Jul 7	12:09	33	Stations 24, 25, 27, 29-33 missed due to low CTD batteries
Jul 14	16:05	41	
Jul 16	09:47	41	
Jul 25	07:34	41	
Jul 29	13:41	40	Station 11 missed due to operating error
Aug 9	9:30	40	Station 25 missed due to operating error
Aug 12	12:44	41	
Aug 21	10:16	41	
Aug 25	9:10	41	
Aug 30	8:08	41	
Sep 3	15:39	41	
Sep 12	15:08	41	
Sep 13	15:31	41	

Table 3 - 1. Summary of sample days.

The profiles were collected using a Seabird 19plus CTD (conductivity, temperature and depth) dropped from the side of a small boat. The CTD was turned on using magnetic switch and soaked at the surface for at least 20-40 seconds before each cast. The decent rate of the CTD was approximately 1m/s. The sampling rate was 4 Hz giving 4 measurements per vertical meter. The Chlorophyll fluorescence was measured using a Wetlabs fluorometer mounted to the CTD. Chlorophyll fluorescence was calibrated with extracted chlorophyll samples following the protocols for the Joint Global Ocean Flux Study (JGOFS) Core Measurements described by Knap *et al.* (1996). Equation 4 in chapter 2 was used for the calibration.

3.2.2. Additional measurements

The buoy at Station 1 measured an array of oceanographic and atmospheric parameters. It was developed by Axys Technologies in Sidney, BC, Canada and used the Watchman 500 acquisition system. At 2m above the water's surface instruments measured wind speed, wind gust, wind direction, air temperature, relative humidity, dew

point temperature, pressure, total solar radiation, and irradiance and radiance in 7 bands ranging from 412nm to 709nm. The current velocity was measured at 1.5m depth, below the buoy float. Dissolved oxygen, conductivity, temperature and chlorophyll fluorescence were measured at 4.5m. The instruments recorded measurements every 30 minutes. The buoy data were used to link the spatial and temporal domain of the buoy and CTD measurements, and to compare ancillary measurements such as wind and current.

3.2.3. Data analysis

The first part of the results describes the vertical and horizontal trends in the CTD profiles. The profiles were processed using the Sea-Bird Electronics software SBE Data Processing, Version 7.12. The processing modules used were Data Conversion, Align CTD, Derive, and Bin Average, which are described at http://www.seabird.com/software/SBEDataProcforWindowsDetails.htm. These modules calculate the depth and salinity from the pressure and conductivity, respectively, correct for response time of the instruments. The CTD profiles were compared the buoy data and used to analyse vertical structure. The profiles were averaged into 1m bins (Figure 3-2). Conductivity was converted to salinity in practical salinity units. The profiles show the horizontal and vertical patterns in the water.

To quantify the strength of stratification in the CTD profiles, the minimum value for each profile was subtracted from the maximum value. Tidal height was taken from the tidal prediction software TideWX (http://wxtide32.com). The tidal height was used as a proxy for current direction and speed, where an ebb tide indicates a current from inlets and a flood tide indicates a current from offshore. Large tidal height range generally correspond with stronger current speeds. The software agrees well with the current meter data and filled in the gaps when current meter data weren't available (June and early July). The tidal range is calculated from the maximum and minimum values of tidal height over 24 hours on the day of sampling as a proxy for the amount of flow. All correlations are performed using Pearsons r coefficient and relationships are significant at the 0.05 level unless otherwise stated.

For the second part of the results an Empirical Orthogonal Function (EOF) analysis was used to decompose the horizontal spatial variance following the approach of

Lagerloef and Bernstein (1988) and Cloern (1996). This technique, also known as principal components analysis (PCA), is used to reduce the dimensionality of large datasets by decorrelating the data into modes representing variability. The original variables are replaced by a smaller number of variables that are transformed linear combinations of the original data. The new variables, or components, represent significant orthogonal modes of variation (Preisendorfer, 1988).

EOFs are a common method of analysis in oceanographic data. Whether the EOF analysis captures the temporal or spatial variability depends on how the data are operated on before transformation (Lagerloef & Bernstein, 1988). In an analysis of spatial variance the space average is removed, while for a temporal analysis the time average is removed.

The analysis was performed for temperature, salinity and chlorophyll fluorescence separately. Of 738 planned stations 11 stations were missed as described in table 3-1. Missing data are replaced by a distance-weighted mean of the closest stations. The average of each cast was used for temperature, salinity and chlorophyll fluorescence. The analysis was performed on the covariance matrix. The output products are the eigenvalues, mode eigenvectors (also referred to as loadings, EOF, coefficients, PC loadings, and modes) and the EOF amplitude function (also referred to as scores and amplitudes). Eigenvalues were ranked by magnitude. The eigenvalues describe how much of the variance can be explained by each eigenvector.

3.3. Results

3.3.1. Spatial and temporal patterns of the CTD measurements

3.3.1.1. Temperature and salinity profiles

The temperature profiles show a strong seasonal signal (Figure 3-2). The time series shows a gradual increase in temperatures up to August 21 followed by cooling into September. There is frequently a gradient from east to west, between the inside and outside stations, with Brabant and Russell stations in between. On June 13 the temperatures are homogenous both vertically and between stations. The inside-outside gradient is most apparent on June 3, July 7, August 9, 12, 25 and 30 with colder water at

outside stations. The strongest example is on July 7. When compared to July 4, the water temperatures on July 7 for the outside stations are almost 2^{o}C cooler on average. As discussed in section 3.4, these cold temperatures, which also have higher salinities, are probably related to a combination of upwelling and onshore winds. Temperatures on August 21 reach close to 15^{o}C for most of the top 15m. On August 25 the cooler water returns at depth. The mean and standard deviation of temperature for all dates per station are calculated from the mean value for each profile (Figures 3-3a and 3-3e, respectively). The spatial pattern of the inside-outside gradient is lost in the mean seasonal signal however the standard deviation shows higher variability for the offshore stations.

Vertical trends in the profiles include stable stratification at nearly all stations with warmer, fresh water near the surface and colder, more saline water at depth. As a proxy for stratification, figure 3-4a shows the time series for the difference between the maximum and minimum temperature averaged for each group of stations. The strength of stratification increases in mid-summer. The inside stations have a significantly higher vertical temperature difference on June 22, June 25 and August 21. Sample dates June 13, July 4, July 14 have little temperature difference between groups of stations. These differences are discussed in terms of mixing in the following sections.

A dominant feature in the salinity data is also the difference between the outside and inside stations, particularly earlier in the time-series (Figure 3-2). The mean salinity (Figure 3-3b) demonstrates this gradient clearly and the standard deviation (Figure 3-3f) is also lower at the outside stations. Salinity values at outside stations generally range between 30 and 31 PSU, while stations inside have salinities around 28 to 30 PSU and as low as 20 PSU. The range of salinities, both vertically and horizontally, decreases later in the year with an increase in the seasonal average. This is consistent with the seasonal decrease in freshwater inputs through the summer. In early September the salinity is nearly homogenous, vertically and horizontally, with a value around 31.

Vertical stratification is strongest at the inside stations where at times the salinity difference is greater than 10. Station groups have similar trends through the time series, however figure 3-4b shows that stratification at outside and Brabant stations are more similar, compared with inside and Russell stations. This contrast is most evident on July 25 when inside and Russell stations show a salinity difference of 2 higher than the

outside and Brabant stations. The decrease in the vertical and horizontal salinity range is evident as salinity difference between station groups decreases in August and September.

The data show a frequent inverse relationship between temperature and salinity. The correlation coefficients are calculated for each sample date comparing temperature and salinity at each 0.5m binned depth for all stations. The time series of the correlation coefficients (Figure 3-5) range between –0.98 and 0.18 (significant at the 0.001 level), and all significant correlations are negative except on July 16. The low temperatures offshore noted on June 3, July 7 and Aug 30 correspond with high salinities and are reflected in the strongly negative correlation coefficients of -.96, -.98 and -.98, respectively. The fresh lens of surface water at the inside stations also corresponds with higher temperatures. On June 13 the temperatures are homogenous but more variable in salinity resulting in a not-significant positive correlation. This is likely a result of mixing after June 3 followed by precipitation and lack of solar heating for several days prior to June 13 (Figure 3-6). Likewise, vertical stratification exists in early September in temperature but not salinity.

The density difference mean plot in figure 3-3d shows the average difference between the lowest and highest density calculated from all sample dates. The highest difference values are found at the north inside stations and inside-Russell Channel stations. These values describe the warm fresh water associated with inside waters. The high values also have the highest standard deviation. Station 23 has the lowest density difference due to mixing over a shallow sand bar.

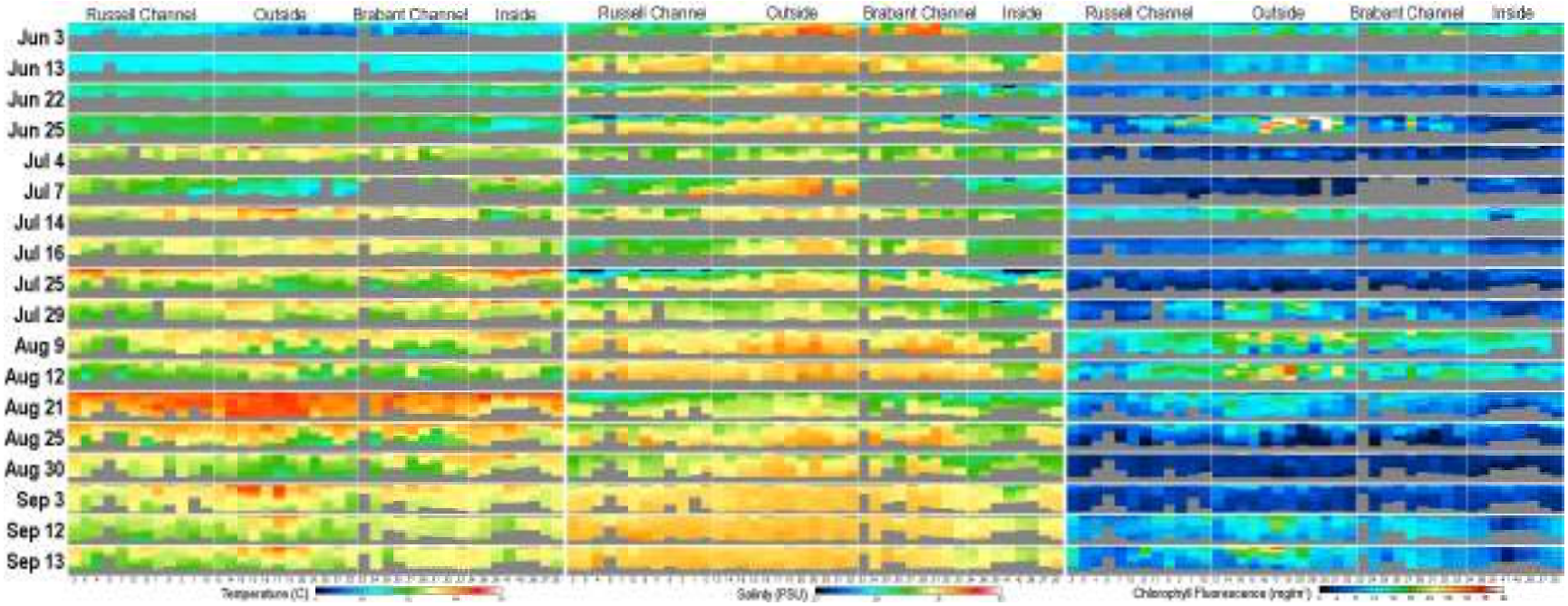

Figure 3 - 2. Temperature (left profile plot), salinity (centre profile plot) and chlorophyll fluorescence (right profile plot) profiles for the region around Bartlett Island. Measurements are averaged into 1m bins. Each date shows 41 casts for the stations (x-axis) grouped by area. Each date shows the top 15 meters (y-axis). The colour grey shows no data and in some cases is the bottom of the seafloor.

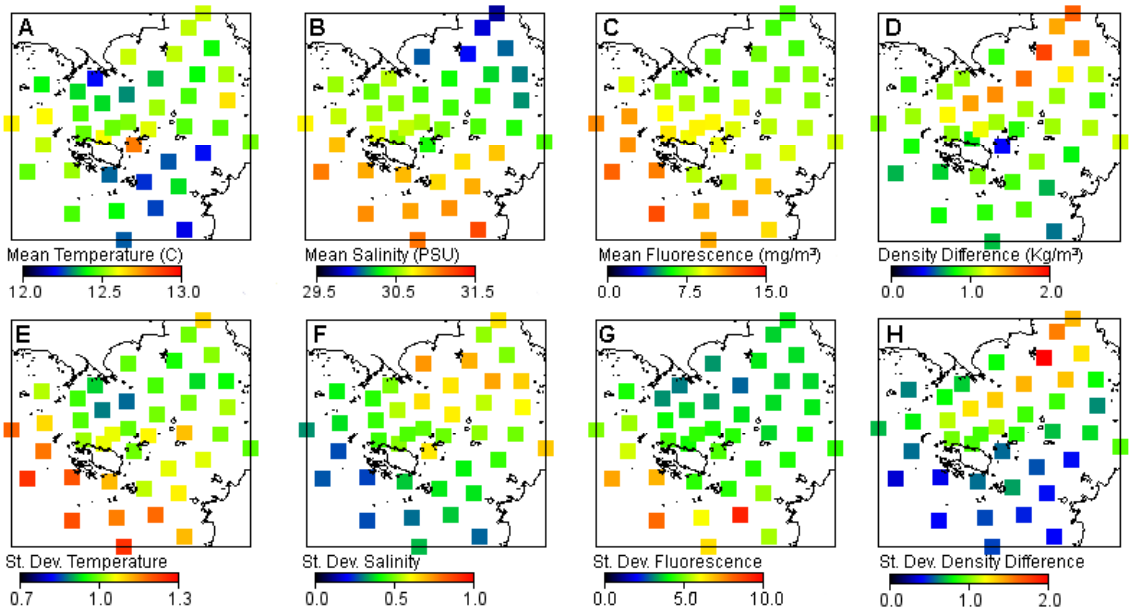

Figure 3 - 3. The mean (top row) and standard deviation (bottom row) for all samples dates for temperature (a and e), salinity (b and f), chlorophyll fluorescence (c and g) and the density difference (d and h). The mean and standard deviation for each station are calculated from the mean of the depth profile at each station, then the mean for all dates.

3.3.1.2. Chlorophyll fluorescence profiles

The chlorophyll plots show high chlorophyll events several times through the summer with the highest concentrations occurring at the outside stations (Figure 3-2). Each event is followed by a period of low chlorophyll. On June 3 the chlorophyll is between 10 and 20 mg/m^3 for the top 10m except for low concentrations at the surface. On June 13 the concentrations are low to moderate with values between 2 and 8 mg/m^3. Fluorescence levels continue to decrease with low levels at all stations and at all depths on June 22. An intense, short-lived bloom is observed on June 25 with chlorophyll fluorescence concentrations over 40 mg/m^3 at stations in the southwest. During this event highest concentrations are measured at stations 17 to 21 outside, stations 25 to 27 in Brabant Channel, and stations 1 and 10. The chlorophyll maximum is between 2 and 5 meters, except for station 26 where it is at the surface and also reaches the highest concentration of 60 mg/m^3. July 4 and 7 show low concentrations at all stations. Another increase in chlorophyll follows on July 14. When matched with the buoy fluorescence data, the July 14 sample date appears to catch the tail end of another bloom. July 16 and July 25 show a subsequent decline in chlorophyll concentration. The sample

dates July 29, Aug 9 and Aug 12 illustrate the development of another longer-lived bloom. Chlorophyll concentrations are highest at the outside stations on all three dates with the chlorophyll maximum near the surface. After August 12 concentrations decline and remain low until mid-September. On September 12 and 13 values at outside stations reach above 20 mg/m^3. This bloom time series was examined in higher temporal detail in chapter 2.

There is a positive correlation between temperature and chlorophyll fluorescence for all sample dates (Figure 3-5) except May 26 and June 3. The correlation between chlorophyll fluorescence and salinity is significant on 16 out of 18 days at the 0.001 level, however it fluctuates between positive and negative coefficients. Chlorophyll fluorescence is more closely related to temperature than to salinity as discussed in section 3.4.

High chlorophyll concentrations occur above the thermocline on July 14, early August and mid-September. Salinity is nearly vertically uniform during these events. The bloom on June 25 occurs in conditions with relatively homogenous temperatures with depth. Salinity is also only weakly stratified at high chlorophyll locations on June 25.

3.3.1.3. Influence of tides, wind, rain and sun

The tidal currents in Clayoquot Sound are strong with velocities measured on the buoy up to 1.3 m/s. At the buoy, measured currents flood to the east and ebb to the southwest. Strongest winds are predominantly from the east-southeast (100^o) and west (265^o). The average tidal range (Figure 3-4d) and wind speed (Figure 3-4e) for each sample day are related to the stratification. The highest tidal range corresponds with the smallest differences in the vertical profiles. The relationship between salinity and tide height is strongest with significant correlation coefficients between –0.45 and –0.65 for the station groups. High tidal range corresponds with low salinity differences on June 3, June 13, July 4, July 14, July 16, July 29, August 12 and August 30. Days with high salinity differences also correspond to lower tidal ranges as seen on June 25, July 7 and July 25. Strong vertical differences with depth in temperature and salinity cannot occur with large tides, while small differences may occur with small tides.

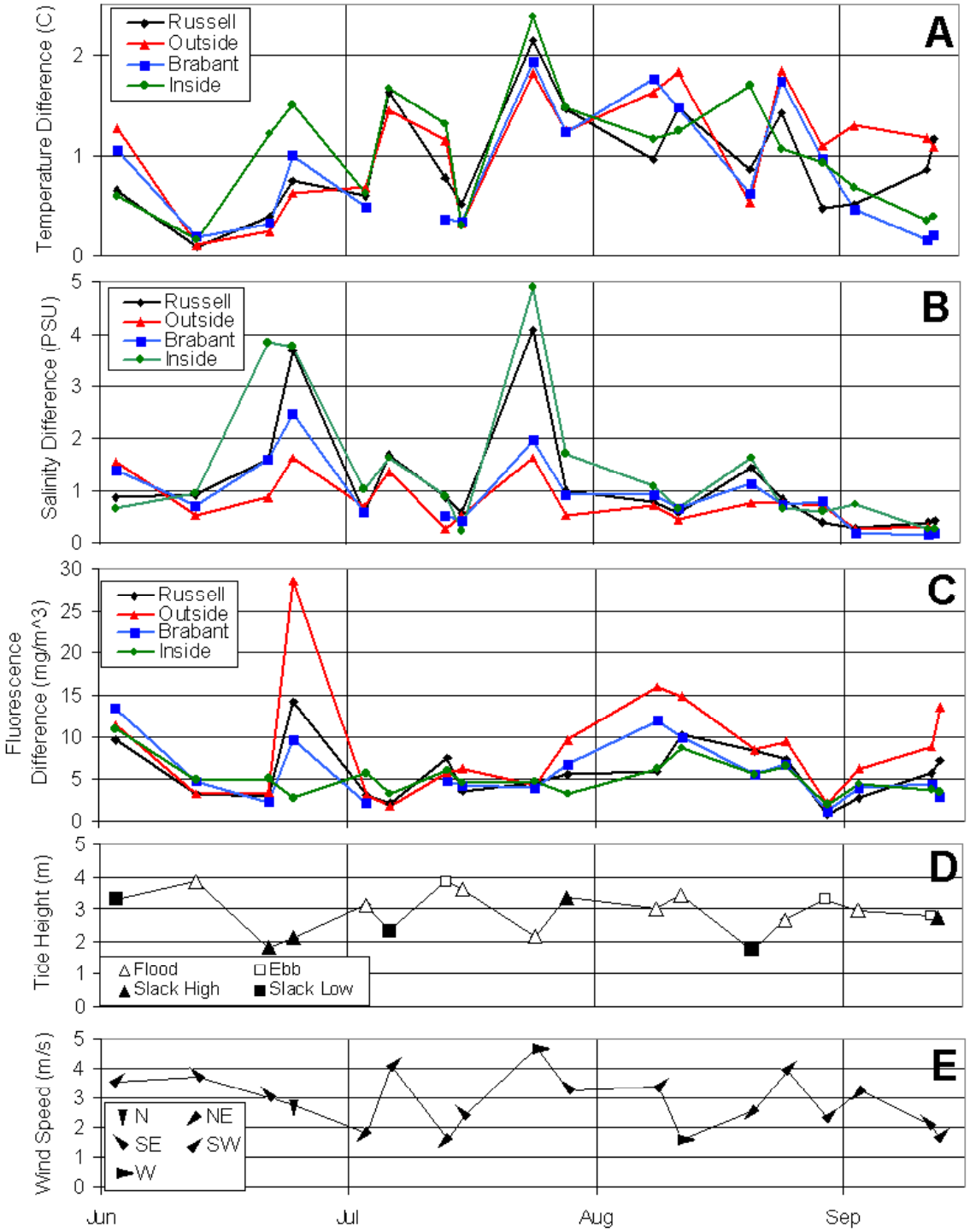

Figure 3 - 4. The difference between the maximum and minimum measurement for each station group set of profiles for temperature (a), salinity (b) and chlorophyll fluorescence (c). Stratification in a, b and c is compared to tidal height range (d) and wind (e). The labels on the plots indicate the start of the month

Temperature and fluorescence vertical difference correlations with tidal range are weak and mostly not significant, however some similarities exist with temperature and tidal height as with salinity. The highest tides on June 13 and July 14 are correlated to lows in the differences with depth and between station groups for all three variables.

The tidal stage, rather than height, may be related to the spatial structure of chlorophyll. The blooms on June 25, in early August, and in mid September are all sampled during flood or slack high-tides. The moderate bloom on July 14 is measured on an ebb tide (Figure 3-4d); however, the Russell Channel and outside stations are sampled at the beginning of the ebb. This is confirmed by the buoy time series compared with tidal height for the June 25 bloom, which shows that the high chlorophyll water is associated with high tides.

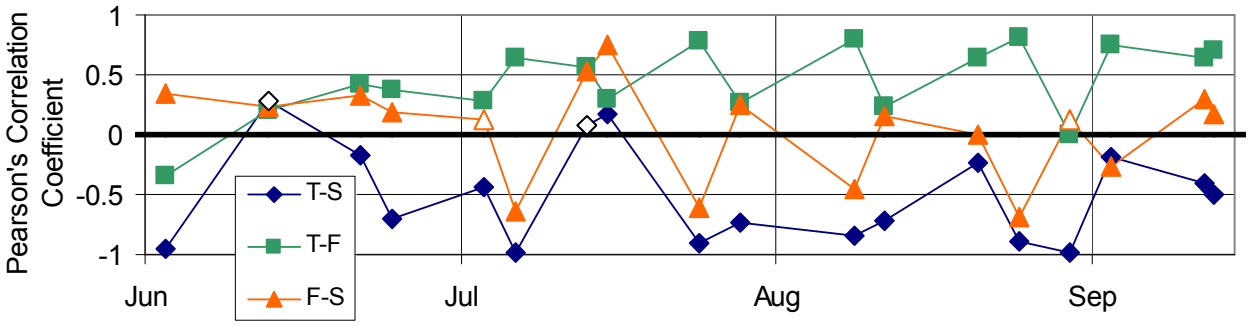

Figure 3 - 5. Correlation coefficients for temperature and salinity (blue series), temperature and fluorescence (green series) and fluorescence and salinity (orange series). For each sample day the correlation coefficient is calculated from all stations comparing each 0.5m binned depth. Solid markers indicate that the correlation is significant at 0.001 level. The labels on the plot indicate the start of the month.

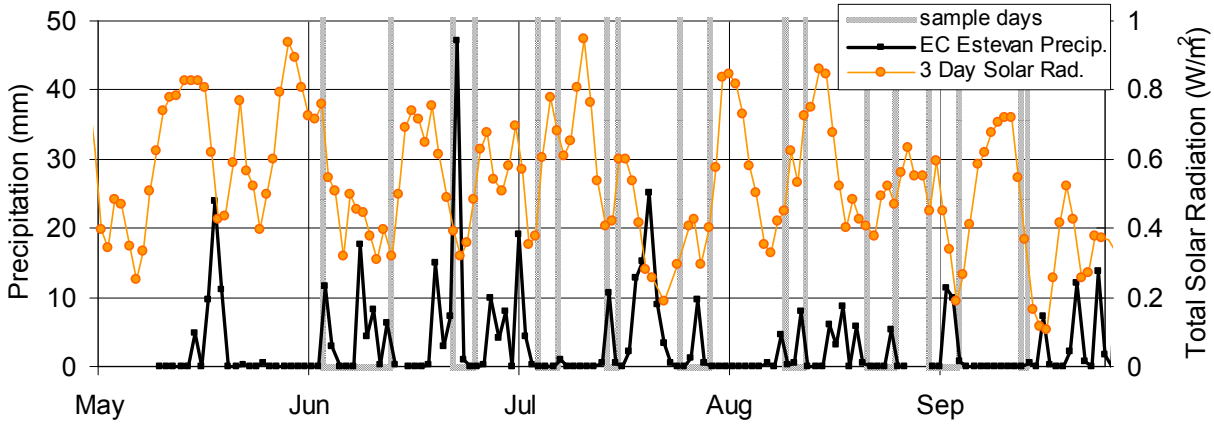

Figure 3 - 6. Daily cumulative precipitation at the Environment Canada weather station at Estevan point (black) with the 3-day cumulative total solar radiation. The labels on the plot indicate the start of the month.

The relationship between the average wind speed measured for 24 hours prior to sampling (Figure 3-4e) and stratification is less clear for the three variables. The expected relationship is that high wind speeds create mixing and are therefore related to low stratification. High winds on July 7 and August 25 correspond with relatively low chlorophyll and salinity differences, but not temperature. High wind speeds on the July 25 correspond to low stratification in chlorophyll fluorescence but high differences in salinity and temperature.

The closest available rainfall data are measured at the Environment Canada Estevan Point CS weather station at 49°22.8N and 126°32.4W, located 37km to the northwest. These data are available online at http://www.climate.weatheroffice.ec.gc.ca/climateData/canada_e.html. When compared to cumulative rainfall (Figure 3-6), high salinity differences show a strong relationship with the periods of precipitation. High rainfall on June 23 results in a large salinity difference at all stations on June 25. Heavy rains occurred close to the end of the sample period on June 22 and is reflected in low surface salinities at the inside stations, which are sampled last. Another peak in the salinity and temperature difference is noted on July 25. This may be a result of rain from July 18 to July 23. The cumulative rainfall for 3 days, 5 days and 7 days before the sample day were compared to the data. The 7-day cumulative rainfall was the only combination showing a significant relationship. The correlation coefficients from the cumulative 7-day rain and salinity difference were 0.82, 0.58, 0.69 and 0.77 for the Russell, outside, Brabant and inside groups, respectively. The lower correlation coefficient for the outside stations can be explained by the greater distance from rivers, less stratification (Figure 3-4b) and by processes outside having a strong influence from upwelling. There are no significant correlations between rain and any of the stations for temperature and chlorophyll fluorescence.

The three-day cumulative total solar radiation (TSR) collected at the buoy (Figure 3-6) can be related to chlorophyll time series. Each chlorophyll bloom follows a peak in the TSR except on July 29, which marks the beginning of a the bloom into mid-August. However, high TSR values in the beginning of August may help fuel and prolong the bloom. Blooms measured on June 3, July 14, and in mid-September are associated with

high TSR 2 to 5 days before. The bloom on June 25 occurs after high TSR a week before. The total radiation is also expected to be related to increased stratification in temperature, but I am unable to see this in the data.

3.3.1.4. CTD profile patterns compared to buoy data

In table 3-2 the representative area of the buoy is determined by the CTD data and compared to the buoy data. The buoy time series can be related to space as described in chapter 2. The time series for temperature, salinity and chlorophyll fluorescence measured on the buoy almost always show a variation that can be related to offshore-onshore differences. The same patterns can be seen in the CTD spatial plots (figure 3-2). The size of the area represented by the buoy was estimated using both figure 3-2 and spatial maps (not shown) for all three parameters. The size of the representative area depended on the range of values. For example when there were low chlorophyll concentrations the buoy represented a larger area (June 3, August 30 and September 3). Spatial patterns in the CTD and buoy data can be related to tide as shown in table 3-2. When the water is close to high tide or flooding during sampling the buoy tends to be more representative of outside stations (June 13, June 22, June 25, July 25, August 12, August 25, September 12 and 13). On June 3, July 7, July 16 the water is close to low tide or ebbing during sampling the buoy tends to be more representative of the inside stations.

CTD date	Tide		Wind speed (m/s) and dir	Spatial description from the buoy data	Spatial description from the CTD data	Representative area around the buoy derived from CTD data	Represe-ntative area (to a max of 40km^2)
	Tidal stage	Height Range					
Jun 3	Slack low	3.3m	3.5 SW	Low T on high tide	Low T at Outside stns.	Most of Russell and Inside stns.	10 km^2 (T)
				High S on high tide	High S at Outside stns.	Most of Russell and Inside stns.	10 km^2 (S)
				Slightly higher C on high tide	Patchy C	Most of Russell and Inside stns.	10 km^2 (C)
Jun 13	Flood	3.9m	3.7 SE	Slightly higher T on low tide Low	Little variation in T	All stns. for T.	> 40 km^2 (T)
				S on low low tide	Low S at stations 40 and 41	All stns. for S except 40 and 41	38km^2 (S)
				Slightly lower C on low tide	Little variation in C	All stns. for C	> 40 km^2 (C)
Jun 22	Slack high	1.8m	3.0 SE	No change in T	No change in T	All stns for T	> 40km^2 (T)
				Lower S on low tide	High S at Outside and outer Brabant and Russell	Outside stns and outer Russell/Brabant stns. for S	30km^2 (S)
				Slightly lower C on low tide	Slightly higher C at Outside stns.	Southern outside and Brabant stns. for C	15 km^2 (C)
Jun 25	Slack high	2.1m	2.8 N	High T on high tide	High T at Outside stns.	Outside, Russell, and Brabant for T	30 km^2 (T)
				High S on high tide	High S at Outside stns.	Outside, Russell, and Brabant for S	25 km^2 (S)
				High C on high tide	Very high C at Outside stns	Stns. 2, 10 and Outside for C	15 km^2 (C)
Jul 4	Flood	3.1m	1.8 NE	No change in T	Patches of high T	Russell and Inside for T	15 km^2 (T)
				Low S on low tide	Low S at Inside stns	Russell for S	10 km^2 (S)
				No change in C	Slightly higher C Outside stns.	Russell, Inside, Brabant for C	20 km^2 (C)
Jul 7	Slack low	2.3m	4.1 SW	Low T on high tide	Low T at Outside stns.	Outer Russell, Outside and Brabant for T	20 km^2 (T)
				High S on high tide	High S at Outside stns.	Outer Russell, Outside and Brabant for S	20 km^2 (S)
				No change in C	Slightly higher C at Inside stns.	Outer Russell, Outside and Brabant for C	20 km^2 (C)
Jul 14	Ebb	3.9m	1.6 NE	Low T on low tide	Low T at north Inside stns..	Russell and Brabant for T	3 km^2 (T)
				Low S on low tide	Low S at Inside stns.	Russell and Brabant for S	3 km^2 (S)
				Patchy C with short high at high tide	Patchy C, higher at Outside stns	Russell and Brabant for C	5 km^2 (C)
Jul 16	Flood	3.6m	2.4 SE	No change in T	Little variation in T	All stns. for T	> 40 km^2 (T)
				Low S on low tide	Low S in Russell and Inside stns.	Russell and Inside for S	15 km^2 (S)
				Patchy C with short high at high tide	Slightly higher C at south Outside stns.	Russell and Inside for C	15 km^2 (C)
Jul 25	Flood	2.2m	4.7 W	High T on low tide	High T at Inside stns.	Outer Russell for T	10 km^2 (T)
				Low S on low tide	Low S at Inside stns.	Outer Russell for S	9 km^2 (S)
				No change in C	Patchy, mostly low C	All stns. for C	> 40 km^2 (C)

Table 3 - 2. Summary of the spatial pattern measured by the buoy and CTDs for temperature (T), salinity (S) and chlorophyll fluorescence (C). . The representative area was estimated from the CTD profiles. Wind speed and tide are the same as in figure 3-4.

CTD date	Tide		Wind speed (m/s) and dir	Spatial description from the buoy data	Spatial description from the CTD data	Representative area around the buoy derived from CTD data	Represe-ntative area (to a max of 40km^2)
	Tidal stage	Height Range					
Jul 29	Slack high	3.4m	3.2 SE	Little change in T	Patchy T, no spatial trend	Closest Russell stns. for T	5 km^2 (T)
				Low S on low tide	Low S at Inside stns.	Russell stns. for S	8 km^2 (S)
				Large peak in C on high tide	High C at most Outside stns.	Stns. 9 and 2 for C	3 km^2 (C)
Aug 9	Flood	3m	3.4 SW	Slightly higher T on low tide	Patchy T, higher at northern Inside and several Outside stns.	Southern Russell for T	10 km^2 (T)
				Low S on low tide	Low S at northern Inside stns.	Southern Russell for S	10 km^2 (S)
				Big C peak on high tide	High C at inner Outside stns.	Southern Russell for C	4 km^2 (C)
Aug 12	Flood	3.4m	1.6W	Low T on high tide	High T at Outside and inside stns.	Southern Russell for T	7 km^2 (T)
				High S on high tide	Low S at Inside stns.	Russell, Outside and Brabant for S except stns. 7, 25, 37	30 km^2 (S)
				Slightly lower C on low tide	High C at outer Outside stns.	Southern Russell for C	6 km^2 (C)
Aug 21	Slack low	1.7m	2.6 NE	Little change in T	Low T at Inside stns.	Russell and Brabant for T	20 km^2 (T)
				Higher S on high tide	High S at Outside stns.	Outer Russell for S	5 km^2 (S)
				Small peak in C on high tide	Slightly higher C at Outside stns.	Outer Russell for C	6 km^2 (C)
Aug 25	Flood	2.7m	3.9 SW	Small increase in T on low tide	Slightly higher T at Outside stns.	Outer Russell, north Outside, and north Inside stns. for T	10 km^2 (T)
				Lower S on low tide	Low S at Inside stns.	Outer Russell, north Outside, and north Inside stns. for S	10 km^2 (S)
				Short peak in C on high tide	High C at north Outside stns.	Closest stns. in Russell for C	3 km^2 (C)
Aug 30	Ebb	3.3m	2.3 SW	Low T on high tide	Low T at Outside stns.	Closest Russell stns. and north Outside for T	10 km^2 (T)
				High S on high tide	High S at Outside stns.	Closest Russell stns. and north Outside for S	10 km^2 (S)
				No change in low C	Little change in low C	All stns. for C	> 40km^2 (C)
Sep 3	Flood	3m	3.3 NE	High T on high tide	High T at Outside stns.	Closest Russell and Brabant for T	10 km^2 (T)
				High S on high tide	Low S at Inside stns.	Outside, Russell and Brabant for S	35 km^2 (S)
				No change in low C	No change in low C	All stns. for C except several outer	37 km^2 (C)
Sep 12	Ebb	2.8m	2.1 SE	Slightly higher T on high tide	High T at Outside	Russell for T	10 km^2 (T)
				Slightly higher S on high tide	Low S at north Inside stns.	Russell, Outside and Brabant for S	37 km^2 (S)
				Very small peak in C on high tide	High C at outside snts.	Closest Russell and Brabant stns for C	4 km^2 (C)
Sep 13	Slack high	2.7m	1.6 SW	Very little change T	High T at Outside stns	Russell for T	12 km^2 (T)
				Very little change in S	Low S at Inside stns	Russell, Outside and Brabant for S	37 km^2 (S)
				Small peak in C on high tide	High C at Outisde stns.	Closest Russell and Brabant stns for C	4 km^2 (C)

Table 3-2. Continued from previous page.

3.3.2. Empirical orthogonal function analysis: spatial variance

To further assess the spatial relationships in temperature, salinity and chlorophyll fluorescence an empirical orthogonal function analysis was applied to the three variables individually. The average value for each profile was used in the analysis. For the EOF analysis of spatial variance the spatial mean was subtracted from each station. The spatial variance is described in terms of the eigenvectors (*loadings*), presented as a time series, and the EOF amplitude function (*score*), presented as a spatial pattern. Figure 3-7 shows the percent of total spatial variance described by each eigenvalue in the spatial EOF analysis for the temperature, salinity and chlorophyll fluorescence. The first three components account for 72.1%, 87.1% and 84.76% of the variation for temperature, salinity and fluorescence, respectively. The break in the curve after the third component in all four cases is considered sufficient to cut off the analysis of the modes after this point and higher modes are considered not significant. In fact, by examining the change between successive eigenvalues (table 3-3) it appears that only the first two modes are significant for temperature and fluorescence. For higher modes the percent change between modes is low and can be considered noise. When the change between modes increases the change is more likely attributed to explainable variance. By the percent change method the third mode for salinity may also be significant. The first three modes for temperature, salinity and chlorophyll fluorescence are shown.

Mode	1	2	3	4	5	6	7	8	9	10	11	12	13	14	15	16	17
Temp	2.3	2.6	1.1	1.3	1.5	1.1	1.5	1.1	1.0	1.4	1.2	1.1	1.2	1.4	1.5	2.1	2.3
Sal	6.3	1.9	2.1	1.2	1.2	1.3	1.6	1.1	1.1	1.3	1.7	1.0	1.1	1.4	1.9	2.4	2.1
Fluoro	5.1	2.3	1.3	1.6	1.2	1.4	1.3	1.4	1.1	1.4	1.5	1.2	1.4	1.3	1.7	1.4	1.7

Table 3 - 3. The percent change between eigenvectors from the spatial analysis EOF for temperature (Temp), salinity (Sal) and chlorophyll fluorescence (Fluoro).

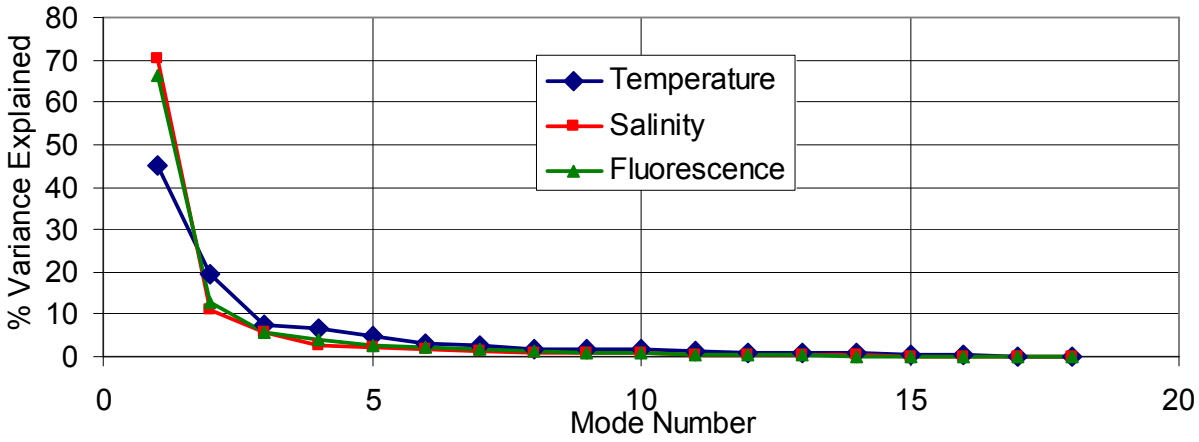

Figure 3 - 7. The eigenvalues for each component from the spatial variance EOF analysis of temperature, salinity and fluorescence.

3.3.2.1. The spatial EOF analysis for temperature

The spatial map of the first mode EOF amplitude function shows a strong inside-outside gradient with positive values at inside stations and negative values at outside stations (Figure 3-8). When this spatial pattern is dominant the corresponding eigenvector time series gives strong positive values. The first mode accounts for 45.1% of the spatial variance. The eigenvector time series closely matches the gradient between the inside and outside stations (Figure 3-9). When there are colder waters at outside stations (June 3, July 7, July 25, August 9 and August 30) the gradient is positive. Likewise, when there is warmer water at outside stations (June 25, July 14 and August 21) both the gradient and corresponding eigenvector is negative. When the eigenvectors for the first mode of the temperature spatial variance EOF are positive the inside-outside gradient is strongest and corresponds with high temperatures inside and cooler temperatures outside. This pattern also occurs when winds are from the southwest (July 7, August 9 and August 30) and west (June 3 and July 25). Similarly, when the eigenvectors are negative and the EOF spatial pattern is reversed (warm temperatures outside and cool temperatures inside) the wind is either from the north (June 25) or northeast (July 14 and August 21). This indicates that the horizontal gradient in temperature is influenced by the wind direction in the first mode. Neither the tidal height nor direction seems to contribute to the eigenvector time series.

The second eigenvector time series accounts for 19% of the total variance and is positive on all dates except July 7 and August 30. This indicates that positive values in the EOF spatial map are usually warmer and negative values are usually cooler. The spatial pattern for the second mode is very similar to the mean temperature field shown in figure 3-3a. This spatial pattern suggests that the cooler water is prevalent to the southwest. The spatial pattern is strongest on August 25 when the average winds are relatively high (4m/s) and aligned in the same direction as the flood tide. Winds from the southwest or west are also aligned with flood tides on July 25, August 9 and August 12. These dates are all positive in the second mode eigenvector time series. The positive peak in the eigenvector time series on July 14 corresponds with alignment of the ebb tide and a northeast wind. Likewise, a low tide and northeast winds on August 21 corresponds with a positive eigenvector. No alignment or opposing directions of tide and wind occurs on the other sample dates, which correspond with lower or negative eigenvectors indicating that the spatial pattern in the second mode does not exist or is reversed on these dates.

The third EOF spatial pattern for temperature shows a contrast with the temperatures in Russell Channel compared with other areas. This mode accounts for 7.4% of the spatial variance. The third eigenvector and EOF spatial patterns have no discernable pattern with respect to other geophysical properties, however high values in Russell Channel may indicate a process unique to this area compared with other locations. However, as indicated in table 3-2 this eigenvector may not be significant.

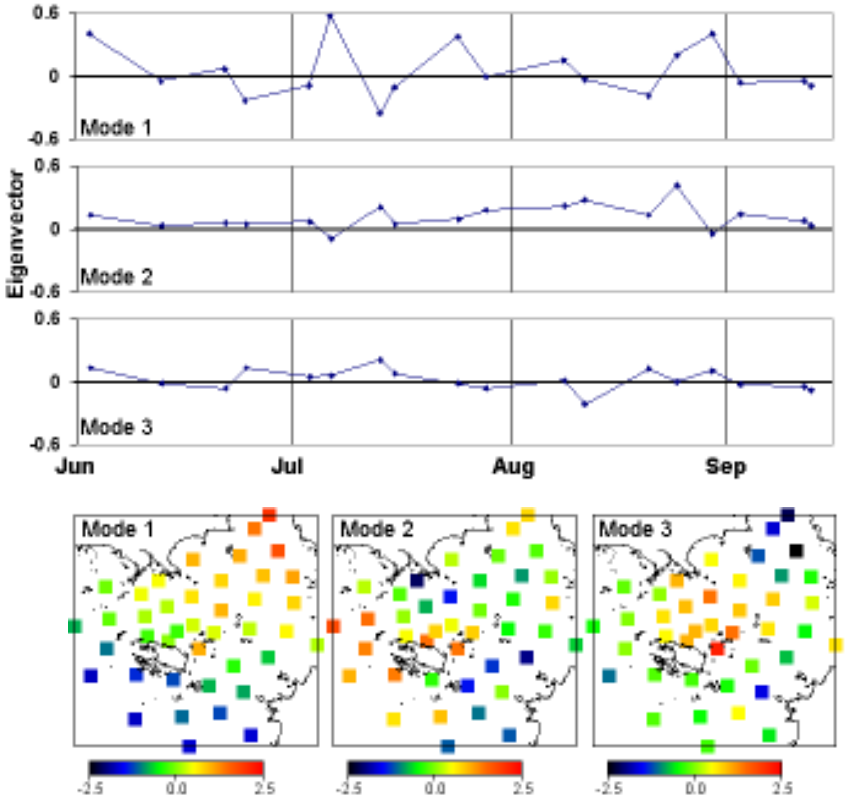

Figure 3 - 8. Temperature eigenvectors (top) and EOF amplitudes (bottom) for the first, second and third modes. The first, second and third modes account for 45.1%, 19.5% and 7.4% of the spatial variability respectively.

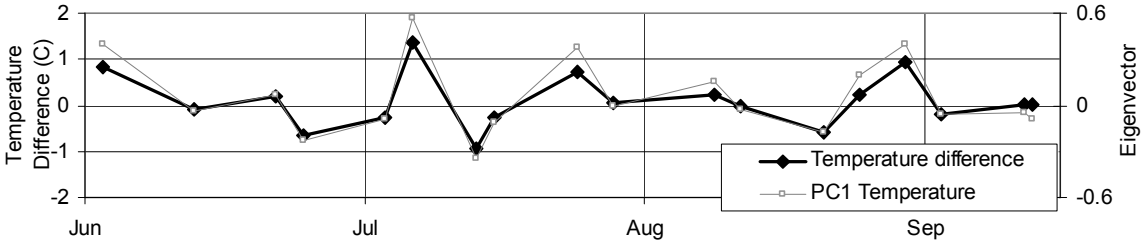

Figure 3 - 9. The average temperature difference between the outside and inside stations (thick line). The spatial variance first mode eigenvector for temperature (thin line) agrees closely with the horizontal gradient.

3.3.2.2. Spatial EOF analysis for salinity

The spatial EOF analysis for salinity accounts for 70.1%, 11.2% and 5.8% of the variance for the first, second and third modes respectively. The first mode eigenvectors are positive for the entire time series indicating that the high values always have high salinity and the low values have always have low salinity in the EOF spatial map. The EOF pattern in the first mode, expressing a high percentage of the total variability, is as expected with low salinities always closer to shore. The spatial map closely resembles the mean salinity field in figure 3-3b. As with the first temperature eigenvector time series this time series closely resembles the inside-outside station gradient time series for salinity (not shown). The eigenvector time series has a decreasing trend with time, which corresponds to the decrease in freshwater input through the summer and the decreasing gradient between outside and inside stations. While the inside-outside gradient is clearly the dominating spatial pattern, the eigenvector time series can not be related to a single geophysical factor as with temperature. Winds from the west and southwest and the corresponding higher salinity water offshore increase the gradient as shown on July 7 and July 25, however the steady decrease in the eigenvector time series is consistent with a decrease in freshwater inputs.

The second mode eigenvector time series represents 11.2% of the total variability. The spatial map of the EOF pattern shows positive values in Russell Channel. This pattern is most prominent on June 22 and July 29. On June 3 and July 16 the pattern is reversed with lower salinity water in Russell Channel. The spatial pattern is similar to the third mode EOF pattern in temperature, however the eigenvector time series do not correspond.

The third mode accounts for 5.8% with the amplitude of the eigenvectors having relatively small values. The spatial EOF amplitude function shows high values for the inside stations of Russell and Brabant, and inside stations except for stations 5, 4, and 38 to 41. This change in amplitude follows the 10m bathymetric contour, which may indicate the mode is related to a process governed by water depth.

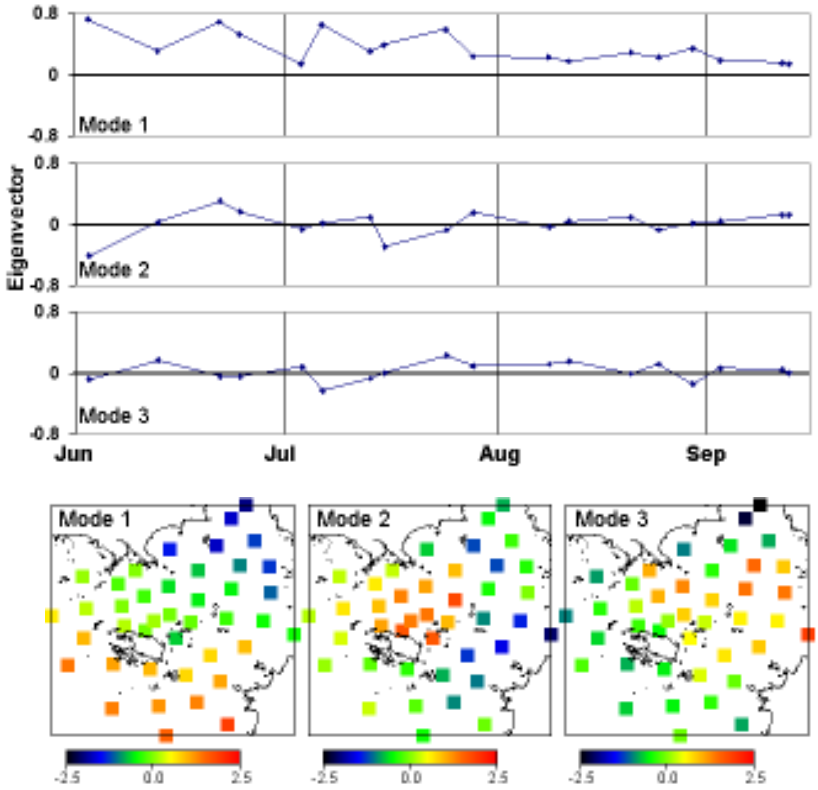

Figure 3 - 10. The results of the spatial EOF analysis for Salinity with the eigenvectors (top) and EOF amplitudes (bottom) for the first, second and third modes. The first, second and third modes account for 70.1%, 11.2% and 5.8% of the spatial variability respectively.

3.3.2.3. Spatial EOF analysis for chlorophyll fluorescence

The first mode eigenvector time series for chlorophyll fluorescence, representing 66% of the variability, is positive for nearly all eigenvectors. It resembles the time series for chlorophyll fluorescence at outside stations with high values on June 25, July 14, July 29, August 9, August 12 and mid-September. It also resembles the inside-outside station gradient time series for chlorophyll fluorescence as with the first modes for temperature and salinity. The EOF spatial map for the first mode in figure 3-11 confirm this. However, this gradient time series is not the same between the physical variables and chlorophyll. The first mode eigenvector time series for temperature and chlorophyll have an inverse relationship. The high eigenvectors in the chlorophyll first mode (indicating high chlorophyll offshore) correspond to negative eigenvectors in the first mode temperature time series (indicating high temperatures offshore) on dates with high chlorophyll values. This is consistent with the positive correlation between temperature

and chlorophyll fluorescence discussed above. The first mode also matches the mean chlorophyll fluorescence field shown in figure 3-3c. No relationship is found between the wind or tidal data and fluorescence.

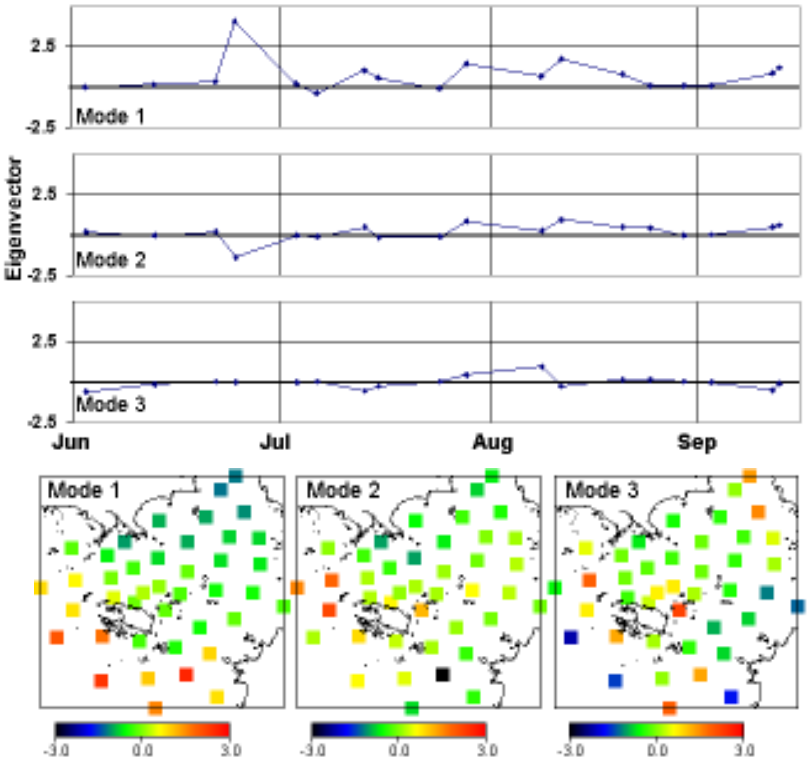

Figure 3 - 11. The results of the spatial EOF analysis for Chlorophyll fluorescence with the eigenvectors (top) and EOF amplitudes (bottom) for the first, second and third modes. The first, second and third modes account for 66.3%, 12.9% and 5.6% of the spatial variability respectively.

The second mode EOF map, representing 12.6% of the spatial variability, is influenced by a strong negative value at station 26, which is related to the intense bloom on June 25, and demonstrated by the negative eigenvector on that date. Positive values at the northwest stations outside correspond with positive eigenvectors most notably on July 14, July 29 and August 12. The third mode represents 5.5% of the spatial variability. The EOF map has a weak outside-inside spatial pattern that is strongest in late July and early August. The second and third modes cannot be related to any geophysical patterns.

3.3.3. Empirical orthogonal function analysis: temporal variance

An EOF was also preformed for temporal variance of temperature, salinity and chlorophyll fluorescence. In this case, the time average was removed from each station. The 41 stations were the variables and each sample date represented a case. The EOF amplitudes are a time series and the eigenvectors are represented in space. The temporal variance described by the first three eigenvalues accounts for 96.3%, 84.9% and 92.4% of the variation for temperature, salinity and fluorescence, respectively (Figure 3-12). The percent change between eigenvalues (table 3-4) suggests that the first two modes of temperature and chlorophyll fluorescence could be significant and that only the first mode is significant for salinity. Only the first mode eigenvectors maps and amplitude time series are shown for temperature, salinity and fluorescence. The temporal patterns are described below.

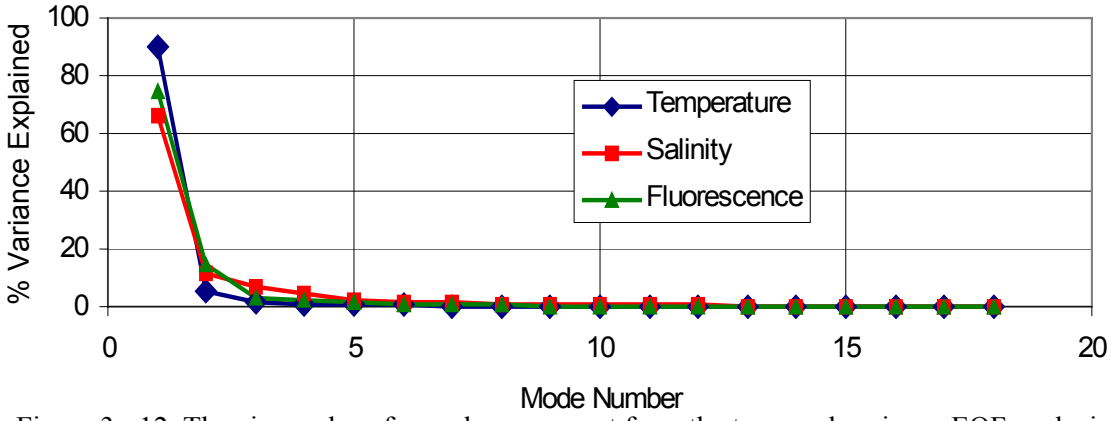

Figure 3 - 12. The eigenvalues for each component from the temporal variance EOF analysis of temperature, salinity and fluorescence.

Mode	1	2	3	4	5	6	7	8	9	10	11	12	13	14	15	16	17
Temp	17.9	3.5	1.6	1.3	1.6	1.3	1.2	1.1	1.1	1.2	1.3	1.1	1.4	1.3	1.5	2.6	
Sal	5.9	1.6	1.7	1.6	1.4	1.0	1.7	1.3	1.2	1.3	1.3	1.4	1.5	1.6	1.9	1.9	
Fluoro	5.1	4.7	1.4	1.5	1.5	1.1	1.5	1.8	1.2	1.4	1.1	1.5	1.4	1.8	1.3	1.2	

Table 3 - 4. The percent change between eigenvectors from the temporal EOF analysis for temperature (Temp), salinity (Sal) and chlorophyll fluorescence (Fluoro).

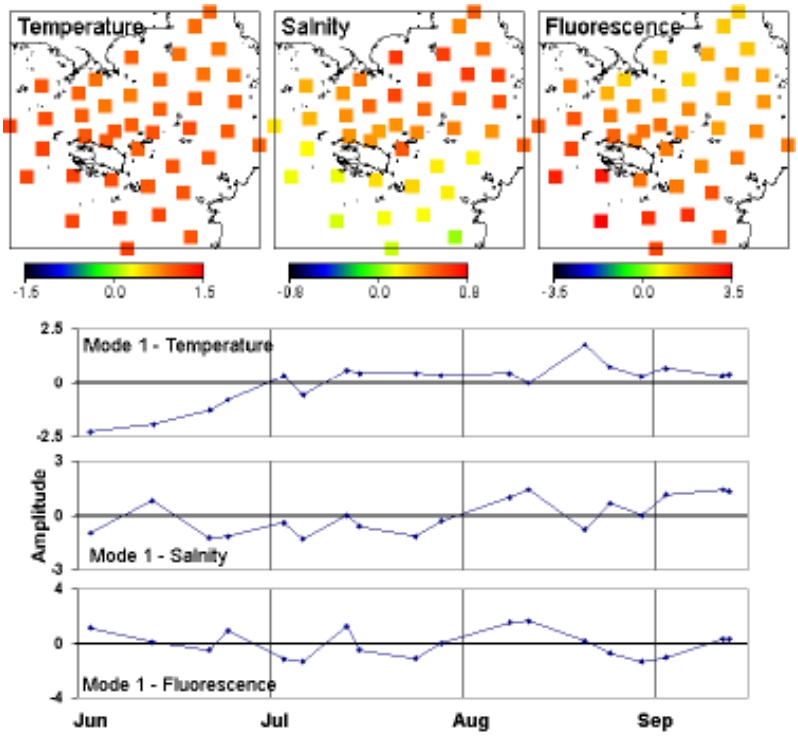

Figure 3 - 13. The results of the temporal EOF analysis for the first modes of temperature, salinity and chlorophyll fluorescence. The eigenvectors are the spatial maps (top) and the EOF amplitudes (bottom) are the time series.

The first mode for the temporal variance of temperature accounts for 89.9% of the temporal variance. The eigenvectors (spatial map) are almost homogenous (figure 3-13). The amplitude function shows a strong seasonal signal, which increases from May to August and then decreases into September. The second mode accounts for 5% of the temporal variance (not shown). It has an identical amplitude to the first mode eigenvector time series for spatial variance (Figure 3-8). Based on the eigenvalue plot in figure 3-12 following modes are not considered significant.

The first mode amplitude function for salinity also resembles the seasonal trend for salinity (figure 3-13). It accounts for 66.5% of the temporal variance. There is a small range in the spatial pattern of the eigenvectors, which shows a gradient between the inside and outside stations. The second mode accounts for 11.3% of the temporal variability. The spatial and temporal patterns are very similar to those in the second

mode of the spatial EOF. The third mode accounts for 7.1% of the temporal variability. Its spatial and temporal patterns cannot be explained in terms of any geophysical patterns or related to other modes in the spatial EOF.

For the chlorophyll fluorescence amplitude function, the first three modes account for 74.7%, 14.6% and 3% of the temporal variance, respectively. The first mode also represents the seasonal trend with peaks in on June 25, July 14, and early August (figure 3-13). The eigenvectors have very little range but a small gradient showing slightly higher values offshore. The second mode patterns reflect the first mode of the spatial EOF. The third mode cannot be explained in terms of any geophysical patterns or related to other modes in the spatial EOF.

3.4. Discussion and conclusions

The correlation and EOF analyses indicate a strong relationship between the temperature and chlorophyll fluorescence data. The EOF analysis shows that the first modes of spatial variation for temperature and chlorophyll are related to each other and linked in time. The first mode of temperature is related to the wind direction, where winds from the west and southwest create a large inside-outside temperature gradient by driving cooler offshore water landward. This is typically followed by a reversal when temperatures increase offshore. This spatial pattern of warm temperatures offshore and cooler temperatures onshore is described by the inverse of the first mode spatial EOF amplitude map and correlated with the first mode chlorophyll EOF amplitude map.

Kerr and Duffus (2005) also associated low temperatures with low chlorophyll concentrations in an area several kilometres north of Russell Channel in Cow Bay (Figure 3-1). Kerr (2005) found that chlorophyll was highly patchy in time and space and with values between 1 and 48 mg/m^3 during the summer of 2002. The study in Cow Bay also linked chlorophyll to temperature where a decrease followed by an increase in temperature could be associated with an increase in chlorophyll. Wieters *et al.* (2003) describe a similar relationship where increased chlorophyll concentrations occur after an initial period of upwelling followed by a period of relaxation on the coast of Chile (Wieters *et al.* 2003).

Mackas *et al.* (1985) showed an inverse correlation (-0.6) between temperature and chlorophyll off Vancouver Island in satellite imagery. This may indicate that the drivers at large scales for blooms are different than the drivers at finer scales. Viewed from a coarse resolution, upwelling of cold nutrient rich water is related to mesoscale blooms; however, closer to shore this nutrient rich water may be at depth or at some distance from shore until current dynamics bring it to the surface and/or onshore. Advection and aggregation of plankton from further offshore, combined with solar heating of cold upwelled water may be a mechanism for the spatial consistency of blooms at outside stations.

Nutrient data is a key component missing from this study. Upwelling is assumed to supply the nutrients and is related to the chlorophyll blooms in Clayoquot Sound. Although, Wieters *et al.* (2003) showed that river flow could be used as a proxy for nutrient input and thereby related to peaks in chlorophyll. Summer rainfall in the Sound might not be enough to be a significant source of nutrients. High rain events on June 23 and July 18 to 23 are followed by strong bloom events on June 25 and July 29 (lasting into August) and may be another source of nutrients supporting bloom growth.

The upwelling indices from the Pacific Fisheries Environmental Lab (PFEL), available online at http://www.pfeg.noaa.gov/products/PFEL/modeled/indices/upwelling/NA/upwell_menu_NA.html, were evaluated for locations north (51º N 131º W) and south (48º N 125º W) of Clayoquot Sound and show no obvious relationship with the low temperatures and high salinities periodically measured at outside stations. The Department of Fisheries and Oceans Canada 2007 State of the Oceans report noted weaker than normal upwelling winds during spring through autumn in 2007 (DFO, 2008). The cold, salty intrusions measured on June 3, July 7, and during the beginning and end of August are likely related to localized upwelling. I expected these cold water events to be associated with upwelling favourable winds (from the north and northwest), however, the EOF analysis clarifies that the large inside-outside gradient, dominated by the appearance of cold water offshore, is more prevalent during southwest and westerly winds. Kerr (2005) found the low temperatures several kilometres to the north of Russell Channel to be coupled with the PFEL upwelling indices. The Kerr study showed some influence from tidal mixing,

however, Cow Bay is more exposed than the location of the buoy. Kerr's study also found that an occasional relationship existed between cold offshore water and large amplitude tides. In the CTD data, cold intrusions were not related to large tides. While both research sites were in a similar area and the same distance from shore, Kerr's site had slightly deeper stations and was more exposed.

Vertical mixing in salinity and to a lesser degree temperature was found to be primarily related to tidal height, which was used as a proxy for currents. Wind was found to have a minimal or no effect on mixing in the near shore zone. We show the average wind speed and direction for the 24hours prior to sampling, but also analysed the average and maximum wind speed and gust for increments of time up to three days prior to sampling. None of these combinations showed a significant relationship with stratification. While Hickey and Banas (2003) describe the Pacific northwest shelf waters to be remarkably similar in stratification, the present study suggests that closer to land and even in the absence of significant fresh water input, stratification is highly variable over small areas. This is likely related to shallower depths where bathymetery and tides create flow that is important for mixing. For example, station 23, on the shallow sandbar connecting Russell and Brabant Channels, is frequently mixed. On the other hand, station 32 is usually stratified, probably as a result of deeper water and the intersection of different water masses from Calmus Passage and Brabant Channel. This is discussed by Cloern (1996) who notes that vertical mixing from tides is sometimes more important than winds in shallow coastal ecosystems.

The depth of the thermocline and mixed layer appears to be related to maximum chlorophyll concentrations. In this study, most station depths were shallower than 20m, and for deeper stations we believe that the mixed layer was captured in the top 15m measured. This is further supported by Taylor and Haigh (1996) who found summer haloclines and thermoclines in nearby Barkley Sound to be no deeper than 5m and 10m, respectively.

Taylor and Haigh (1996) found plankton communities entering Barkley Sound to be largely dependent on the dominant winds, currents and tidal forcing. They found that diatoms dominate in Barkley Sound as a result of offshore upwelling followed by onshore advection by winds. Under calm, stratified conditions they found that

dinoflagellates and other species dominate. In this study, species composition wasn't recorded. However, the mechanisms for bloom development are similar to those described in Barkley Sound. Chlorophyll fluorescence does not have a distinguishable relationship with tidal height or with stratification. It can be related to temperature and thereby to winds from the southwest and west as a result of onshore advection.

Scaling problems were an issue in the analysis of the CTD data. While dynamic processes and complex patterns demand that measurements be made in fine detail, efficient analyses must make generalizations at some scale. I grouped the stations in terms of area. However, variability within the groups was sometimes high (Figure 3-2). For example, on July 4 Station 15 had a temperature range between 13C and 14.9C and station 16 had a temperature range between 12.6C and 12.9C. This also applies to the EOF analysis, where CTD profiles were averaged before input into the analysis.

The EOF spatial analysis clarifies some of the spatial relationships and describes the dominant patterns. The inside-outside gradient is most pronounced in the first modes for temperature, salinity and chlorophyll fluorescence. The spatial map for the second mode of temperature may suggest that cooler temperatures are associated with Brabant Channel from the south. There are no similarities between the second and third mode time series for temperature and salinity. The eigenvector time series for the second mode of salinity and the third mode of chlorophyll show a similar pattern; however, the spatial maps are different. The EOF spatial maps from the third temperature mode and the second salinity show spatial similarities in Russell Channel indicating that some unique process exists in this area.

The temporal EOFs describe the seasonal patterns in the first mode for all three variables. Temporal EOFs tend to describe structures with strong temporal variability (Fang & Hsieh, 1993). The spatial patterns continued to show a strong inside-outside gradient similar to those observed in the spatial EOF analysis. The second and third modes for the temporal EOF analysis resembled the first and second modes from the spatial analysis. Particularly in the case of temperature, the first mode represents so much of the variability that the following modes are probably not significant; the second mode represents 5% of the variability compared to 90% in the first mode. Lagerloef and Bernstein (1988) describe an earlier paper where the temporal eigenvectors (spatial maps)

are nearly homogenous and associated with large-scale seasonal change. This is also the case here. The temporal EOF analysis does not reveal as much information about the spatial structure in the CTD time series because the seasonal temporal patterns are stronger than the spatial patterns. However, the third mode of the salinity EOF does reveal an offshore-shore gradient with an amplitude function pattern not found in the spatial EOF. Fang and Hsieh (1993) found that spatial variance is often more appropriate for studies that have more spatial data than temporal data. The CTD data has higher spatial resolution then temporal resolution, which makes the spatial analysis more revealing in terms of modes of variability.

The representative area of the buoy was described using the CTD data. For the majority of the CTD sample dates the agreement between the two datasets was good (table 3-2). The range of values seen in the CTD data for temperature, salinity and chlorophyll fluorescence was also measured at the buoy over a range of tidal heights. CTD profiles show spatial patterns that can be described by the buoy data in time.

3.5. Literature cited

Denman, KL, JF Dower. 2001. Patch dynamics, pp. 2107-2114, In: J.H. Stee. e-Prints Soton - Encyclopedia of Ocean Sciences. http://eprints.soton.ac.uk/58872/.

Cloern, JE, 1996. Phytoplankton bloom dynamics in coastal ecosystems: A review with some general lessons from sustained investigation of San Francisco Bay, California. Reviews of Geophysics 34, no. 2 (May): 127-168.

Cloern, JE, and AD Jassby. 2008. Complex seasonal patterns of primary producers at the land-sea interface. Ecology Letters 11, no. 12 (December): 1294-1303. doi:10.1111/j.1461-0248.2008.01244.x.

Crawford, WR and RE Thomson. 1991. Physical oceanography of the western Canadian continental shelf. Continental Shelf Research 11, no. 8-10 (October): 669-683. doi:10.1016/0278-4343(91)90073-F.

DFO, 2008. State of the Pacific Ocean 2007. DFO Can. Sci. Advis. Rep. 2008/028. Available online at: http://www.pac.dfo-mpo.gc.ca/media/back-fiche/2008/pr16-eng.htm

Emery, WJ and RE Thomson. 2001. Data analysis methods in physical oceanography, 2nd edition. Elsevier, Amsterdam, 638pp.

Environment Canada, 2009. National Climate Data and Information Archive. http://www.climate.weatheroffice.ec.gc.ca. Accessed March 2009.

Fang, WD and WW Hsieh. 1993. Summer sea-surface temperature variability off Vancouver Island from satellite data. Journal of Geophysical Research – Oceans C8, 14391-14400.

Jassby, AD and TM Powell. 1990. Detecting changes in ecological time series. Ecology 71, no. 6, 2044-2052.

Kerr, KA and DA Duffus. 2005. Timing of larval release in the porcelain crab, *Petrolisthes cinctipes* (Decapoda, Anomura), in Clayoquot Sound, British Columbia. Crustaceana 78, 1041-1051.

Kerr, K. 2005. Nearshore Oceanography and Planktonic Prey (Family Porcellanidae) of Gray Whales, *Eschrichtius robustus*, in Clayoquot Sound, British Columbia. Masters Thesis, University of Victoria, Victoria, Canada.

Knap, A, A Michaels, A Close, H Ducklow and A Dickson. 1996. Protocols for the Joint Global Ocean Flux Study (JGOFS) Core Measurements. JGOFS Report Nr. 19, 170pp. Reprint of the IOC Manuals and Guides No. 29, UNESCO 1994.

Lagerloef, G.S.E., Bernstein, R.L., 1988. Empirical orthogonal function analysis of advanced very high-resolution radiometer surface-temperature patterns in Santa-Barbara Channel. Journal of Geophysical Research – Oceans 93, C6, 6863-6873.

Mackas, DL, KL Denman, MR Abbott. 1985. Plankton Patchiness – biology in the physical vernacular. Bulletin of Marine Science 37, no. 2, 652-674.

Moore, SK, NJ Mantua, JA Newton, M Kawase, MJ Warner and JR Kellogg. 2008. A descriptive analysis of temporal and spatial patterns of variability in Puget Sound oceanographic properties. Estuarine Coastal and Shelf Science 80, no. 4, 545-554.

Mulkins, LM, Jelinski, D.E., Karagatzides, J.D., Carr, A., 2002. Carbon isotope composition of mysids at a terrestrial-marine ecotone, Clayoquot Sound, British Columbia, Canada. Estuarine Coastal and Shelf Science 54, no. 4, 669-675.

Nelson, T.A., Duffus, D.A., Robertson, C., Feyrer, L.J., 2008. Spatial-temporal patterns in intra-annual gray whale foraging: Characterizing interactions between predators and prey in Clayquot Sound, British Columbia, Canada. Marine Mammal Science, no. 2, 356-370.

Otero, M.P., Siegel, D.A., 2004. Spatial and temporal characteristics of sediment plumes and phytoplankton blooms in the Santa Barbara Channel. Deep-sea Research Part II-Topical Studies in Oceanography 51, no. 10-11: 1129-1149.

Preisendorfer, R.W. 1988. Principal Component Analysis in Meteorology and Oceanography. Elsevier Science Ltd., 426pp.

Seuront, L., Lagadeuc, Y., 2001. Variability, inhomogeneity and heterogeneity: Towards a terminological consensus in ecology. Journal of Biological Systems 9, no. 2, 81-87.

Thomson, R.E. 1981. Oceanography of the British Columbia Coast. Ottawa, Ont: Canada Dept. of Fisherie,s and Oceans.

Whitney, F.A., Crawford, W.R., Harrison, P. 2005. Physical processes that enhance nutrient transport and primary productivity in the coastal and open ocean of the subarctic NE Pacific. Deep-sea Research Part II-Topical Studies in Oceanography 52, no. 5-6: 681-706.

Wieters, EA, DM Kaplan, SA Navarrete, A Sotomayor, J Largier, KJ Nielsen, and F Veliz. 2003. Alongshore and temporal variability in chlorophyll a concentration in Chilean nearshore waters. Marine Ecology-Progress Series 249, 93-105.

Chapter 4. Bio-fouling rates on the Clayoquot Sound buoy

4.1. Introduction

In this chapter I describe the rates of fouling and fouling prevention techniques on the Clayoquot Sound buoy. Biogenic fouling was a major challenge for the Clayoquot Sound Buoy. This is a well-known problem in making long-term oceanographic measurements, particularly in the coastal ocean where increased nutrient loads yield high biological productivity. The rates of fouling are determined by several factors including type of organism, depth, light availability, nutrients, surface roughness and instrument orientation (Manov *et al.* 2004). Long-term moorings must address fouling either in terms of maintenance or in terms of an antifouling system.

Biofouling can be caused by a range of organisms, from microbial and algae films to large macrophytes, barnacles and mussels (Chavez et. al, 1997). Algae thrive in high nutrient, shallow waters typical of coastal zones. Organisms such as larvae can adhere to surfaces for their sessile life stage. For upward facing sensors detritus settling out of the water column is also a problem. While fouling can alter the calibration on any oceanographic instrument it is particularly a problem for optical instruments, which rely on a clear lens or window to make the measurements. If the window is obstructed, the measurement represents the obstruction rather than what is actually in the water column.

Various fouling prevention techniques have been developed by both researchers and private companies (www.wetlabs.com; Chavez *et al.*, 2000, Wolk & Li, 2005). For non-optical instruments such as CT sensors and transducers, chemical coatings and solutions are viable antifouling options. Preventing fouling of optical instruments is more difficult as the window must be free while sampling. This limits the use of agents that coat surfaces such as copper paints and tributyl tin based products. Dilute bleach, chlorine and bromine use are described by some authors but with less success (Chavez et al, 1997; Mclean 1996; Manov, 2004). Instrument manufactures describe successful reduction of biofouling using copper shutters for optical windows (www.wetlabs.com; http://www.satlantic.com/). Dickey *et al.* (2009) reported success using copper shutters

as well as bleach and air to flush flow-through instruments. Copper is frequently described as the most effective fouling deterrent (Manov *et al.*, 2004; Jannasch *et al.*, 2008; Chavez, 2000). However, it is also susceptible to corrosion during long deployments (Dickey *et al.* 2009). Dickey *et al.* (2009) also found that a 70:30 Cu:Ni alloy was resistant to corrosion and still effective for anti-fouling. Other methods for handling fouling include zinc anondes (Nittis *et al.*, 2001; Manov *et al.*, 2004), mechanical wipers, copper tubing (Chavez *et al.*, 2000), mechanical cleaners (Wirick, 1994), baseline subtraction (Davis *et al.*, 1997) and statistical methods (Dickey & Stramska, 1992 cited by Davis *et al.*, 1997).

4.2. Fouling and maintenance of the Clayoquot Sound Buoy

The buoy collected physical, biological and optical data from March to October 2007. All of the underwater instruments experienced varying degrees of fouling. The spectrometer, CT sensor and fluorometer were cleaned manually every 5 to 10 days during the deployment (table 4-1). The current meter was cleaned four times through the summer. The fluorometer was part of the Wetlabs biowiping series, which have copper shutters. In addition, copper wire and sheeting was wrapped around the DO sensor, CT sensor and spectrometer on June 21. The spectrometer, fluorometer and CT cell were cleaned periodically with a dilute (%10) bleach solution.

The temperature, salinity and chlorophyll fluorescence time series have been calibrated as described in chapter 2 (figures 2-2 to 2-4). Time series are drawn with lines between measurements. This is for visualization purposes only and there is no data between points. The dates labeling vertical lines on plots are the start of the day or month with which it's labeled. All times are in UTC unless otherwise stated.

Date in 2007	Instruments cleaned	Days since last cleaning					Instruments calibrated	Comments
		S	F	CT	DO	CM		
Mar 24	-						-	Deployment
Apr 29	SF	36	36				-	
May 16	SF	17	17				-	
May 23	SF	7	7				-	
May 26	SFCT-b, DO	3	3	63	63		-	
May 30	SFCT-b	4	4	4			-	
Jun 3	SFCT-b	4	4	4			-	S 2/10
Jun 5	S	2					CTF	
Jun 21	SCT-b	16		8			CTF	S 10/10, copper added
Jun 22	-						CTF	
Jun 25	SFCT-b, DO	4	22	4	30		CTF	Strong bloom
Jul 4	SFCT-b, CM	9	9	9		102	CTF	S 5/10 fouling
Jul 7	SFCT-b	3	3	3			CTF	
Jul 13	SFCT-b	6	6	6				
Jul 16	SF	3					CTF	Kelp
Jul 25	SFCT-b, DO, CM	9	12	12	30	21	CTF	S and CT 8/10
Jul 29	SFCT-b	4	4	4			CTF	
Aug 7	SFCT-b	9	9	9			CTF	
Aug 9	-						CTF	
Aug 12	SFCT-b, DO, CM	5	5	5	18	18	CTF	
Aug 21	SFCT-b	9	9	9			CTF	Copper replaced
Aug 25	SFCT-b	4	4	4			CTF	
Aug 30	SFCT-b	5	5	5			CTF	
Sep 3	SFCT-b, DO	4	4	4	22		CTF	
Sep 12	SFCT-b	9	9	9			CTF	Kelp
Sep 13	CM					32		

Table 4 - 1. Schedule for cleaning. Letters are: S – spectrometer, F – fluorometer, C – conductivity cell, T – temperature sensor, DO – dissolved oxygen sensor, CM – current meter, b – cleaned with bleach. The fractions in the comments indicate the rating out of 10 that the spectrometer was fouled.

The chlorophyll fluorescence time series shows no sign of fouling in the time series (Figure 4-1). When there was growth on the instrument the lens remained clear as a result of the copper shutter. Fouling in a chlorophyll fluorescence dataset is identified by a slow increase with time as algae grow on the window. If biogenic fouling exists there is should be a sudden drop in the fluorescence after cleaning. The average and standard deviation for the 6 hours before cleaning and after cleaning are compared in table 4-2. On 7 of 20 days there is a drop in the chlorophyll fluorescence after cleaning. However, there is no correlation with the length of time since cleaning and the before and after difference. Fouling should be most apparent when the instrument was not serviced for a long period. The longest the fluorometer went without maintenance was for 36 days between March 23 and April 29. After servicing on April 29 the chlorophyll

fluorescence increases (Figure 4-2a). This is well within the range of the variability inherent to chlorophyll fluorescence shown in the dataset. On June 25 the fluorometer had not been serviced for 22 days and also shows an increase in the average chlorophyll after cleaning. A fouled fluorometer might have a decreased standard deviation due to a constant high signal. The 6-hour before and after standard deviation also shows no trend with servicing (table 4-2).

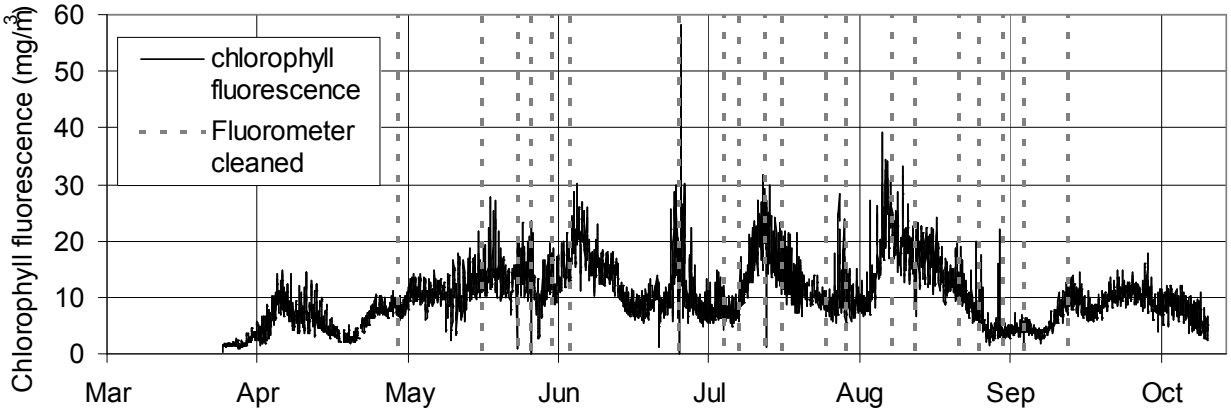

Figure 4 - 1. Chlorophyll fluorescence time series. The vertical dashed lines are dates of cleaning. Variations in chlorophyll are discussed in chapter 2. The labels on the plot indicate the start of the month.

Gelatinous algal films were common on the conductivity-temperature sensor between visits. However, it is difficult to determine whether fouling affected the data quality. One potential characteristic of fouling on the conductivity cell would be a reduction in variability. Algal films growing on conductivity cells may also reduce the range of salinity because the conductivity of the algae is measured rather than the water. Table 4-2 shows no obvious trend of fouling when comparing the average and standard deviations for the 6hours before cleaning and 6hours after cleaning. If fouling were a problem in these data, an increase in the standard deviation after cleaning should correspond with the longer time periods without cleaning. A film or algal mat could also act as insulation for the thermistor and therefore reduce the range of values in temperature, although not likely at the time scales of the buoys measurements (ihalf hourly). Figure 4-2b shows the temperature and salinity before and after cleaning on May 26. This is the longest period of time that the CT sensor went without cleaning. While there is little difference in the values immediately before and after cleaning, the

comparison of the standard deviation for the 6 hours before and after cleaning shows an increase for both temperature and salinity. Other dates with long times between visits include June 21 (18 days) and July 25 (12 days). June 21 shows no difference in the standard deviations before and after cleaning. July 25 shows a small increase for temperature and a large decrease for salinity.

Date of service	Fluorescence				Days since serv.	Temperature				Days since serv	Salinity				Days since serv
	6hrs Ave.		6hrs St dev.			6hrs Ave.		6hrs St dev.			6hrs Ave.		6hrs St dev.		
	B	A	B	A		B	A	B	A		B	A	B	A	
Apr 29	7.3	7.9	0.4	0.7	36										
May 16	**12.9**	**12.1**	2.1	1.3	17										
May 23	13.5	14.0	1.6	3.2	7										
May 26	13.6	17.2	3.4	2.9	3	10.2	10.8	**0.1**	**0.4**	63	29.7	29.1	**0.2**	**0.4**	63
May 30	13.9	16.1	2.6	2.1	4	9.9	10.6	**0.2**	**0.4**	4	30.9	30.2	**0.2**	**0.7**	4
Jun 3	14.7	16.5	2.0	1.5	4	10.2	10.0	**0.5**	**0.4**	4	30.5	30.7	0.8	0.7	4
Jun 21	11.1	5.9	1.2	1.3		10.8	11.0	0.1	0.1	18	30.1	30.1	0.2	0.2	18
Jun 25	10.5	14.4	4.6	2.4	22	11.3	11.7	0.3	0.1	4	29.5	29.9	0.5	0.5	4
Jul 4	**7.3**	**6.9**	1.3	1.8	9	12.5	12.9	**0.1**	**0.2**	9	28.8	30.4	0.5	0.4	9
Jul 7	7.5	7..9	0.8	1.3	3	11.4	11.5	0.3	0.3	3	30.7	30.7	0.4	0.4	3
Jul 13	**20.6**	**16.0**	2.4	1.5	6	12.8	12.7	0.2	0.2	6	30.3	30.7	**0.3**	**0.4**	6
Jul 16	13.6	15.7	3.7	3.8	3										
Jul 25	**9.5**	**8.0**	1.4	0.9	9	13.6	13.6	**0.3**	**0.4**	12	29.2	29.7	0.9	0.3	12
Jul 29	8.5	10.3	2.6	2.7	4	12.9	13.1	**0.1**	**0.3**	4	30.0	30.1	0.4	0.4	4
Aug 7	**26.8**	**22.3**	2.4	1.6	9	13.3	14.3	**0.4**	**0.5**	9	30.5	31.0	0.1	0.1	9
Aug 12	13.2	16.4	1.1	4.9	5	12.8	12.4	**0.1**	**0.5**	5	30.4	31.0	**0.2**	**0.3**	5
Aug 21	11.5	11.6	1.3	1.3	9	14.4	14.5	0.2	0.1	9	30.0	30.2	0.2	0.2	9
Aug 25	**6.6**	**6.3**	0.5	1.1	4	14.1	13.6	0.1	0.1	4	30.3	30.7	0.2	0.1	4
Aug 30	**4.0**	**3.5**	0.6	0.4	5	12.3	12.4	**0.2**	**0.4**	5	31.0	30.9	**0.1**	**0.3**	5
Sep 3	4.4	4.8	1.3	0.9	4	13.2	13.2	0.2	0.2	4	30.6	30.9	**0.2**	**0.3**	4
Sep 12	9.0	10.6	1.3	0.4	9	12.7	12.8	0.1	0.1	9	30.8	31.1	0.1	0.1	9

Table 4 - 2. Comparison of the average and standard deviation for 6 hours before (B) and 6 hours after (A) cleaning the fluorometer and CT sensor. Highlighted in bold are values that may indicate fouling.

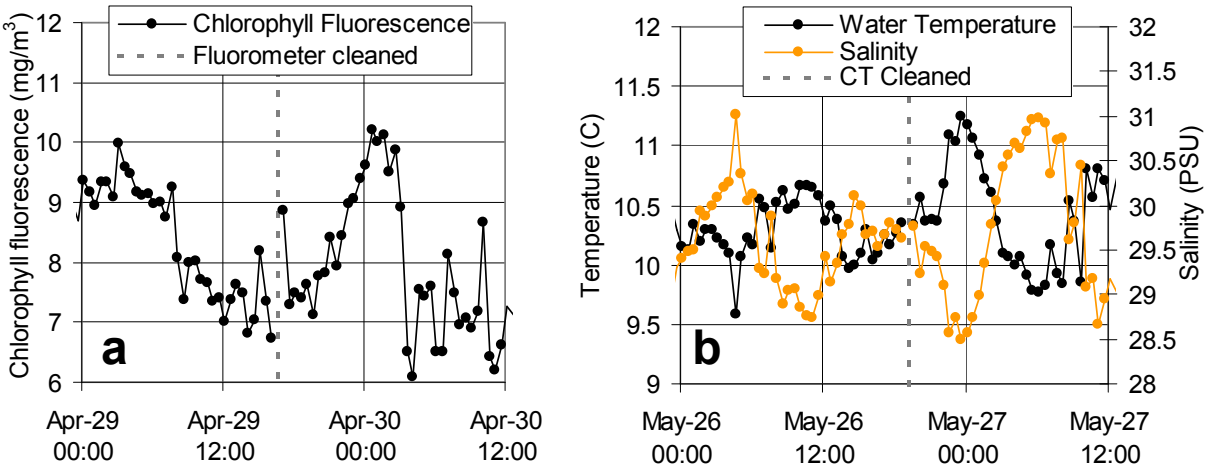

Figure 4 - 2. a) Chlorophyll fluorescence for before and after cleaning on April 29, 36 days after last cleaning. b) Temperature (black series) and salinity (orange series) for before and after cleaning on May 26, 63 days after last cleaning. The labels on the plots indicate the start of the day (UTC).

The uplooking Satlantic underwater spectrometer had major problems with fouling. An immediate increase in signal was noted after each servicing (Figure 4-3). In March to June, fouling occurred after about 10 days after servicing (March 24 – in 10 days, April 29 – in 11 days, June 10 – in 10 days). From late June into September fouling occurred in less than 9 days after servicing (June 25 – in 7 days, July 7 – in 4 days, July 16 – in 6 days, July 29 – in 5 days, September 3 – in 6 days, September 12 – in 8 days). These high fouling rates correspond with persistent high chlorophyll concentrations in July and August (Figure 4-1). Figure 4-4 shows the underwater irradiance for the last visit of the field season. Data appear to be unaffected by fouling for about 8 days after servicing on September 12. The decay in signal is seen clearly when compared to the above water irradiance.

The ADCP, measuring current speed and direction, was located near the surface in a moon pool in the buoy's hull. Initially, cleaning the ADCP was not part of the regular servicing schedule because instrument access was difficult. After 61 days the data became intermittent and eventually stopped. Barnacles covered the instrument and also wedged the instrument in the moon pool (Figure 4-5). The data are good until the instrument stopped working.

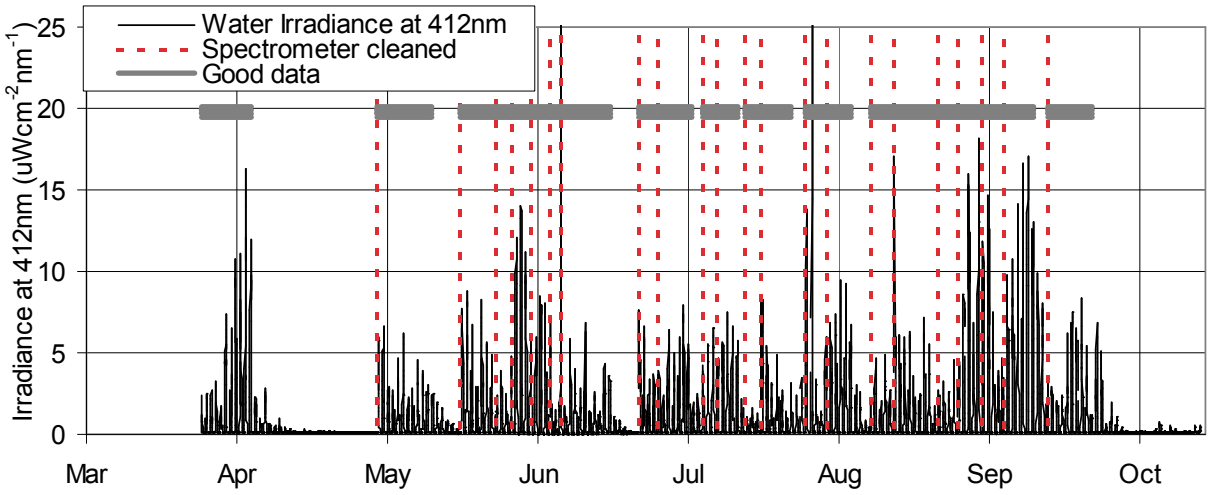

Figure 4 - 3. The irradiance at 412nm for the 2007 deployment. The vertical red dotted lines show where the sensor was cleaned. The gray blocks show where data appears to be unaffected by fouling. The labels on the x-axis denote the start of each month in 2007.

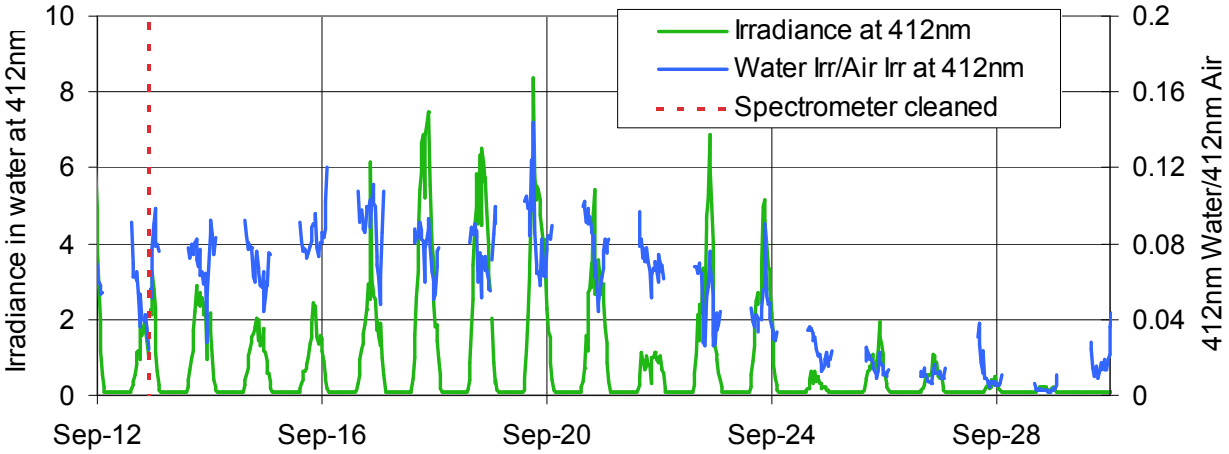

Figure 4 - 4. The time series for the underwater irradiance at 412nm and the ratio between the above water irradiance (green series, left axis) and underwater irradiance at 412nm (blue series, right axis). The vertical red dotted line denotes the last visit to the buoy for the season.

Another problem for the optical instruments was kelp becoming tangled around the buoy. On July 16 masses of kelp were cut free from the buoy. The kelp in the field of view of the above water radiometer. There is a large difference in the reflectance spectra from before and after the kelp was cut away (Figure 4-6a). The peak at 705nm is characteristic of floating vegetation with high reflectance in the near infrared. The spectrum for underwater irradiance, normalized by the above water irradiance, shows

little difference in the spectrum shape before and after servicing (Figure 4-6b). However, the overall increase in signal after the kelp is removed indicates the kelp was shading the underwater instrument.

Figure 4 - 5. The ADCP covered in barnacles after being wedged in the moon pool for 102 days. The instrument gave data for 61 days after deployment before stopping due to fouling.

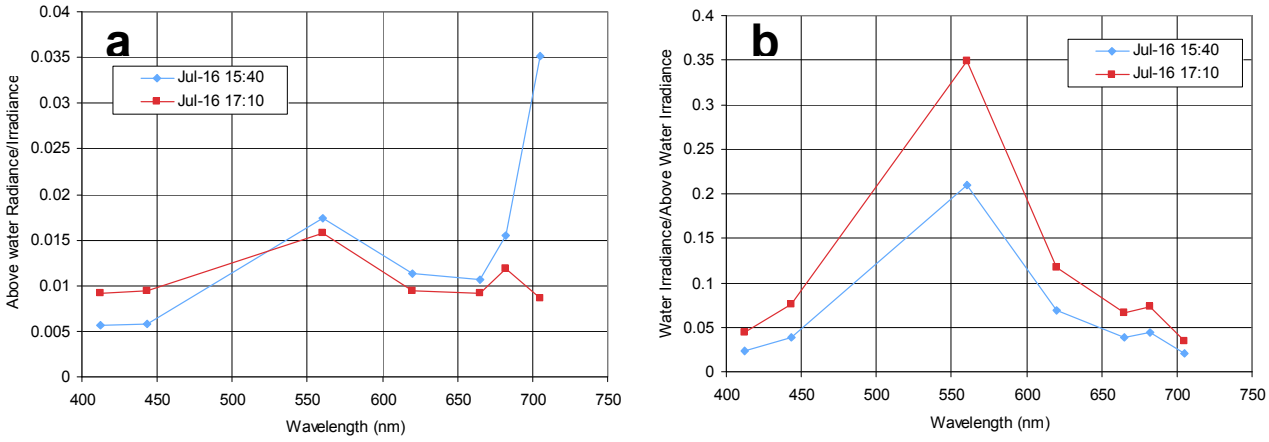

Figure 4 - 6. a) Reflectance spectra (above water radiance / above water irradiance) from before servicing (blue series) and after servicing (red series). During servicing large amounts of kelp were cut away from the buoy. b) Normalized underwater irradiance (underwater irradiance / above water irradiance). Kelp signature not seen but the instrument is shaded in the earlier measurement.

The oxygen sensor also had major problems with fouling (Figure 4-7). No calibration was performed on the sensor and therefore quantifying the rate of fouling is difficult. The sensor used was a YSI 5775 which measures dissolved oxygen (DO) across a semi-permeable membrane using an electrode system. This sensor is designed to be a field or lab sensor and not to be used on extended deployments (YSI support, pers. comm.). Algae grow on the membrane and cannot be wiped off so the membrane must be changed. Changing the membrane was difficult and time consuming under field conditions. Another problem with this oxygen sensor is that fouling can restrict flow across the membrane making it too low (a few cm/s) to replenish oxygen passing through the membrane while making measurements.

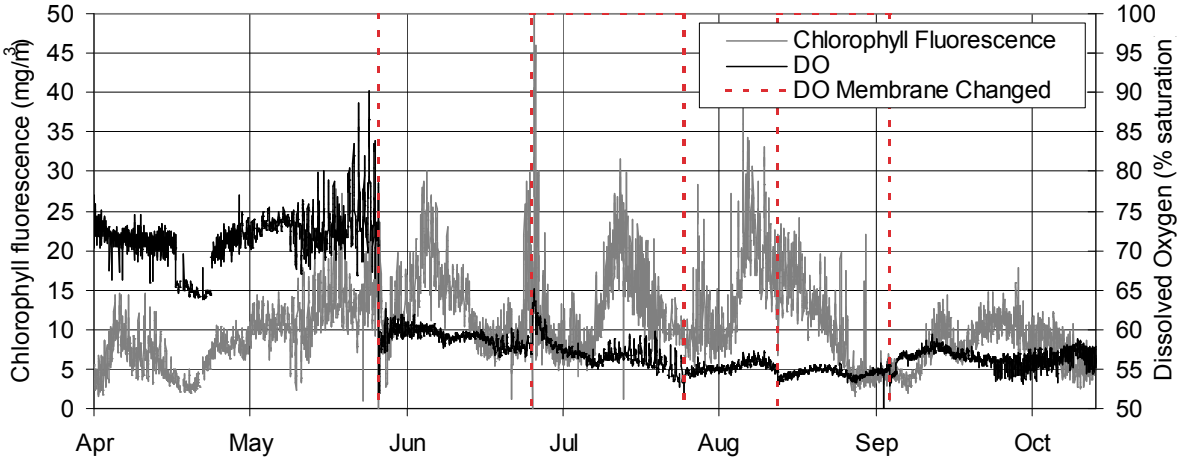

Figure 4 - 7. Dissolved oxygen and chlorophyll time series with times that the DO membrane was changed (red dotted lines). The labels on the x-axis denote the start of each month in 2007.

The uncalibrated time series shows high dissolved oxygen levels between 65 and 90 % saturation before May 26 and 55 to 65% saturation after May 26 (Figure 4-7). The membrane was changed for the first time since deployment on May 26. Leading up to this servicing date the data show increased variability. This may be a result of the algae attached to the membrane growing and respirating. The oxygen levels never return to the post-deployment levels which may indicate that the sensor was damaged during this first cleaning. Other dates where the membrane was changed also show a step in the data. There is an increase in the before-after values on Jun 25 which may coincide with increased chlorophyll values and therefore an actual increase in dissolved oxygen. On

the other dates when the membrane was changed there is either a very small decrease or very little change. Without calibration understanding this time series is difficult. Further problems with the sensor are indicated between April 17th to 24th. The large drop in dissolved oxygen cannot be explained in terms of maintenance or any real feature related to water properties.

4.3. Discussion and conclusion

Fouling rates on the buoy varied with instrument type and time. The conductivity cell, thermistor, fluorometer and DO sensor were all at a similar depth and all oriented downward. The hyperspectral sensor was oriented upwards, and about 1m above the CTF and DO sensors. More light optimized growing conditions for algae on the hyperpsectral sensor and therefore it showed higher fouling rates. Table 4-3 compares other rates of fouling found in the literature. For coastal applications fouling rates are higher. Shuttered windows on instruments clearly reduce fouling rates.

There is no significant sign of fouling in the temperature and salinity datasets. Fouling on the conductivity cell can change the size of the cell and also affect the conductivity of the electrodes (Wolk & Li, 2005, Schmitt, 2005). On a coastal mooring at the depth of 1m the in waters of southern Japan fouling is evident after 7 days in the salinity data shown by a steady decline in signal (Wolk & Li, 2005). The salinity is initially steady near 35PSU and decreases to 26PSU with fouling. Their temperature data shows no observed fouling for the same 30-day deployment. Other papers describe salinity measurements 'plagued' by fouling problems (Schmitt *et al.* 2005), and Seabird adds the toxic TBT as a standard method for biofouling control (www.seabird.com). There is no explanation found for the absence of fouling in the Clayoquot Buoy salinity dataset. The calibration of the buoy CT sensor with the CTD was always preformed after the instruments were cleaned. This was to measure the drift of the sensors and not the fouling. However, the similarities in values before and after cleaning suggest that fouling wasn't a problem. The standard deviation was used to determine if the response was affected, but the range the temperature and salinity from the tidal cycle dominated the signal.

Author	Location	Instrument	Fouling rates	Depth
Wirick, 1994	Coastal mid-Atlantic bight	Fluorometer /w wiper	No fouling in 4 months Low chlorophyll concnts.	20m
Wolk and Li, 2005	Coastal Southern Japan	Salinometer	7 days	1m
		Salinometer /w cleaner	>30 days	
Manov *et al.*, 2004	Arabian sea	Fluorometer	<3 weeks	
		Fluorometer /w TBT	3-4 months	
Manov *et al.*, 2004	Sargasso Sea	AC meter /w chlorine	< 20 days	
Manov *et al.*, 2004	Sea of Japan (open ocean)	Fluorometer /w copper shutter	> 1 year	35m
Davis *et al.*, 1997	Bering Sea	AC meter /w bromine	> 8 months	40m
Pettigrew and Roesler, 2005	Gulf of Maine	Fluorometer and AC meter with copper shutter	3-6 months	3m
Orrico *et al.* 2007	Coastal California	FLNTU w/o copper shutter	23 days	2m
		FLNTU /w copper shutter	3-5 months	
Nittis, 2001	Agean Sea	Fluorometer /w	40 days	3m
Chavez, 2000	Mid-Pacific	Fluorometer w/o wiper	52 days	10m
Jannasch, 2008	Monterey Bay estuary	Oxygen optode	2-8 weeks	Surface
		Fluorometer w/ shutter	> 4months	Surface

Table 4 - 3. Fouling rates found in other projects.

The hyperspectral sensor had severe problems with fouling. Decay in the signal occurred in 10 days in the spring and early summer and in 4 to 6 days in mid-summer. The method for determining fouling on the hyperspectral sensor was by visual inspection of the time series. Steady growth of organisms in the water column rather than growth on the sensor may also have the same affect. However, the immediate increase in light after cleaning suggests this wasn't a problem.

The fluorometer also showed no sign of fouling. This instrument also measures turbity which was not discussed in this thesis. Orrico *et al.* 2007 suggest that the turbity is more sensitive to biofouling and although measured by the same instrument will degrade more quickly than chlorophyll fluorescence. Turbity in the Clayoquot Buoy time series also did not show any sign of biofouling.

The ADCP had extreme barnacle growth which eventually stopped it from working. In Texas, Walpert et al, (2001) had the same problem on an ADCP 5.5months after deployment. The manufactures of the ADCP suggested severe barnacle growth would have caused attenuation of the signal which will result in missed returns or returns with a weak signal strength (Aquadopp, personal communication).

4.4. Literature cited

Chavez, FP, JT Pennington, RHH Jannasch, G Thurmond, and GE Friederich. 1997. Moorings and Drifters for Real-Time Interdisciplinary Oceanography. Journal of Atmospheric and Oceanic Technology 14, no. 5 (October 1): 1199-1211.

Chavez, FP, D Wright, R Herlien, M Kelley, F Shane, and P Strutton. 2000. A Device for Protecting Moored Spectroradiometers from Biofouling. Journal of Atmospheric and Oceanic Technology 17, no. 2 (February 1): 215-219 .

Davis, RF, CC Moore, JRV Zaneveld, and JM Napp. 1997. Reducing the effects of fouling on chlorophyll estimates derived from long-term deployments of optical instruments. Journal of Geophysical Research-Oceans 102, no. C3 (March 15): 5851-5855.

Dickey, T, N Bates, RH Byrne, G Chang, FP Chavez, RA Feely, AK Hanson, *et al.* 2009. The NOPP O-SCOPE and MOSEAN projects advanced sensing for ocean observing systems. OCEANOGRAPHY 22, no. 2 (June): 168-181.

Field B. 1981. Marine Biofouling and its Control*:* History and State of the Art Review. Oceans 81 IEEE 81, CH1685-7.

Jannasch, HW, LJ Coletti, KS Johnson, SE Fitzwater, JA Needoba, and JN Plant. 2008. The Land/Ocean Biogeochemical Observatory: A robust networked mooring system for continuously monitoring complex biogeochemical cycles in estuaries. Limnology and Oceanography-Methods 6 (July): 263-276.

Manov, DV, GC Chang and TD Dickey. 2004. Methods for Reducing Biofouling of Moored Optical Sensors. Journal of Atmospheric and Oceanic Technology 21, no. 6 (June 1): 958-968 .

McLean, S, B Schofield, G Zibordi, M Lewis, S Hooker, and A Weidemann. 1997. Field evaluation of anti-biofouling compounds on optical instrumentation. Proceedings of SPIE 2963, 708–713.

Nittis, K, V Zervakis, L Perivoliotis, A Papadopoulos, and G Chronis. 2001. Operational monitoring and forecasting in the Aegean Sea: System limitations and forecasting skill evaluation. Marine Pollution Bulletin 43, no. 7-12 (December): 154-163.

Orrico CM, C Morre, D Romanko, A Derr AH Barnard, C Janzen, N Larson, D Murphy, R Johnson, J Bauman. 2007. WQM: A New Integrated Water Quality Monitoring Package for Long-Term In-Situ Observation of Physical and Biogeochemical Parameters. Proceedings of Oceans 2007 MTS/IEEE Vancouver, B.C., Canada, October 1 - 4, 2007.

Schmitt, RW, R Petitt, F Thwaites, and N Brown. 2005. A fouling protected conductivity sensor for long-term salinity measurements in the upper ocean. Oceans 2005, VOLS 1-3: 1652-1655.

Walpert, JN, NL Guinasso JR, LC Bender, and LL Lee III. 2001. The effects of marine fouling on the performance of a single-point acoustic Doppler current sensor mounted on a TABS-II spar buoy. Oceans 2001 MTS/IEEE Proceedings p. 9956–9961. Marine Technology Society, Washington DC. 5–8 Nov. 2001.

Wirick, CD. 1994. Exchange of phytoplankton across the continental shelf-slope boundary of the middle Atlantic Bight during spring – 1988. Deep-Sea Research Part II-Topical Studies in Oceanography 41, no. 2-3: 391-&.

Wolk, F, and H Li. 2005. Self-cleaning sensors for long-term moorings - Wiper technology proves effective in tests in Japan's coastal waters. Sea Technology 46, no. 2 (February): 43-+.

Chapter 5. Concluding thoughts

Before looking at long-term/large-area coastal processes it is important to understand how small-scale processes and patterns are related. In this thesis I used the buoy data and CTD profiles separately to describe these fine-scale conditions. Combining the results and conclusions from chapters 2 and 3 a more complete picture is formed. In this concluding chapter I summarize the small-scale conditions and the processes driving these conditions, and discuss the advantages of each approach to oceanographic measurements in terms of scale.

In chapter 2 the buoy made measurements of oceanographic and atmospheric parameters every 30 minutes for almost 7 months. I found that large-scale upwelling in combination with the localized winds and tidal currents affect water properties at temporal scales of hours. Understanding these driving processes allows the spatial extent of the buoy to be extended from single point measurement to a larger area. In Russell Channel the water masses represent an inland source on a low tide and an offshore source on a high tide. With an onshore wind there is a greater range in water properties. A fine scale current model in the region would give this spatial interpretation more precision.

In chapter 3, the conditions are described at a high spatial scale with CTD profiles at 41 stations over 18 sample days. A strong positive correlation was found between temperature and chlorophyll fluorescence. The dominant modes of variability found in the spatial EOF analysis showed a strong offshore-onshore gradient. Variability in this gradient is likely governed by wind, particularly from the west and southwest. Vertical variability is influenced mainly by tide, but also by rainfall, which creates a fresh surface layer. The regional upwelling indices were not related to the fine-scale patterns in the CTD profiles.

Both approaches identify a strong offshore/onshore gradient. This gradient is strongest in salinity with high values offshore and low values onshore. It also exists in temperature and chlorophyll fluorescence, but with less regularity. Low temperature and high chlorophyll fluorescence are most common offshore. The profiles and buoy data show a strong inverse relationship between horizontal temperature and salinity. The profiles show the relationship exists vertically as well. The CTD data shows that outside

waters are most similar to Brabant stations, especially for salinity. This is corroborated in the buoy data in May where water from Brabant Channel is cold and salty.

The differences between the conclusions in the two chapters are related to the temporal scale at which the measurements were made. The CTD sampling, done every 3 to 10 days, captures about 5 blooms (June 3, June 25, July 14, Aug 9-12, and September 13), all with strongest concentrations offshore. The buoy chlorophyll fluorescence time series shows that the CTD sampling captures the major events for the June to mid-September period. However, the CTD time series can say little about the duration and peak concentrations of these blooms. For example, the CTD time series suggests a bloom starting around July 29 and extending through early August. In comparison, the buoy time series shows two separate blooms. Another difference is that the buoy data show that most of the temperature variation comes from offshore. This is deduced from figure 2-7 where the there is more variability in the temperatures at high tide than at low tide. The spatial EOF identifies the gradient between the offshore and onshore but does not attribute greater variability to the outside stations.

The buoy time series shows higher chlorophyll at low tide in early spring and during several short periods through the summer. Higher chlorophyll is interpreted as blooms coming from inlets and is never observed in the CTD profiles. The buoy data showed that cold, salty intrusions were sometimes related to large tides. This was also not seen in the CTD data. However, Kerr's 2005 study, described in chapter 2, used CTD data to describe oceanographic patterns and did observe this relationship. The CTD data in the present study show a strong positive correlation between temperature and chlorophyll. This relationship exists at times in the buoy data however not with same strength as in the CTD data. This is likely because the strength of the correlation comes from the depth component in the CTD data where low temperatures and low chlorophylls at depth increase the correlation coefficient. It is difficult to draw a relationship between the intrusions of cold salty water in the CTD data and the PFEL upwelling index. On the other hand, the link becomes clear in the buoy data with a finer temporal resolution.

The CTD measurements were limited to 18 days during the summer months. They require significant time and resources. Managing the buoy also requires time,

however the high temporal resolution dataset is necessary to capture the range of conditions in the coastal waters.

One major problem with data collection on a coastal mooring is biogenic fouling. It was largely overcome in this project by anti fouling devices and intensive servicing. This amount of maintenance can be time consuming and costly. The optical instruments on the buoy needed cleaning every 4-6 days in mid summer. This is particularly a problem for monitoring in remote locations.

The final points that address the questions asked in the first chapter can be summarized as follows:

- The fine-scale temporal and spatial patterns in the region are characterized by a strong gradient between offshore and onshore waters.
- The key processes driving these patterns are large-scale upwelling in combination with the localized winds and tidal currents operating at time scales of hours.
- An autonomous mooring such as the Clayoquot Sound buoy requires a significant amount of maintenance. Cleaning the instruments must be done regularly. Optical sensors without wipers require cleaning every 4-6 days.
- The representative area of the buoy varied with tide and wind. On a high tide with an onshore wind the area represented was larger than the extent of the CTD measurements. At high tide the buoy represented offshore conditions. At low tide the buoy represented onshore conditions.

The fine scale approach demonstrated in this study has high potential for future applications. Increased anthropogenic pressure on the coastal ocean means that more research is required in this area. An example of an application for this type of fine scale monitoring is in for aquaculture; detailed information on water masses is important for raising fish. Understanding and predicting bloom timing is another application; however, would require more information on nutrients and phytoplankton grazing.

In both cases fine-scale patterns and processes were used to make a link between the physical and biological domains. While phytoplankton have many contributing factors that influence the spatial and temporal variability, we show that for the exposed

coastal waters in Clayoquot Sound, winds play a dominant roll in horizontal spatial variability and tides influence the vertical spatial variability. I relate patchiness and spatial uniformity to the physical mechanisms that drive these patterns. We are not aware of any other work that has been conducted with such fine three-dimensional resolution. This study contributes to the small but growing body of literature that aims to provide a descriptive analysis of a coastal ecosystem at a small scale. Many fields, particularly biological, assume spatial homogeneity in the physical field of coastal environments with variability driven by seasonality. In addition many papers are based on measurements with a temporal resolution of 2 or 3 times a year, which form a picture that may be inadequate for the coastal ocean. We conclude that the physical properties of the coastal ocean are highly variable in small spaces and short time scales and can be related to the biological variability at similar scales.